



AL-TR-89-015

AD:

Final Report
for the Period
December 1987 to
January 1989

Combustion Characteristics of Sprays

August 1989

Author:

S. H. Sohrab

Northwestern University
Department of Mechanical Engineering
Research Institute
2145 Sheridan Road
Evanston IL 60298

F04611-87-K-0067

AD-A213 651

Approved for Public Release

Distribution is unlimited. The AL Technical Services Office has reviewed this report, and it is releasable to the National Technical Information Service, where it will be available to the general public, including foreign nationals.

Prepared for the

Astronautics Laboratory (AFSC)

Air Force Space Technology Center
Space Systems Division
Air Force Systems Command
Edwards Air Force Base, California 93523-5000

NOTICE

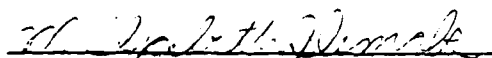
When U.S. Government drawings, specifications, or other data are used for any purpose other than a definitely related Government procurement operation, the fact that the Government may have formulated, furnished, or in any way supplied the said drawings, specifications, or other data, is not to be regarded by implication or otherwise, or in any way licensing the holder or any other person or corporation, or conveying any rights or permission to manufacture, use, or sell any patented invention that may be related thereto.

FOREWORD

This final report was submitted by Northwestern University on completion of contract F04611-87-K-0067 with the Astronautics Laboratory (AFSC), Edwards AFB, CA. AL Project Manager was M. Elizabeth Slimak.

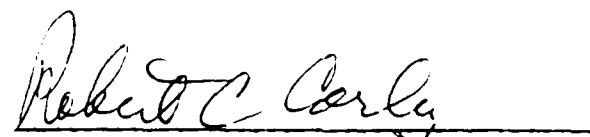
Copywritten articles are reprinted with permission from Gordon and Breach Science Publishers, Inc., 30 May 1989.

This report has been reviewed and is approved for release and distribution in accordance with the distribution statement on the cover and on the DD Form 1473.


M. ELIZABETH SLIMAK
Project Manager


LAWRENCE P. QUINN, Ph.D.
Chief, Aerothermochemistry Branch

FOR THE DIRECTOR


ROBERT C. CORLEY
Deputy Director, Astronautical Sciences
Division

REPORT DOCUMENTATION PAGE

1a. REPORT SECURITY CLASSIFICATION UNCLASSIFIED		1b. RESTRICTIVE MARKINGS	
2a. SECURITY CLASSIFICATION AUTHORITY		3. DISTRIBUTION/AVAILABILITY OF REPORT Approved for Public Release; Distribution is Unlimited	
2b. DECLASSIFICATION/DOWNGRADING SCHEDULE			
4. PERFORMING ORGANIZATION REPORT NUMBER(S)		5. MONITORING ORGANIZATION REPORT NUMBER(S) AL-TR-89-015	
6a. NAME OF PERFORMING ORGANIZATION Northwestern University	6b. OFFICE SYMBOL (If applicable)	7a. NAME OF MONITORING ORGANIZATION Astronautics Laboratory (AFSC)	
6c. ADDRESS (City, State and ZIP Code) Department of Mechanical Engineering Technological Institute 2145 Sheridan Road, Evanston IL 60208		7b. ADDRESS (City, State and ZIP Code) AL/LSCF Edwards AFB CA 93523-5000	
8a. NAME OF FUNDING/SPONSORING ORGANIZATION	8b. OFFICE SYMBOL (If applicable)	9. PROCUREMENT INSTRUMENT IDENTIFICATION NUMBER F04611-87-K-0067	
8c. ADDRESS (City, State and ZIP Code)		10. SOURCE OF FUNDING NOS.	
		PROGRAM ELEMENT NO. 61101F	PROJECT NO. 5730
		TASK NO. 00	WORK UNIT NO. 2N
11. TITLE (Include Security Classification) Combustion Characteristics of Sprays			
12. PERSONAL AUTHOR(S) Sohrab, Siavash H.			
13a. TYPE OF REPORT Final	13b. TIME COVERED FROM 87,12 TO 89,01	14. DATE OF REPORT Yr., Mo., Day 89,08	15. PAGE COUNT
16. SUPPLEMENTARY NOTATION Copywritten papers reprinted with permission			
17. COSATI CODES		18. SUBJECT TERMS (Continue on reverse if necessary and identify by block number)	
FIELD	GROUP	SUB. GR.	
19. ABSTRACT (Continue on reverse if necessary and identify by block number) This report provides a general description of the results of research studies aimed at providing a basic understanding of turbulent spray combustion. The environment in a liquid rocket engine can lead to complex flow/flame/droplet interactions which can substantially modify the droplet evaporation and combustion processes which can affect the stability characteristics of the rocket engine. The various studies conducted during this research project were: spray combustion in stagnation-point flow, thermo-diffusive flame instabilities, the influence of vorticity on flame stability/stabilization, non-planar flame configurations. Areas of future research are presented along with a discussion as to how the results of the investigation can be applied to liquid rocket engine combustion.			
20. DISTRIBUTION/AVAILABILITY OF ABSTRACT UNCLASSIFIED/UNLIMITED <input checked="" type="checkbox"/> SAME AS RPT. <input type="checkbox"/> DTIC USERS <input type="checkbox"/>		21. ABSTRACT SECURITY CLASSIFICATION UNCLASSIFIED	
22a. NAME OF RESPONSIBLE INDIVIDUAL M. Elizabeth Slimak		22b. TELEPHONE NUMBER (Include Area Code) (805) 275-5199	22c. OFFICE SYMBOL LSCF

FINAL REPORT

to

AIR FORCE ASTRONAUTICS LABORATORY

Contract No. F04611-87-0067

Principal Investigator

Siavash H. Sohrab

Assistant Professor of Mechanical Engineering

NORTHWESTERN UNIVERSITY
Department of Mechanical Engineering
Technological Institute
2145 Sheridan Road
Evanston, Illinois 60208

A-1

<i>X</i>

INTRODUCTION

Combustion in liquid rocket motors, like that in the diesel engines or gas turbines, occur as a rule under fully turbulent hydrodynamics. The turbulent fluctuations lead into complex flow/flame/droplet interactions which substantially modify the droplet evaporation and combustion processes (Faeth, 1983). Because of the large number of parameters that influence the reactive flow, systematic investigation of turbulent spray combustion requires consideration of small local flow models which aim at illuminating one particular aspect of the complex problem. For example, many model studies consider combustion of a single droplet or an array of droplets in stagnant atmosphere or under specified flow conditions. The results of such studies could then be collectively employed in the development of more comprehensive models of the turbulent spray combustion.

In the following, a general description of the results of the research studies aimed at the understanding of the various aspects of turbulent spray combustion will be presented. In particular, the relevance of the model studies to the simulation of the local flow/flame conditions within turbulent combustion in liquid rocket motors will be emphasized. The detailed discussion of each study are presented in the Appendices I through VI at the end of the present report. In the sequel, a brief description of major findings in each of the studies will be presented, and their impact on the global aspects of turbulent spray combustion will be assessed. In addition, some suggestions for research areas in need of further future exploration will be identified. Also, some discussions will be presented as to how the ideas and the results obtained in these investigations may help the modeling of turbulent spray combustion in liquid rocket engines.

SPRAY COMBUSTION IN STAGNATION-POINT FLOW

The detailed discussion of the study on the combustion of sprays in the stagnation-point flow has been presented in Appendices I and II. As is described in the Appendix I, turbulent spray is considered as a jet of liquid hydrocarbon spray which is injected into a turbulent oxidizing environment, a condition which closely simulates rocket motors using hydrocarbon fuel. Therefore, from the central core of the spray to the far field regions of the oxidizing atmosphere, an entire spectrum of concentrations from, pure fuel (F), fuel-rich ($F+\epsilon O$), near-stoichiometric ($F+O$), fuel-lean ($\epsilon F+O$), and pure oxidizer (O) may be encountered. Such regions of gaseous mixtures will be under constant random motion and may contain fuel droplets. Therefore, the concentrations of the regions will be changing because of the turbulent mixing, molecular diffusion and droplet evaporation.

In the presence of chemical reactions, the interfaces between the (F) and (O) regions identified above may support diffusion flames. Also, partially premixed flames will be encountered between the regions (F)-($\epsilon F+O$) and (O)-(F+ ϵO) with the flame receiving either fuel or oxidizer from both sides of its reaction zone. Finally, premixed flames will occur in regions which have near stoichiometric concentrations. It is emphasized that while the premixed flames are dynamic because of their propagation,

the diffusion flames only move due to the motion of the burning droplets or the bulk convection of the burning (F)-(O) interfaces. Under the velocity fluctuations, the interactions between the droplets and the randomly moving flame surfaces are inevitable. Clearly, the understanding of the problem requires knowledge of the transient interactions between the flow, the flame, and the droplets.

One of the important problems to be addressed in such turbulent spray combustion is the behavior of the individual droplets as they approach and pass through the flame surfaces. Because of the expansion of the gas, the velocity normal to the flame surface will experience a sudden jump across the flame. Another significant hydrodynamic parameter which influences the flame behavior is the rate of change of the flame surface area, i.e. flame stretch (Williams, 1985). It is expected that the rate of strain will also have substantial effects on the spray combustion similar to that in homogeneous turbulent combustion. We emphasize that thus far little is known about the subject of droplet-flame interactions, which was one of the facts that motivated the present research effort. In addition, the influence of aerodynamic stretching on the behavior of flames within sprays is almost totally unknown.

In the Appendix I, the results of our study on the behavior of reactive and non-reactive sprays in stagnation-point flow are discussed. An important finding in these tests was the pronounced change in the droplet slip velocity as it crosses the flame surface. Thus, the expansion of the gas within flames resulted in appreciable droplet deceleration (acceleration) in the pre-flame (post-flame) regions. Clearly, the change in the droplet slip velocity will have substantial effects on the droplet evaporation and combustion. We emphasize that the knowledge of the droplet trajectory as it passes through flames are quite significant for our understanding of turbulent spray combustion. Possible application of the experimental technique for the evaluation of flame propagation velocity in sprays was also described (Chen, et al., 1988). Finally, the addition of water spray to lean methane-air flames was shown to result in the formation of a yellow-orange radiation layer downstream of the flame surface. We note here that the problem of soot formation and accumulation poses severe difficulties in methane and propane-fueled rocket motors. More detailed description of the findings are available in the Appendix I (Chen, et al., 1988).

Another important result of the experimental investigation is concerning the occurrence of acoustic instabilities in the sprays when certain critical values of the fuel concentration or the flow velocity are exceeded. In particular, the concentration domains for acoustic flame were determined for both methane-air as well as methane-air-ethanol spray systems, as described in the Appendix II. The coupling with the acoustic waves produced within the burner cavity were found responsible for the observed phenomenon (Zinn, 1986). Because the present experimental model provides steady and stationary flames, the diagnostics of the properties and structure of such acoustically unstable flames is facilitated. Another significant finding in the experimental investigation was the occurrence of the so called hysteresis phenomenon shown in Fig. 1. In the tests, the contour of maximum fuel molar concentrations X_F at various nozzle velocities V corresponding to the onset of acoustic flame instability were determined. Next, the fuel concentration of the already acoustic flames was gradually reduced until the flames ceased to be acoustic and the minimum critical fuel

concentration was noted. As shown in Fig. 1, the two contours for the critical values of fuel concentrations just defined do not coincide leaving a hysteresis band in the middle. This behavior is a direct indication of the significance of the role of the non-linear phenomenon in the process of acoustic-chemically coupled flame instabilities (Zinn, 1986). Clearly, the results have direct bearing on the understanding of the mechanisms for initiation/suppression of acoustic instabilities and is in need of further investigation.

In the course of our investigation of spray combustion, an electrical heating system was developed for the evaporation of the spray in order to perform experiments on the combustion of vapors of fuels such as heptane and kerosene. The system could also be used for performing tests on the combustion of sprays in the background of their own vapors. Because of the budgetary constraints, this system was only partially developed and some preliminary results were obtained on heptane-vapor combustion. A most interesting result of these tests was the occurrence of the star-shaped flame predicted earlier by Sivashinsky (1983). Because of the transparent quartz plate used in our burner system, the geometry of the star flame could be clearly visualized as seen in the direct photograph shown in Fig. 2. Thus in agreement with the theory, as the rate of stretch was steadily increased, the cellular flame first assumed the star-shaped geometry and eventually at higher stretch rates the flame surface became flat. We emphasize that the geometry of the flame surface relates to the total flame surface area which in turn controls the turbulent burning rates.

It is emphasized again here that the results of the basic research efforts outlined above are for application to modeling of turbulent combustion process in liquid rocket motors. The goal of these basic research studies is to provide a fundamental insight into the local dynamics of the reactive flow and thereby help to improve our capability for modeling the more complex global process. For example, presently baffles are being used in the rocket motor cavity in order to modify the standing acoustic wave patterns within the cavity and thereby prevent the coupling between chemical heat release and the acoustic waves. Studies that improve our understanding of the acoustic-wave/flame interactions may be helpful in future development of better techniques for designing safe and more economic rocket motors. Also, it is emphasized that the present experimental model provides a stationary acoustically unstable flame which will facilitate the diagnostic investigation of these unstable flames. Finally, we note that only preliminary data was obtained on the acoustic frequency and the temperature fluctuations of the unstable flames, Appendix II. Clearly, more research is needed to further explore these and other important aspects of the unstable flames which is of central significance to the liquid rocket combustion phenomenon (Williams, 1985).

THERMO-DIFFUSIVE FLAME INSTABILITIES

Another important type of flame-front instability in premixed systems is the thermo-diffusive flame instability (Sivashinsky, 1983) which is caused by the preferential diffusion of heat versus reaction-controlling species. Thus, when the

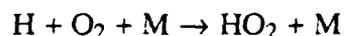
Lewis number $Le = \alpha/D$ (α and D refer to the diffusivity for heat and the deficient component) of the mixture is less than a critical value $Le^* < 1.0$, small corrugations of the flame surface will grow, leading to the formation of regularly spaced cells hence cellular or polyhedral flames. Although the phenomenon of thermo-diffusive flame instability is primarily controlled by the processes at the molecular scales, i.e. molecular diffusion, it is expected to have a pronounced influence on the burning rate in turbulent flames (Williams, 1985). This is in part because of the fact that turbulent flames are often composed of an ensemble of stretched laminar flamelets whose surface corrugation may be modified by the thermo-diffusive instability mechanism. The influence of Le on the turbulent propagation velocity has been discussed by Williams (1985).

In a previous experimental study (Bidinger and Sohrab, 1985), it was shown that the chemical kinetic mechanisms may play a significant role in the amplification/sustenance of thermo-diffusive flame instabilities. This hypothesis was tested by observation of the effects of bromo-trifluoro-methane, CF_3Br , on polyhedral butane Bunsen flames. We note here that besides the early investigations by Markstein (1964), relatively little experimental work has been devoted to the study of the temperature profiles in cellularly unstable flames. In particular, few experiments have been performed on the periodic temperature variations in rotating polyhedral flames (Sohrab and Law, 1985). Because of the important fundamental as well as practical value of the problem, the influence of radical species on cellular flames was re-examined and the temperature of the trough and crest regions of the polyhedral flames of butane were measured.

The results of the experimental investigation of polyhedral butane flames are presented in the Appendix III. In accordance with the earlier observations (Bidinger and Sohrab 1985), it was established that the radical species may indeed play a significant role in the process of thermo-diffusive flame instabilities. On the basis of the observations and in terms of the known radical scavenging properties of halogens, a phenomenological mechanism for the observed effects of CF_3Br on the polyhedral flames was presented. Another significant aspect of the study, Appendix III, was the description of the lean flammability limit of mixtures on the basis of the chemical kinetic mechanisms. Thus, it was described how the different temperature sensitivities of the important chain branching reaction such as



and a chain terminating reaction such as



may describe the occurrence of a critical minimum temperature, and hence fuel concentration, below which steady combustion will not be possible (Appendix III).

The fundamental significance of the results described above to the understanding of turbulent combustion in liquid rockets is apparent. It is emphasized here that in rocket motors using $H_2 + O_2$ as reactant, the large difference between the molecular diffusivity of the fuel versus oxidizer makes the mixture particularly susceptible to

preferential-diffusion effects. Almost every aspect of the problems studied in the Appendix III are in need of further research. Chemical kinetic description of the limits of flammability is of central significance to the understanding of local flamelet extinction in turbulent premixed flames. Also, it is emphasized that the thermo-diffusive instabilities were found to be enhanced in the oxygen-rich environments which are expected to predominate in liquid rocket motors. In turbulent combustion fields, multiple flame surfaces occur which are in constant random motion due to the turbulent fluctuations (Williams, 1985a). Because of the thermo-diffusive instabilities, the interactions between corrugated flame surfaces may occur which will modify the nature of the reactive flow (Sohrab and Chao, 1984). The central importance of studies on various mechanisms of the flame front instabilities to the understanding of turbulent combustion has been emphasized (Williams, 1985).

INFLUENCE OF VORTICITY ON FLAME STABILITY/STABILIZATION

Two hydrodynamic parameters which are of central significance to the understanding of turbulent combustion are the rate of stretch (Williams, 1985a) and the vorticity (Chen, et al., 1987; Lin and Sohrab, 1987; Sivashinsky and Sohrab, 1987). In liquid rocket motors, the presence of two phases further complicates the dynamics of the reactive field. Turbulent eddies are expected to interact with the flame surfaces as well as the moving droplets in a complex and transient fashion (Faeth, 1983). Therefore, the understanding of the interactions between vorticity and premixed and diffusion flames is of central importance to the global modeling of turbulent premixed and diffusion flames. For example, in recent theoretical (Sivashinsky and Sohrab, 1987) and experimental (Chen, et al., 1987; Lin and Sohrab, 1987) studies, it was shown that flow rotation can reduce the minimum fuel concentration at flame extinction. In addition, it was found that the rotation of the gas will enhance the formation of soot particles in opposed-jet counter-rotating flows when oxygen-enriched air is used. Such results have direct relevance to the problem of local flame extinction and soot formation in turbulent combustion environments of the rocket motors using hydrocarbon fuel.

The influence of slow rotation on the geometry and stability of flames propagating in a rotating cylindrical tube was theoretically investigated in the limit of weak thermal expansion (Sivashinsky, et al., 1988). Thus, the effects of centrifugal and Coriolis accelerations on the premixed flames were illuminated. In the study, a discrete set of angular velocities were identified at which resonance effects occurred, leading to unbounded amplification of the flame propagation speed. Of course, in real situations the dissipative viscous effects will prevent the occurrence of such resonance points (Sivashinsky and Sohrab, 1987). An important prediction of the theory was concerning the suppression of thermo-diffusive instabilities, i.e. cellular flame structures, by the flow rotation which was also substantiated experimentally (Sivashinsky, et al., 1988). On the basis of this result, we expect that turbulent eddies may tend to suppress the flame corrugations induced by thermo-diffusive instabilities. The experimental observation of the shape of the flame surface in the rotating tube also showed good qualitative agreement with the theoretical predictions. The central importance of these findings to the understanding of turbulent combustion

has been emphasized (Sivashinsky, 1983). Many other aspects of the problem thus described require further future exploration both experimentally as well as theoretically. In particular, the theoretical analysis may be extended to include the effects of strong heat release. Also, the effects of preferential diffusion and non-unity Lewis number require further experimental study.

In another theoretical investigation (Sheu, et al., 1989), the effects of the flow rotation on the geometry and stabilization of Bunsen flames were investigated. It was found that flow rotation first buckled the central portion of the otherwise conical flame and eventually, at higher rotation velocities, the stabilization of the flame on the burner rim became impossible and the flame flashed back into the burner tube (see Appendix V). The predictions of the theory just described were also substantiated by the experimental observation of methane and butane premixed flames stabilized on a rotating Bunsen burner. Both the geometry as well as the flame flash-back characteristics observed experimentally were in good qualitative agreement with the theory. Many aspects of the theoretical and experimental investigation just described are in need of further future exploration. For example, because of the importance of the flame stabilization phenomenon, the theoretical model may be extended to include the effects of the heat loss to the burner rim. Also, additional experiments are needed to improve our understanding of the transient process of flame flash-back. We emphasize again that even though the studies described herein are necessarily confined to a certain geometrical model flow fields, their aim is more general in that they may help to improve our understanding of the local flow/flow, flow/flame and flame/flame interactions in turbulent reactive flows.

NON-PLANAR FLAME CONFIGURATIONS

Flame stabilization on nozzles is a common occurrence in many combustion devices. In a theoretical investigation (Sheu and Sivashinsky, 1989) the non-planar solutions for nozzle-stabilized premixed flames were determined for reactive jets impinging on a plane wall in the stagnation-point configuration. The results of the theory (see Appendix VI) were found to be in close qualitative agreement with the experimental observations. In particular, it was established that in the stagnation flow configuration, besides the usual planar flame, other non-planar flame surfaces may also occur whose dynamic stability require further experimental and theoretical investigation. Model problems such as the one being discussed here may be considered as the first step towards the simulation of flame stabilization on injector ports and flame holders. Indeed, it is expected that future stability analysis of the cylindrical, nozzle-stabilized flames would reveal more detailed aspects of the flame stand-off as well as the flame blow-off mechanisms. More experimental investigations would also be needed in order to allow comparisons with the theoretical results of the flame stability/stabilization characteristics just described.

ACKNOWLEDGEMENTS

The research efforts reported here have been supported by the Air Force
Astronautics Laboratory under contract No. F04611-87-K-0067 and in part by the
AFOSR contract No. F49620-85-C-0013.

17. Sohrab, S. H. and Law, C. K. (1985) Influence of burner rim aerodynamics on polyhedral flames and flame stabilization, Combust. Flame 62, 243.
18. Williams, F. A. (1985) Combustion Theory, 2nd. Ed., Benjamin Cummins, Palo Alto, California.
19. Williams, F. A. (1985a) Turbulent combustion, in The Mathematics of Combustion, J. D. Buckmaster, ed., SIAM, Philadelphia, p. 97.
20. Zinn, I. B. (1986) Pulsating combustion, in Advanced Combustion Methods, F. J. Weinberg (Ed.), Academic Press, New York, p.113.

REFERENCES

1. Bidinger, D. F. and Sohrab S. H. (1986) Chemical kinetic mechanisms as amplifiers of diffusional-thermal instabilities, Central States Section Meeting, The Combustion Institute, May 5-6, Cleveland, Ohio.
2. Chen, Z. H., Liu, G. E. and Sohrab, S. H. (1987) Premixed flames in counterflow jets under rigid-body rotation, Combust. Sci. and Tech. 51, 39.
3. Chen, Z. H., Lin, T. H. and Sohrab, S. H. (1988) Combustion of liquid fuel sprays in stagnation-point flow, Combust. Sci. and Tech. 60, 63.
4. Faeth, G. M. (1983) Evaporation and combustion of sprays, Prog. Energy Combust. Sci. 9, 1.
5. Libby P. A. and Williams ,eds.(1980) Turbulent Reactive Flows, Springer Verlag, Berlin.
6. Lin, T. H. and Sohrab, S. H. (1987) Influence of vorticity on counterflow diffusion flames, Combust. Sci. and Tech. 52, 75.
7. Lin, T. H. and Sohrab, S. H. (1989a) Finite jets with/without rigid-body rotation, J. Fluid Mech., to appear.
8. Markstein, G. H. (1964) Nonsteady Flame Propagation, Pergamon Press.
9. Sheu, W. J. and Sohrab, S. H. (1989) On upstream interactions between flamelets in turbulent premixed flames, Combust. Sci. and Tech., to appear.
10. Sheu, W. J. , Sohrab, S. H. and Sivashinsky, G. I. (1989) Effects of rotation on Bunsen flame, Combust. Flame, to appear.
11. Sheu, W. J. and Sivashinsky, G. I.(1989) Nonplanar flame configurations in stagnation point flow, to appear.
12. Sivashinsky, G. I. (1976) On a distorted flame as a hydrodynamic discontinuity, Acta Astronautica 3, 889.
13. Sivashinsky, G. I. (1983) Instabilities, pattern formation, and turbulence in flames, Ann. Rev. Fluid Mech. 15, 79.
14. Sivashinsky, G. I. and Sohrab, S. H. (1987) The influence of rotation on premixed flames in stagnation-point flow. Combust. Sci. and Tech. 53, 67.
15. Sivashinsky, G. I., Rakib, Z., Matalan. M. and Sohrab, S. H. (1988) Flame propagation in a rotating gas, Combust. Sci. and Tech. 57, 37.
16. Sohrab, S. H. and Chao, B. H. (1984) Influence of upstream versus downstream heat loss/gain on stability of premixed flames, Combust. Sci. and Tech. 38, 245.

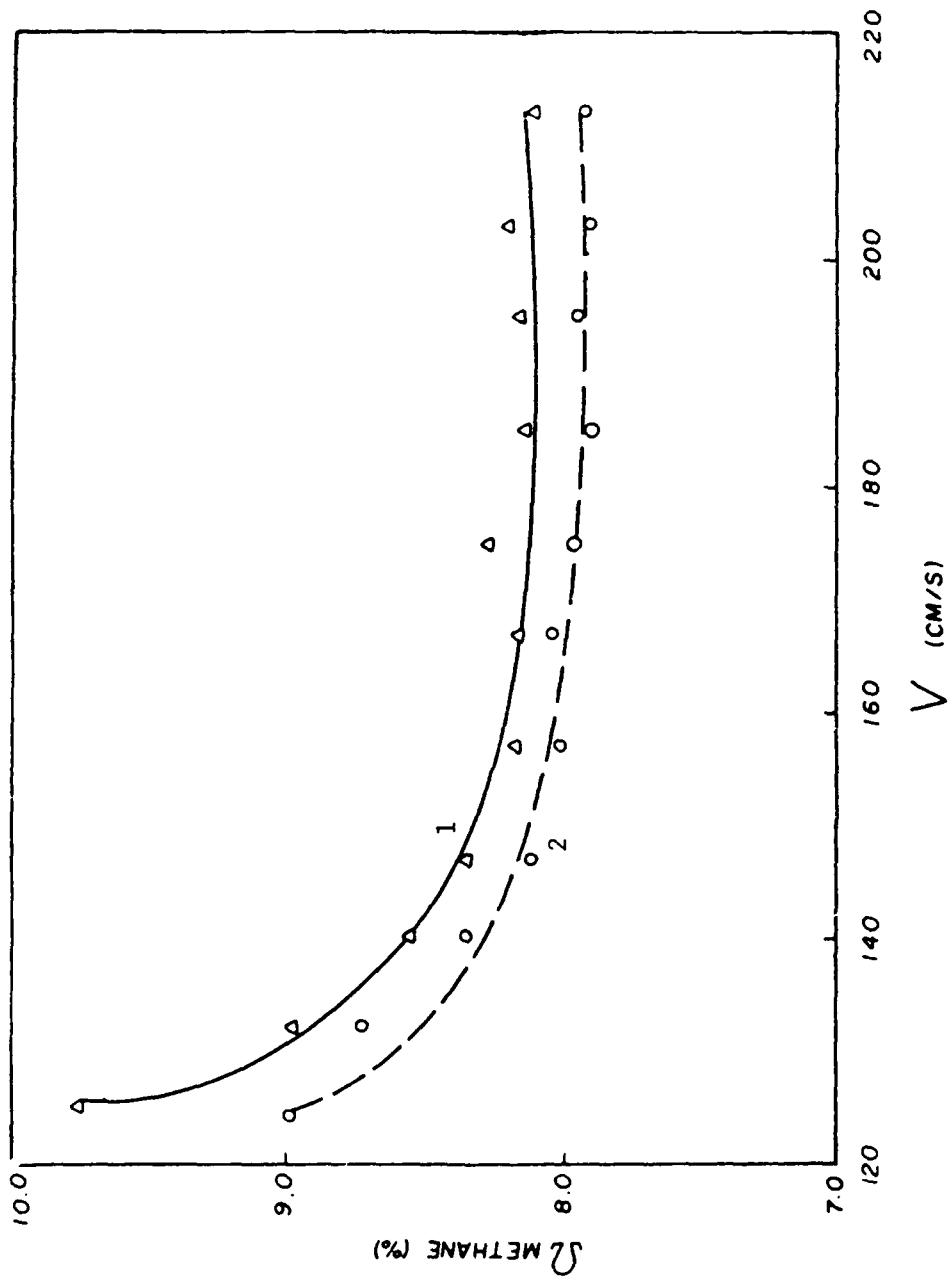


Figure 1 (1) Maximum methane concentration for onset of acoustic instability.
 (2) Minimum methane concentration for re-stabilization of acoustically unstable flame



Figure 2 Direct photograph of star shaped flame of rich butane-air mixture in stagnation - point flow Photographed from the top through quartz plate(see Appendix I. Fig 1)

APPENDIX I

Combustion of Liquid Fuel Sprays in Stagnation-Point Flow

Z. H. CHEN, T. H. LIN and S. H. SOHRAB *Department of Mechanical Engineering, Northwestern University, Evanston, Illinois 60208, U.S.A.*

(Received November 11, 1987; in final form March 3, 1988)

Abstract—The steady combustion of polydispersed sprays of ethanol and kerosene in the stagnation-point flow of lean methane-air mixtures is experimentally investigated. Using laser Doppler velocimetry, the axial and radial velocity profiles of the droplets are measured for water sprays in the presence or absence of lean methane-air flame. These results are then compared with the velocity profiles obtained for small MgO particles under identical flow conditions. The results show the effects of gas expansion on droplet deceleration (acceleration) in the pre-flame (post-flame) regions. Also, it is found that addition of water spray results in the formation of a distributed region of yellow-orange emission downstream of the lean methane flame. In combustion of ethanol spray, certain critical fuel-concentration-velocity limits are identified above which the flame becomes acoustically unstable. The implications of the study to the modeling of turbulent spray combustion are discussed.

INTRODUCTION

Studies on combustion of liquid fuel sprays help to improve the understanding of burning processes in gas-turbine, liquid-rocket and diesel engines, among many other important applications. The complications due to the simultaneous presence of two phases and uncertainties in droplet size and distribution are compounded by the presence of turbulence in most practical applications. Turbulent fluctuations modify the mixing, evaporation and combustion processes and lead to transient interactions between droplet flow/flame dynamics (Faeth, 1983). Because of the large number of parameters, analytical and experimental studies often aim at modeling the separate effects of individual parameters which are known to locally govern the reactive flow field. The results of such studies will help the future development of more comprehensive global models for turbulent spray combustion.

The evolution of theoretical models of spray combustion has been discussed by Williams (1985). Recent developments in the field, including the progress made in turbulent spray combustion, have been reviewed by Faeth (1983). Because of the complexity of the problem, besides the full-scale studies, two distinct and complementary classes of investigations have been found necessary. First are studies which aim at understanding of local phenomena, and consider combustion of single droplet or an array of droplets. Second, which includes the work reported herein, are studies concerned with the global effects and investigate combustion of mono- or poly-dispersed sprays in laboratory scale burners. For example, spherical propagation of flames in mono-dispersed sprays of ethanol and *n*-octane has been studied in Wilson-cloud-chamber type apparatus (Hayashi and Kumagai, 1974; Hayashi *et al.*, 1976). In another experimental model, combustion of poly-dispersed sprays in propane-kerosene drop-air (Mizutani and Nakajima, 1973) and kerosene-air (Polymeropoulos and Das, 1975) systems were studied in inverted-cone-flame-burner configuration. Also, the propagation of planar flames in poly-dispersed sprays in cylindrical vessel have been studied (Ballal and Lefebvre, 1981). In these studies, among other important findings, the propagation speed of the flames in sprays were determined.

In modeling of turbulent spray combustion, one of the major difficulties to be addressed is the way in which the multiple flame surfaces and the individual droplets

behave under the large velocity fluctuations (Faeth, 1983). Thus, the problem in part involves interaction of a burning droplet with severe velocity non-uniformities. It is expected that, similar to homogeneous turbulent combustion, the flame stretch-compression effects (Karlovitz *et al.*, 1953) will also play an important role in turbulent spray combustion. We note that in passing through the flame sheet, droplets experience a sudden velocity jump induced by the expansion of the gas. Also, besides the transient interactions between flamelets (Sohrab *et al.*, 1984; 1986), mixing non-homogeneities may lead to transitions between premixed and diffusion burning regimes (Lin and Sohrab, 1987).

The present experimental investigation is an extension of an earlier study (Sohrab, 1985) on combustion of hydrocarbon sprays in laminar stagnation-point flow. The study is motivated by the fact that in such flow configuration, not only the fluid mechanics of the gaseous flow is relatively well understood, but the effects of stretch rate on the flame can be systematically studied. Also, since steady combustion of planar flames can be achieved, the investigations of the droplet/flame interactions and flame diagnostics are facilitated. In the following, the stagnation flow spray-burner is described and the axial and radial velocity profiles of the gas as well as non-reactive droplets in (water spray-methane-air) systems are presented. Next, the results on combustion and acoustic flame instabilities observed in (ethanol spray-methane-air) and (kerosene spray-methane-air) systems are discussed. A summary of our principal findings is given in the concluding remarks.

SPRAY BURNER SYSTEM

The stagnation flow spray burner is composed of a quartz contoured nozzle with 32 mm exit diameter and 10 to 1 area contraction, a flat quartz plate and a liquid fuel atomizer. In Figure 1 the schematic of the spray burner is shown. Air and gaseous fuel are metered by conventional rotameters and premixed in the lower chamber of the burner as shown in Figure 1. The combustible mixture then enters the 102 mm diameter extension tube containing small glass beads thus producing a uniform velocity profile within the tube. A liquid fuel atomizer is situated at the center of the extension tube as shown in Figure 1.

Two types of atomizers with fundamentally different working mechanisms are considered for generation of polydispersed sprays. The first type of atomizer employs ultrasonic vibration of a specially designed nozzle using piezo-electric crystals for liquid atomization. The liquid fuel is fed into the atomizer by gravity from a specially designed supply system which maintains an optimum constant liquid level at all times. The atomizer produces 20–50 μm droplets in a narrow jet, about 40 degree cone angle, with negligible spillage and axial momentum. The second atomizer is a high-pressure atomizer that is used in conventional oil spray burners. The liquid is introduced to the atomizer from a 1 liter storage tank pressurized to 100 psig by nitrogen gas. The cone angle of the spray is about 80 degrees.

The droplets are convected by the coflowing methane-air mixture as shown in Figure 1. In passing through the contoured nozzle, a uniform-velocity polydispersed spray is formed at the exit plane of the nozzle. This flow subsequently impinges on a flat quartz plate located at a specified and fixed height, 14 mm, above the nozzle rim. As shown in Figure 1, a ring of cooling water with small water jets surrounds the nozzle for cooling the rim as well as the exhaust system. A fuel drain pipe is provided for droplets which may accumulate within the glass bead region. An exhaust system is surrounding the nozzle, Figure 1, to prevent the

COMBUSTION OF LIQUID FUEL SPRAYS

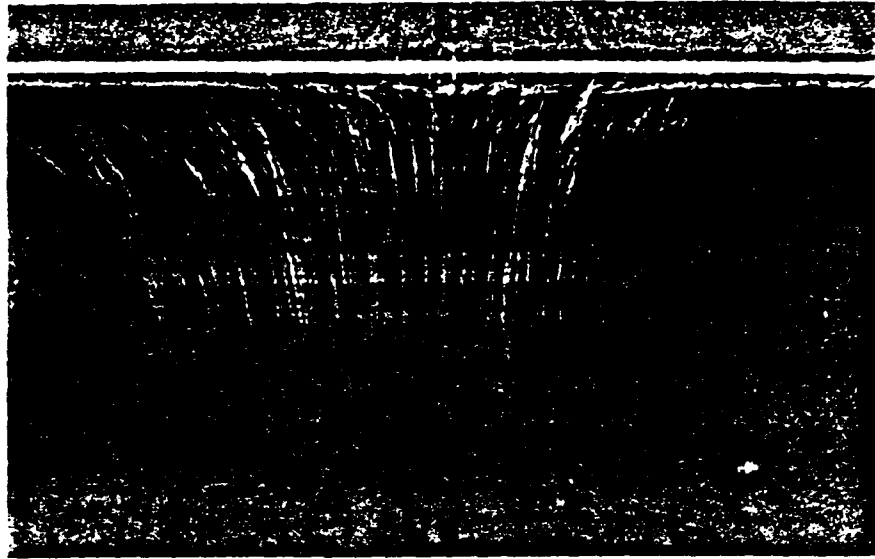


FIGURE 3 Direct photograph of streamlines in nonreactive spray of water in air. $U^* = 125 \text{ cm/s}$

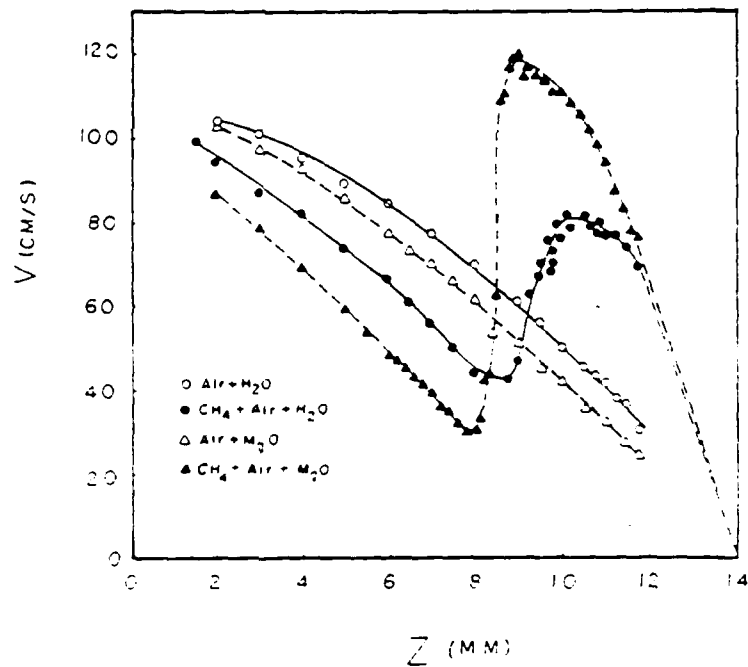


FIGURE 4 Axial velocity profiles of water droplets and MgO particles in reactive and non-reactive flows. $U^* = 125 \text{ cm/s}$, $H_2O = 0.019 \text{ cc/s}$, $\Omega = 7.7^\circ/\text{s}$, $r = 0 \text{ mm}$

compared to particles (Figure 4). On the other hand, the radial velocity of droplets is slightly smaller, $< 2 \text{ cm/s}$, than that of particles (Figure 5). Also, the small but finite value of the radial velocity about 15 cm/s , at $Z = 0$ shows that the flow at the nozzle rim is not purely axial. This early divergence is apparently caused by the overall pressure distribution in the flow field since it remains nearly constant even in the absence of the exhaust suction.

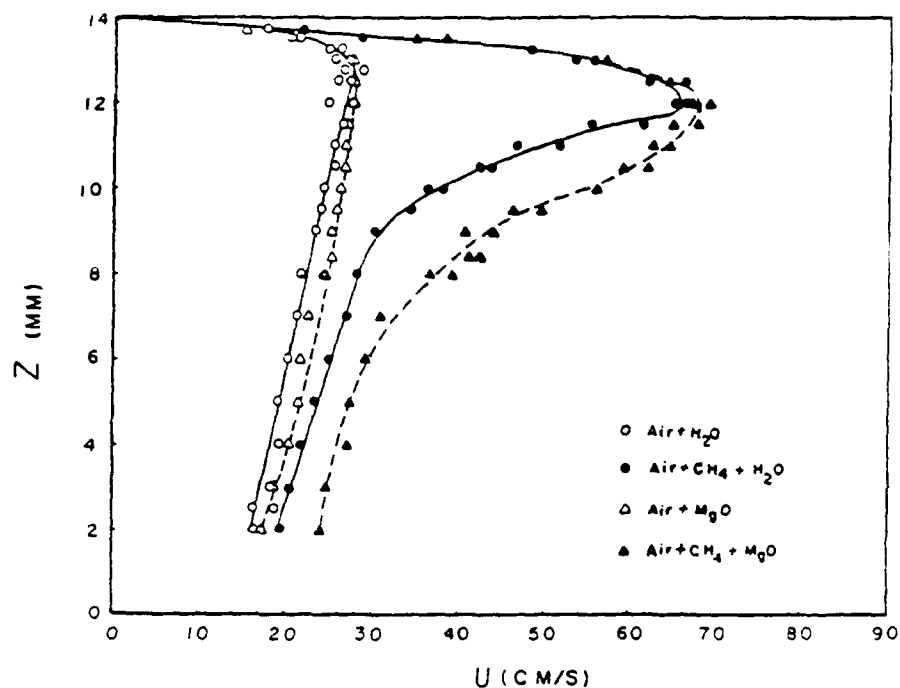


FIGURE 5 Radial velocity profiles of water droplets and MgO particles in reactive and non-reactive flows. $U'' = 125$ cm/s, $H_2O: 0.019$ cc/s, $\Omega_f = 7.7\%$, $r = 6$ mm.

The characteristics of water spray in the presence of lean methane-air flames are examined next. At nozzle velocity of $U'' = 124$ cm/s, a lean methane-air flame with volumetric fuel concentration $\Omega_f = 7.5\%$ is established first. Small quantity, 0.02 cc/s, of water spray is then introduced into the flow field. The direct photograph of the initial blue-violet lean methane flame is shown in Figure 6a. After introduction of water spray, a homogeneous region of yellow-orange radiation occurs downstream of the blue-violet flame as shown in Figures 6b-6d. This is quite interesting, since the lean methane flame is not easily susceptible to soot formation. This phenomenon is in part caused by the cooling effects of evaporating droplets in the hot post-flame regions. It is known that the slow combustion of carbon monoxide is not complete until about 2 mm downstream of the flame zone (Tsuji and Yamaoka, 1982). Hence, the cooling effects due to droplet evaporation may suppress CO combustion and lead to polymerization. Also, scavenging of radicals, such as OH, due to heterogeneous surface recombination may occur. Hydroxyl radical is known to be effective in combustion of soot precursors.

Similar phenomena were observed when distilled water was used instead of the tap water. Therefore, the yellow-orange radiation could not be associated with emission from possible sodium salt impurities in water. Small quantities of soot were found to deposit on thin metallic wires inserted in the yellow post-flame regions. The yellow-orange radiation zone ended abruptly about 2 mm from the quartz plate; a position corresponding to the edge of the boundary layer (Figure 7). Hence, no accumulation of soot particles on the hot quartz plate was observed. The exact nature of the yellow-orange radiation region and its possible relation to soot formation requires further future exploration. Figures 6c-6d are direct photographs of droplet streamlines that are illuminated by a narrow vertical laser sheet-light, respectively upstream and downstream of the flame zone. Comparisons of Figures 6a with 6b-d show that the flame thickness increases in the presence of water spray.

COMBUSTION OF LIQUID FUEL SPRAYS

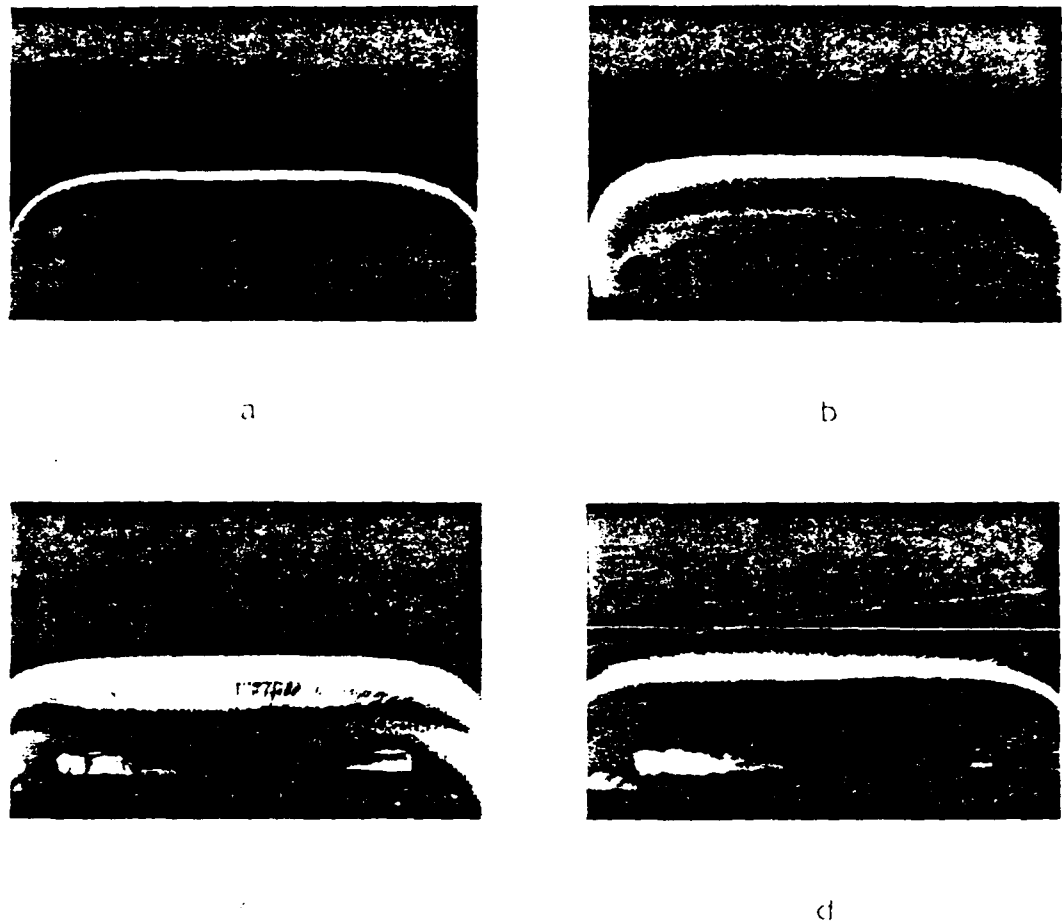


FIGURE 6 Direct photograph of CH_4 air flames in presence of water droplets (a) Pure CH_4 air flame (b) CH_4 air flame with water drops (c) CH_4 air flames with water drops under pre-flame illumination (d) CH_4 air flames with water drops and post-flame illumination. $U = 124 \text{ cm s}^{-1}$, $\Omega_f = 7.5\%$, H_2O 0.02 cc s $^{-1}$

The axial temperature profiles for the lean methane air flames, $\Omega_f = 7.7\%$ and $U = 125 \text{ cm s}^{-1}$, with and without water spray are shown in Figure 7. The data are obtained by axial traverse of a silica-coated Pt-Pt-13% Rh thermocouple with 0.1 mm wire diameter at a constant radial position $r = 6 \text{ mm}$. Clearly, the measured temperatures represent a mean value since droplet collisions with the thermocouple junction occur. The cooling effects of water spray reduce the flame propagation speed, which is manifested by the relocation of flame closer to the stagnation plane, $Z = 14 \text{ mm}$. The axial thickness of the orange-yellow layer is identified in Figure 7. The upper surface of the yellow emission layer abruptly ends at a finite distance from the hot quartz plate (Figure 6b), it is noted that relatively small changes of the mean temperatures, $< 75^\circ\text{C}$, have resulted in substantial change in radiation characteristics in post-flame regions. Of course, because of the vaporizing droplets, the local temperature fluctuations are much larger than 75°C .

The variations of the axial and radial velocity as functions of Z for droplets and MgO particles in the presence of lean methane air flame are also shown in Figures 4 and 5. As seen in Figure 4, the differences between axial velocity of particles and droplets are quite substantial. The data show that droplet deceleration (acceleration) induced by the gas expansion in the pre (post) flame zones is smaller than that

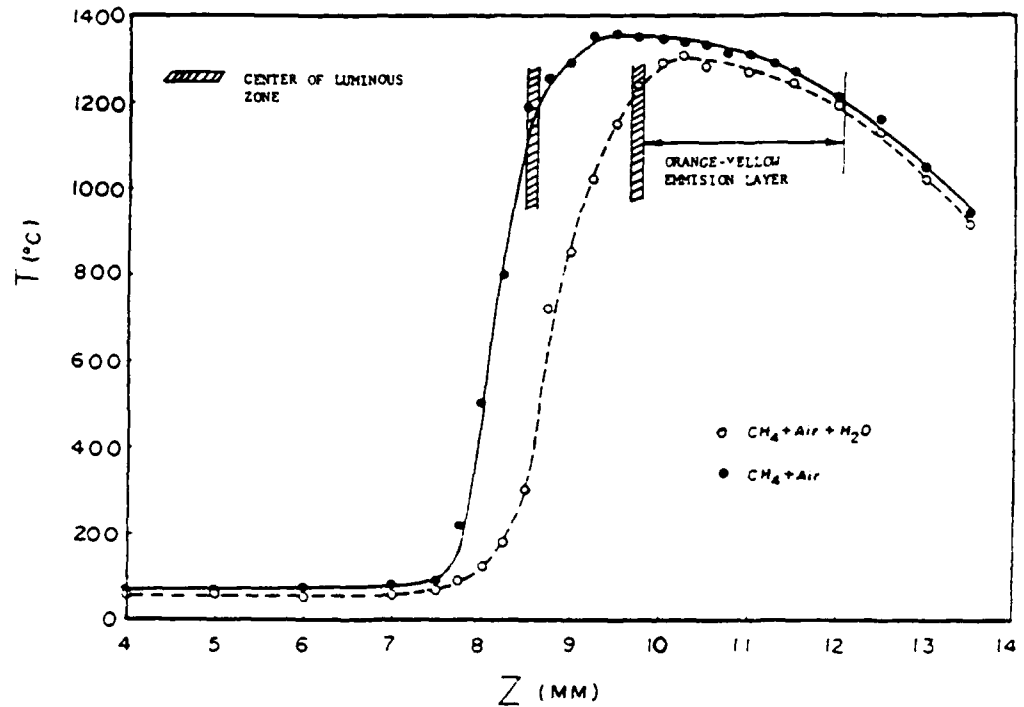


FIGURE 7 Axial temperature profiles in lean methane-air flames (a) without, (b) with water spray. $\Omega_f = 7.7\%$, $U^0 = 125 \text{ cm/s}$, $\text{H}_2\text{O} = 0.019 \text{ cc.s}$, $r = 6 \text{ mm}$.

corresponding to particles. While the particle velocity V jumps from 30 to 120 cm/s across the flame front, that of droplets is from 40 to 80 cm/s. This is to be expected in view of the larger inertia of the droplets and their higher resistance to velocity changes as compared to the particles. That is, since the droplets are heavier than the MgO particles, their acceleration by the expanding gas will be more difficult. Obviously, such velocity jumps result in enhanced droplet slip velocity which will substantially alter droplet evaporation/combustion in chemically reactive sprays.

In the stagnation-point flow configuration, the axial velocity at the upstream edge of the preheat zone may be defined as the laminar propagation speed of the stretched flame which differs from the propagation speed in the absence of stretching. According to Figure 4, this axial velocity is about 30 cm/s at the position $Z \approx 8 \text{ mm}$, based on the MgO velocity profile, in agreement with prior observations for lean methane flames (Yamaoka and Tsuji, 1984; Wu and Law, 1984) under similar stretch and concentration conditions. Because of the inertial effects, the velocity profile based on droplet motion differs from that of the gas and cannot be used to deduce the flame speeds in the presence of water spray. However, for the flame cooled by water spray, an approximate and lower propagation speed, about 20 cm/s, is estimated when the velocity profile based on MgO particles is linearly extrapolated to the corresponding flame position (Figure 4).

The differences between axial distribution of radial velocity for particles versus droplets, shown in Figure 5, also reflect the effects of higher droplet inertia. It is noted that the boundary layer thickness δ for reactive flow is about twice, $\delta = 2 \text{ mm}$, that of the cold flow (Figure 5). This tendency is anticipated since for the present flow field δ is proportional to $\sqrt{\bar{v}}$ (Batchelor, 1970) and the kinematic viscosity ν is an almost linearly increasing function of temperature. In addition, because of the composition

differences, the value of v is different for the reactive and non-reactive flows. The data in Figure 5 also show that the measured maximum radial velocities of droplets and particles are nearly the same, 66 and 68 cm/s, while those within the boundary layer are identical.

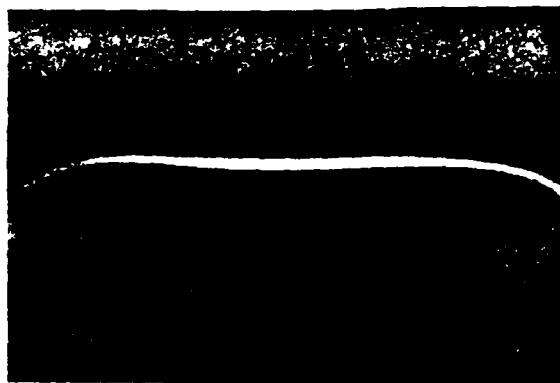
REACTIVE SPRAY IN REACTIVE FLOW

In this section, the combustion of fuel sprays in lean methane-air mixtures are discussed. Basically, two distinguishable burning modes may be identified depending on the volatility of the liquid fuels. For less volatile fuels, such as kerosene, droplets remain intact until they closely approach the methane flame. Hence, evaporation occurs primarily in the preheat zone and downstream of the reaction zone. For more volatile fuels, such as heptane and ethanol, on the other hand, droplet evaporation begins immediately after atomization. Hence, in this case smaller droplets burn in the gaseous mixture of their own vapor and methane-air. For heptane sprays, the concentration of methane in air could be reduced to zero while maintaining steady combustion of the spray.

Direct photographs of flames in sprays of ethanol and kerosene have been obtained and typical samples are shown in Figures 8 and 9, respectively. In Figure 8, the side view as well as the top view, through the quartz plate, are shown. A horizontal sheet of laser light was axially positioned 5 mm upstream of the flame surface in Figure 8b to illuminate the droplets. It is evident that with higher intensity and narrower thickness of the laser sheet-light, such photographs will allow for approximate evaluation of droplet size and distribution in the pre-post-flame regions. Preliminary observations of magnified photographs, such as Figure 8b, showed that most of the droplets are not spherical in shape. For kerosene sprays, Figure 9, envelope flames are observed to surround the individual droplets downstream of the flame front. Also, severe sooting and eventual accumulation of soot on the quartz plate occurs as the kerosene flow rate is increased. The photographs for kerosene sprays were taken when the high-pressure atomizer was being used (Sohrab, 1985). It was found that with dense sprays, kerosene drops actually impinge on the hot plate and support a partially premixed flame (Sohrab *et al.*, 1984) adjacent to the hot plate. In this burning regime, a thick layer of soot develops on the quartz plate which is difficult to remove.

The variation of axial flame position Z , and the mean flame temperature T , with methane concentration in air Ω_1 for ethanol and kerosene sprays are shown in Figures 10 and 11. In these tests, the total liquid flow rate into the burner is held fixed by maintaining a constant atomizer frequency and liquid level in the supply tank. However, the quantities of liquid fuels which actually reach the flames will depend on the gas velocity U'' . The effective values of liquid flow rates given in Figures 10 and 11, are obtained by subtraction of the measured rates of liquid drainage from the burner from those introduced into the atomizer. Such experiments are difficult since the system must reach a steady state operation before the measurements are made. Moreover, with the ultra-sonic atomizer, our ability to prescribe a certain desired rate of liquid flow is limited. Such limitations could be overcome by the use of more advanced aerosol generators.

For both ethanol and kerosene sprays, the flames extinguished below a minimum methane concentration $\Omega_1 < 2\%$. Hence, under the present rate of stretch and droplet size, 20–50 μm , steady flame propagation in such sprays is not possible. The luminous flame zone in the presence of sprays appeared thicker than that of homogeneous lean methane/air flame, about 1 mm. The variation of Z , with Ω_1 , Figures 10 and 11, is in



a



b

FIGURE 8. Direct photographs of lean CH_4 air flames with ethanol spray (a) side view (b) top view with laser sheet lighting.

accordance with the known dependence of flame propagation speed on the mixture stoichiometry. For ethanol spray, Figure 10, at $\Omega_f \approx 3.77$ the flame flashes back into the nozzle. We note, however, that at $U'' = 121 \text{ cm/s}$, flame flash-back does not occur for methane-air flames even under stoichiometric, $\Omega_f = 9.5$, conditions. Moreover, the flame propagation speeds in the range 45–25 cm/s have been reported for pure ethanol sprays (Hayashi and Kumagai, 1974; Hayashi *et al.*, 1976). Therefore, the observed phenomenon shows that higher laminar flame propagation speed has occurred in the heterogeneous system as compared to those achievable in homogeneous mixture of either fuel. Such tendencies have been observed earlier (Mizutani and Nakajima, 1973a; Polymeropoulos and Das, 1975) when, under fixed overall stoichiometry, the flame propagation speed was found to first increase and then decrease with droplet diameter. This tendency is in agreement with the early predictions by Williams (1960).

Unfortunately, the variation of flame propagation speed with Ω_f in sprays could not be measured because of the difficulty in obtaining the axial velocity of the gas in

COMBUSTION OF LIQUID FUEL SPRAYS



a



b



c



d



e

FIGURE 9 Direct photograph of lean CH_4 air flame with kerosene spray.

reactive sprays. Here, the laser velocimetry based on droplet motion cannot be used since droplets do not follow the gas (Figure 4). On the other hand, addition of MgO particles to the sprays is not feasible, since particles tend to agglomerate within the liquid fuel. When values of Z , in Figures 10 and 11 are linearly extrapolated to $\Omega_r \rightarrow 0$ limit, it is found that Z is about 14 mm, i.e. position of the stagnation plane. This

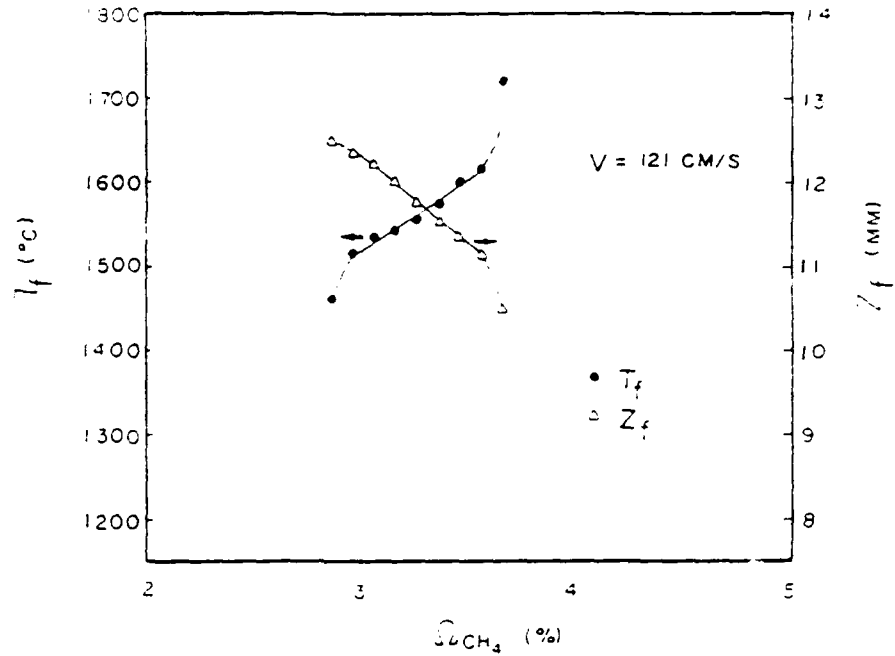


FIGURE 10 Flame temperature and position as a function of Ω_f for ethanol spray in lean methane air mixtures. Ethanol flow rate = 0.062 cc s.

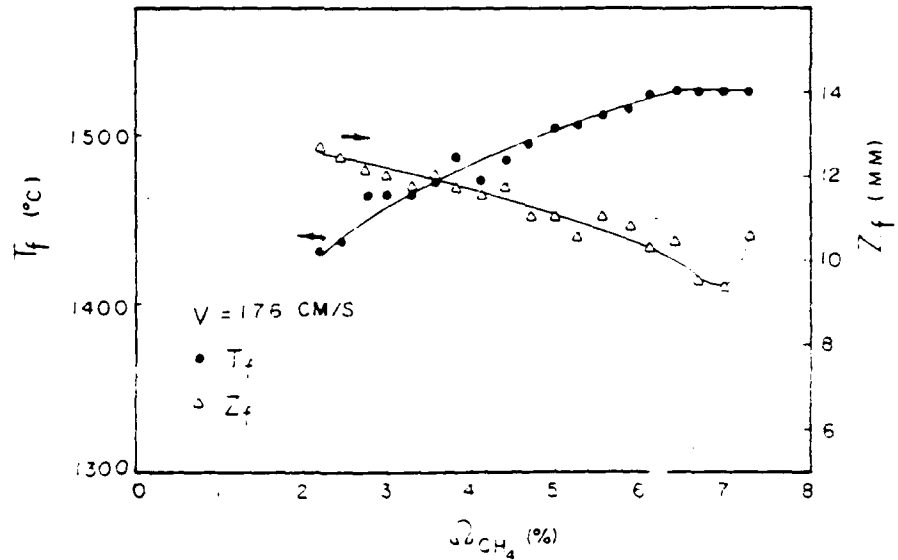


FIGURE 11 Flame temperature and position as function of Ω_f for kerosene spray in lean methane air mixtures. Kerosene flow rate = 0.0135 cc s.

tendency suggests that the flame propagation speed in pure sprays, in absence of methane, is zero which corresponds to extinction condition. hence, in absence of sufficient gas-phase fuel, the gasification rate in spray is unable to support self-sustaining flames in ethanol and kerosene sprays considered herein.

COMBUSTION OF LIQUID FUEL SPRAYS

An interesting observation made in connection with the tests on reactive sprays was the occurrence of acoustically unstable flames in certain range of nozzle velocity and fuel concentration. For example with $U^* = 174 \text{ cm/s}$ and ethanol flow rate of 0.085 cc/s , it was found that near $\Omega_F \approx 4\%$, the flame started to vibrate and emit audible acoustic sound. Such acoustically unstable flames persisted beyond $\Omega_F \sim 4\%$ until the eventual extinction of flame at the rich flammability limit. The acoustic flames showed small, $< 2 \text{ mm}$, axial oscillations at high frequency, about 120 Hz , measured from amplified microphone signal. The extent to which hydrodynamic, thermo-diffusive and chemical flame instability mechanisms are effective in promotion and sustenance of such acoustic flames are as yet not understood. The hydrodynamic and thermo-diffusive aspects of premixed flame instabilities have been discussed by Sivashinsky (1976). It appears that resonance effects with the acoustic waves within the burner cavity play a dominant role in the present situation (Zinn, 1986). Similar acoustically unstable flames were also observed earlier in kerosene, heptane, octane and methanol sprays (Sohrab, 1985). Since the onset of acoustic instability was found to be repeatable, the present experimental model may be used for systematic study of this interesting phenomenon.

DISCUSSIONS

In the sequel, the relevance of some of the results obtained for non-reactive and reactive sprays to the global aspects of turbulent spray combustion will be described. As in many applications, the spray is assumed to be injected into a hot and turbulent oxidizing atmosphere. Thus, from the central core of the spray to the far field regions of the atmosphere, an entire spectrum of compositions, from pure fuel to pure oxidizer are expected to occur. Since chemical reactions are considered to occur only in the gas phase, in the following discussions the concentrations refer to those in the gaseous phase. We may then expect that in addition to regions of pure fuel (F) and oxidizer (O), other intermediate premixed regions composed primarily of fuel ($F + \alpha O$) or oxidizer ($O + \alpha F$) will also occur. Finally, there will be regions where near stoichiometric mixtures ($F + O$) are encountered. Such regions may contain fuel droplets and will be under constant random motion due to turbulent fluctuations. Hence, the composition of various regions may change due to droplet evaporation and by fast turbulent mixing or the relatively slow molecular diffusion. However, under strictly homogeneous turbulent situations, the stochastic averages in the multi-phase field may remain invariant in time.

In the presence of chemical reactions, some of the interfaces between the regions identified above may support diffusion flames (DF) or partially premixed (PPF) flames (Sohrab *et al.*, 1984, 1986). Also, in the regions ($F + O$), premixed flames (PF) may occur which will be dynamic due to their propagation. The diffusion flames, which do not propagate, may be convected by the motion of burning droplets or by the bulk motion of the entire interface between (F) and (O) regions. The existence of these multiple flame surfaces is known to depend on both local fuel and oxidizer concentrations as well as the local rate of stretch. The critical limits of fuel and oxidizer concentration for flammability of (DF) and (PF) have been extensively studied. Moreover, the influence of the rate of stretch on the flame extinction has been discussed (Williams, 1985). Thus, the combustion field may be composed of many (PF), (DF) and (PPF) surfaces that are in random motion as droplets cross such flame surfaces. Clearly, to understand the complex dynamics of the flow flame droplet interactions, simple models of the local flow conditions should be studied first.

In view of the above considerations, it is evident that the study of spray combustion in stagnation flow will help to simulate the local flow conditions within the combustion field. For example, the problem of non-reactive spray discussed earlier is also relevant to situations where fuel droplets pass through rich premixed flame surfaces. Under such conditions, only droplet evaporation and the consequent cooling effects will occur, since downstream of the rich (PF) no more oxygen will be available for further combustion. We note however that the behaviour of fuel droplets after rich (PF) will be somewhat different than water droplets since the former may undergo pyrolysis. Nonetheless, similar to the observed effects of water sprays on lean methane-air flames, fuel sprays in fuel rich mixtures are also expected to influence the process of soot formation in the post flame regions.

The knowledge of velocity and trajectory of droplets as they approach and pass through flames is quite important for the understanding of turbulent spray combustion. For example, the observed enhancement of droplet slip velocities across flame fronts are expected to result in local strained, stagnation flow fields in the proximity of the individual droplets. Such local stretch rates will then alter the structure and extinction behavior of the diffusion flames (Williams, 1975) which may surround the droplets. Another important problem to be addressed is the evaluation of the critical minimum concentration of gaseous fuel which would insure steady combustion within the spray. For example, the combustion of (ethanol spray-methane-air) system discussed earlier was symbiotic in that individually, both (methane-air) and (ethanol-spray-air) mixtures were incapable of supporting self-sustained flames under the specified flow conditions. The relevance of studies on spray combustion in counterflows to turbulent spray combustion modeling were discussed in more detail elsewhere (Sohrab, 1985).

CONCLUDING REMARKS

In this study, the behavior of reactive and non-reactive sprays within methane air mixtures in the stagnation-point flow configuration were investigated. In particular, the motion of water sprays in lean methane air flame was studied. It was found that water spray resulted in the formation of a yellow-orange radiation layer downstream of the flame zone. The axial and radial velocity profiles of water droplet and small MgO particles were measured in both reactive and non-reactive flows. Thus, the effect of gas expansion on the droplet motion in the pre- and post-flame regions were determined and compared to those for MgO particles.

For combustion of ethanol and kerosene sprays in methane air mixtures, the variation of flame temperature and position with methane concentration was determined. It was found that below a minimum methane concentration, steady flame propagation in the sprays was not possible. Also, above certain critical methane concentrations, the flames became acoustically unstable. This interesting and complex phenomena relates to acoustic-chemically coupled flame instabilities and requires further systematic investigation. Since steady and stationary flames were achieved, the present experimental model provides a good vehicle for future investigations of spray combustion.

ACKNOWLEDGEMENTS

This research has been supported by Air Force Astronautics Laboratory under Contract No F04611-87-0067, and in part by AFOSR Contract No. F49620-85-C-0013.

COMBUSTION OF LIQUID FUEL SPRAYS

REFERENCES

- Ballal, D. R., and Lefebvre, A. H. (1981). Flame propagation in heterogeneous mixtures of fuel droplets, fuel vapor and air. *18th Symposium (International) on Combustion*. The Combustion Institute, p. 321.
- Batchelor, G. K. (1970). *An Introduction to Fluid Dynamics*. Cambridge University Press, p. 288.
- Faeth, G. M. (1983). Evaporation and combustion of sprays. *Prog. Energy Combust. Sci.* **9**, 1.
- Hayashi, S., and Kumagai, S. (1974). Flame propagation in fuel droplet-vapour-air mixtures. *15th Symposium (International) on Combustion*. The Combustion Institute, p. 445.
- Hayashi, S., Kumagai, S., and Sakai, T. (1976). Propagation velocity and structure of flames in droplet-vapor-air mixtures. *Combust. Sci. and Tech.* **15**, 169.
- Karlovitz, B., Denniston, D. W., Knapschaefer, D. H., and Wells, F. E. (1953). *Studies in turbulent flames. 4th Symposium (International) on Combustion*. Williams and Wilkins, Baltimore, MD, p. 613.
- Lin, T. H., and Sohrab, S. H. (1987). On the transition of diffusion to premixed flames in conserved systems. *Combust. Flame* **68**, 73.
- Mizutani, Y., and Nakajima, A. (1973a). Combustion of fuel vapor-drop-air systems: Part I—Open burner flames. *Combust. Flame* **21**, 343.
- Mizutani, Y., and Nakajima, A. (1973). Combustion of fuel vapor-drop-air systems: Part II—Spherical flames in a vessel. *Combust. Flame* **20**, 351.
- Polymeropoulos, C. E., and Das, S. (1975). The effect of droplet size on the burning velocity of kerosene-air sprays. *Combust. Flame* **25**, 247.
- Sivashinsky, G. I. (1976). On a distorted flame as a hydrodynamic discontinuity. *Acta Astronautica* **3**, 589.
- Sohrab, S. H. (1985). *Studies on Combustion of Liquid Fuel Sprays in Stagnation Flows*. AFOSR UES Final Report, AFRPL.
- Sohrab, S. H., Ye, Z. Y., and Law, C. K. (1984). An experimental investigation on flame interaction and the existence of negative flame speeds. *20th Symposium (International) on Combustion*. The Combustion Institute, p. 1957.
- Sohrab, S. H., Ye, Z. Y., and Law, C. K. (1986). Theory of interactive combustion of counterflow premixed flames. *Combust. Sci. Tech.* **45**, 27.
- Tsuji, H., and Yamaoka, I. (1982). Structure and extinction of near limit flames in a stagnation flow. *19th Symposium (International) on Combustion*. The Combustion Institute, Pittsburgh, Pennsylvania, p. 1533.
- Williams, F. A. (1985). *Combustion Theory*, 2nd Edition. Benjamin Cummings, Menlo Park, CA.
- Williams, F. A. (1960). Monodisperse spray deflagration. *Prog. Astronautics and Rocketry* **2**, 223.
- Williams, F. A. (1975). A review of some theoretical considerations of turbulent flame structures. *AGARD Conference Proceedings, No. 164*, M. Barrere (Ed.), III, 1.
- Wu, C. K., and Law, C. K. (1984). On the determination of laminar flame speeds from stretched flames. *20th Symposium (International) on Combustion*. The Combustion Institute, Pittsburgh, Pennsylvania, p. 1941.
- Yamaoka, I., and Tsui, H. (1984). Determination of burning velocity using counterflow flames. *20th Symposium (International) on Combustion*. The Combustion Institute, Pittsburgh, Pennsylvania, p. 1883.
- Zinn, T. B. (1986). Pulsating combustion, in *Advanced Combustion Methods*, F. J. Weinberg (Ed.). Academic Press, New York, p. 113.

APPENDIX II

THE COMBUSTION AND ACOUSTIC INSTABILITY OF ETHYL-ALCOHOL SPRAY IN STAGNATION-POINT FLOW

J. H. TIEN and S. H. SOHRAB
Department of Mechanical Engineering
Northwestern University
Evanston, Illinois 60208

INTRODUCTION

In almost all practical applications, such as liquid rocket motors, diesel engines and gas-turbines, spray combustion occurs in turbulent flows. Because of the large number of parameters, and interactions between flow/flame/droplet, the description of the combustion field is exceedingly complex [1,2]. Therefore, most modelling techniques first attempt to identify the role of the individual parameters which influence the combustion field and investigate their separate effects in simple analytical models or controlled laboratory experiments. Such information may then be collectively applied to the development of comprehensive models with proper measures taken to include the interactions between the individual processes.

Two important hydrodynamic parameters, among others, which are known to influence the turbulent combustion are the rate of stretch and vorticity. The importance of flame stretch in turbulent combustion within homogeneous gaseous flows is well established [2]. Relatively less is known about the role of vorticity in flame-front dynamics [3-5]. In turbulent sprays, on the other hand, the importance of the interaction between droplets and turbulent eddies has been recognized [1]. In general, turbulent fluctuations will induce flame stretching and effect the motion of droplets. For example, the nature of droplet evaporation and drag force on droplets are known to depend on relative speed between the droplet and gas [1]. Hence, studies on the effects of stretch on spray combustion in laminar flows may help the understanding of the mechanisms through which both the flame and droplets improve for large velocity gradients which predominate the turbulent sprays.

In recent experimental investigations [6,7], the combustion of hydrocarbon sprays in stagnation-point flow was studied. Such flow configuration is best suited for systematic study of the effects of controlled velocity nonuniformity on flames [2]. In application to spray combustion, since steady and planar flames can be stabilized within the flow, the flame diagnostics and evaluation of droplet trajectory through the flame are facilitated. In the present experimental study, certain combustion characteristics of ethyl-alcohol sprays in lean methane/air mixtures are investigated.

EXPERIMENTS AND DISCUSSIONS

The spray combustion is studied in a burner which is schematically shown in Fig. 1 and was described previously [6,7]. The polydispersed spray of ethyl-alcohol, 20-50 μ droplets, is generated by an ultra-sonic atomizer which is surrounded by uniform-velocity flow of lean methane-air mixture. After passage through a contoured nozzle, the spray impinges on a planar quartz plate. The trajectories, flow streamlines, of the droplets are schematically illustrated in Fig. 2. Also, direct photograph of the streamlines have been

made using laser sheet-lighting for illumination. Planar flames can be obtained in the ethyl-alcohol spray with small volumetric concentration Ω of methane in air, $\Omega = 2$.

A constant total flow rate of atomized liquid, $\dot{Q} = 0.0833 \text{ cm}^3/\text{sec.}$, is maintained by controlling the level of fuel-supply and the ultra-sonic frequency of the atomizer. Air and methane flow rates are controlled by conventional rotameters. Using a pt-pt-10% Rh thermocouple, .10 mm wire, the temperature T_c and position Z_c , measured from nozzle exit plane, of the planar flame are then measured as Ω is increased at fixed air flow rate. Hence, the mean gas velocity at the exit plane of the nozzle V is nearly constant at 157 cm/s. In this flow configuration, the flame position can be related to the laminar flame propagation velocity S_L for stretched flames [7]. The results of such measurements for pure methane/air flames and those in presence of ethyl-alcohol spray are shown in Figs. 3 and 4. As is to be expected, Z_c decreases (S_L increases) with Ω until the mixture has reached an effective stoichiometric composition, $\Omega = 9.5$ and 5.4 in Figs. 3 and 4, and thereafter increases (decreases) for fuel-rich mixtures.

An interesting observation made in the test was concerning the occurrence of certain acoustic instabilities in both pure lean methane/air flames and those with spray of ethyl-alcohol. It is found that the planar flames start vibrating, emitting sound waves, over certain composition range, $\Omega_L < \Omega < \Omega_U$, identified in Figs. 3 and 4. Some of the acoustic frequencies as well as the vibration frequencies of the flames have been measured. More detailed study of the complex coupling between the hydrodynamic flow instabilities and the intrinsic flame instabilities [9] are presently being further investigated.

ACKNOWLEDGMENTS

This research is supported by the Air Force Astronautics Laboratory, under the contract No. F04611-87-0067.

REFERENCES

1. Faeth, G. M., "Evaporation and Combustion of Sprays", Prog. Energy Combust. Sci. 9, (1983).
2. Williams, F. A., Combustion Theory, 2nd Edition, The Benjamin/Cummings, Menlo Park, CA, 1985.
3. Chen, Z. H., Liu, G. E., and Sohrab, S. H., "Premixed Flames in Counterflow Jets Under Rigid-Body Rotation", Combust. Sci. Tech. 51, 39 (1987).
4. Lin, T. H., and Sohrab, S. H., "Influence of Vorticity on Counterflow Diffusion Flames", Combust. Sci. Tech. 52, 75 (1987).
5. Sivashinsky, G. I., and Sohrab, S. H., "The Influence of Rotation on Premixed Flames in Stagnation-Point Flow", Combust. Sci. Tech. 53, (1987).
6. Sohrab, S. H., Studies on Combustion of Liquid Fuel Sprays in Stagnation Flows, AFORS Final Report (1985).

7. Chen, Z. H., Lin, T. H., and Sohrab, S. H., "Combustion of Liquid Fuel Sprays in Stagnation Flows", Eastern States Section Meeting, The Combustion Institute, Dec. 21-24, Puerto Rico (1986).
8. Daneshyar, H., Mendes-Lopes, J. M. C., and Ludford, G. S. S., "Effect of Strain Fields on Burning Rate", 19th Symposium (International) on Combustion, The Combustion Institute, p. 413 (1982).
9. Sivashinsky, G. I., "On a Distorted Flame as a Hydrodynamic Discontinuity", Acta Astronautica 3, 889 (1976).

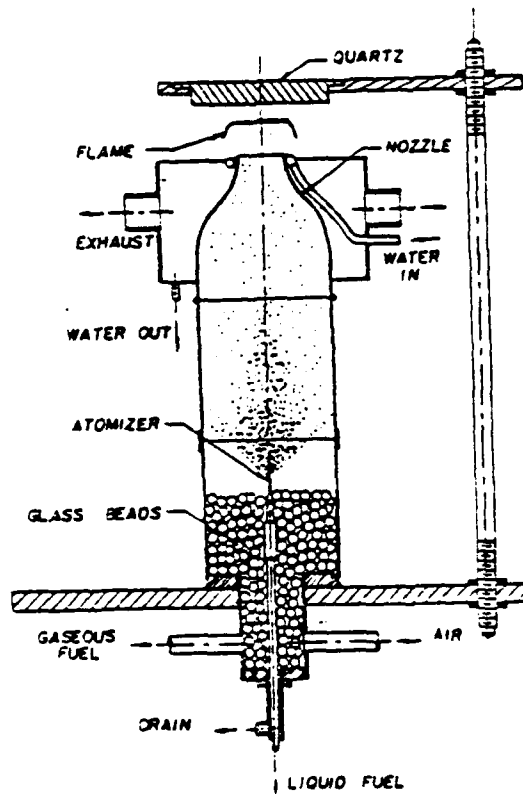


Fig. 1 Spray Burner

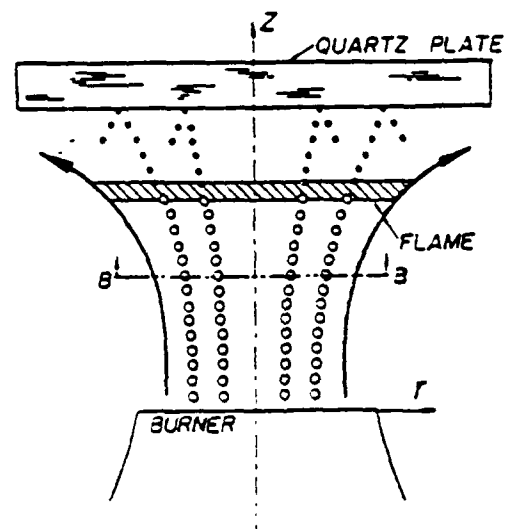
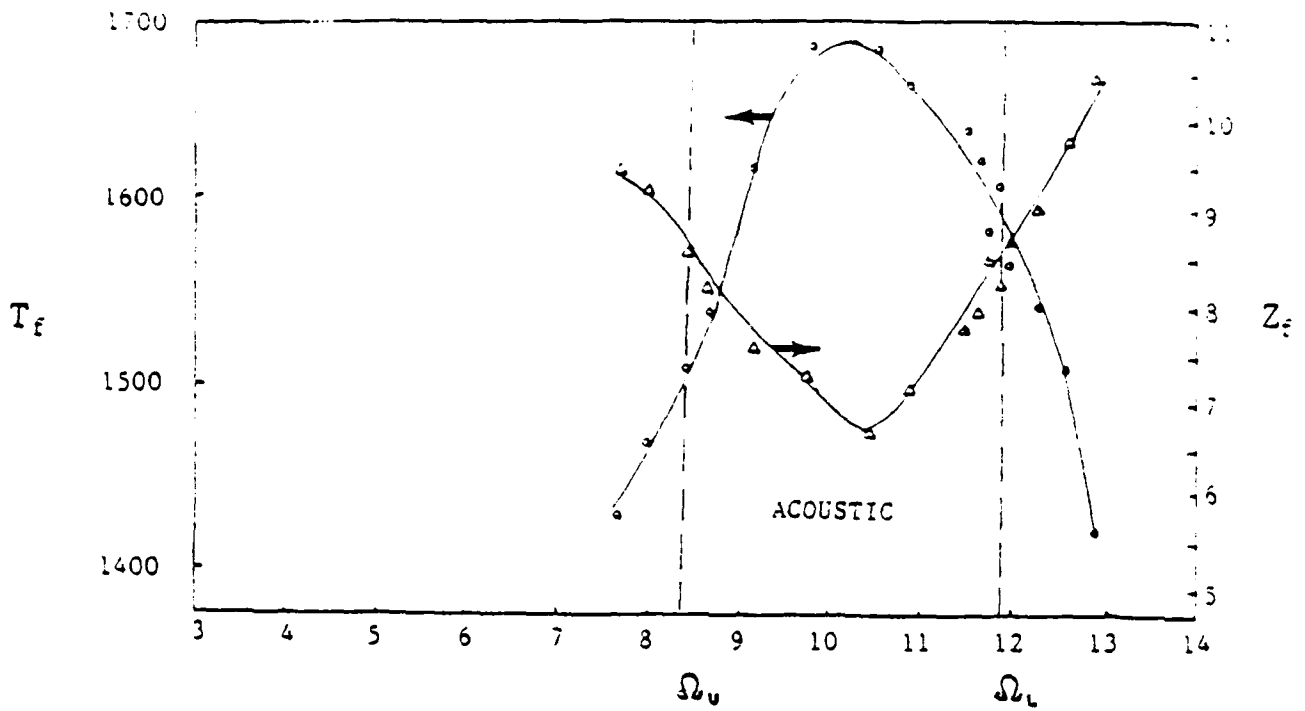
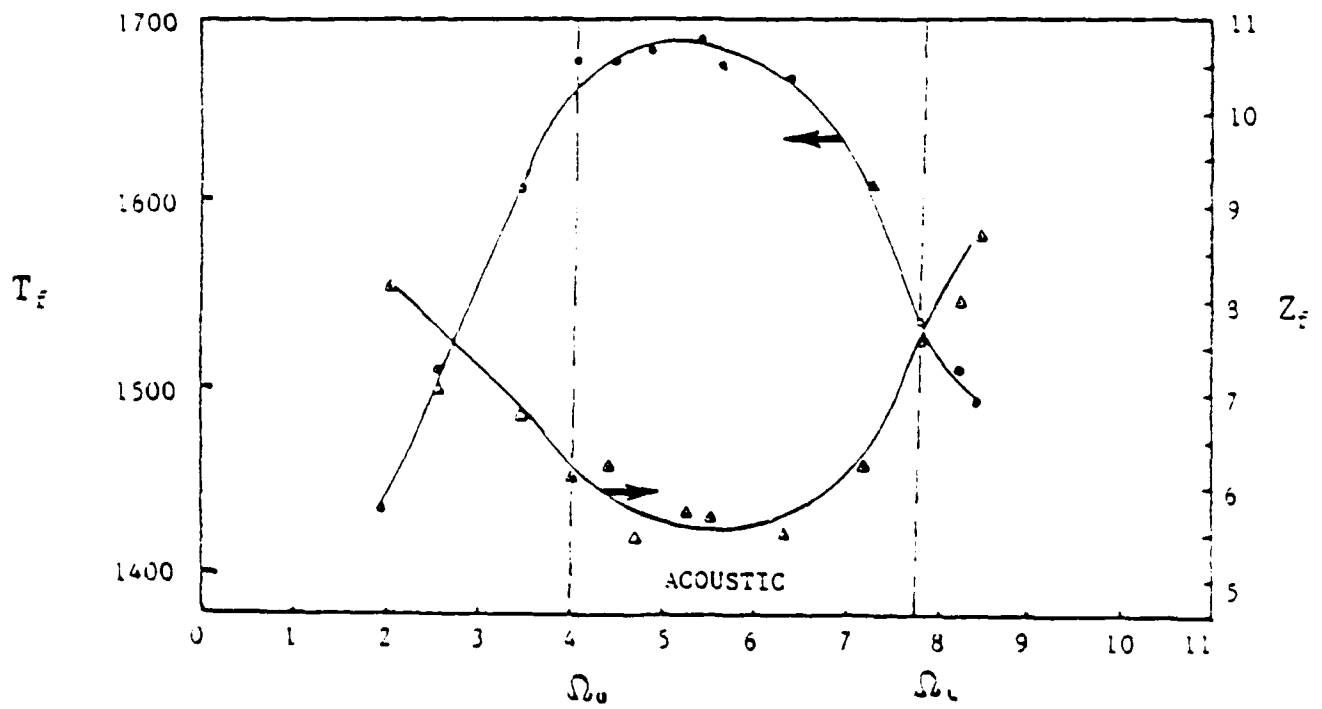


Fig. 2 Spray Flow Field



Ω CH₂

FIG 3



Ω CH₂

FIG 4

APPENDIX III

CHEMICAL KINETIC AND THERMAL ASPECTS

OF CELLULAR PREMIXED FLAMES

A. N. Jacobi and S. H. Sohrab
Department of Mechanical and Nuclear Engineering
Northwestern University, Evanston, Illinois 60201

ABSTRACT

The temperature fields of stationary and rotating polyhedral Bunsen flames of butane-air are experimentally investigated. As the additives CF_3Br and N_2 are gradually introduced into the combustible mixture, the variation of the temperature in the trough and crest regions of the polyhedral flames are examined. It is found that addition of 0.36 (5.0) molar percentage of CF_3Br (N_2) completely removes the cellular structure of the polyhedral flame. The results suggest that in conjunction with the preferential-diffusion mechanism, chemical-kinetic effects also play some role in the formation, amplification or sustenance of cellular flame structures. Some phenomenological arguments which are based on kinetics of branched-chain reactions are presented in support of the empirical observations. Also, in butane/air mixtures of different velocity, the critical flame temperatures corresponding to the onset of cell formation are found to be nearly identical. The periodic circumferential-fluctuations of the temperature at different radial positions within rotating polyhedral flame of butane are measured and the angular speed of rotation is determined.

INTRODUCTION

Investigation of flame-front instabilities has been recognized as a significant branch of the combustion science (Williams, 1985). In the purely fluid mechanical systems, the flow stability is related to the Reynolds number which describes the eventual onset of turbulence. If, in addition to the velocity gradients, both temperature and concentration gradients are also present, the flow stability is further complicated due to the simultaneous transport of momentum, heat and mass. Thus, inclusion of two additional parameters, namely Prandtl, Pr (ratio of momentum to heat diffusivity) and Lewis, Le (ratio of heat to mass diffusivity) numbers will be needed. Finally, if the non-homogeneous flow field is also chemically-reactive, the chemical-kinetic effects also induce their direct or indirect influences on the flow/flame stability. Thus, in general the stability of flames may be said to be governed by hydrodynamic, thermal, diffusional as well as chemical effects. One of the objectives of the present investigation is to ascertain the extent to which the last category, namely chemical-kinetic effects, influences the stability of premixed Bunsen flames, such as polyhedral flames.

The first report about polyhedral flames (PHF) was given by Smithells and Ingle (1892). They reported the existence of stationary or rotating polyhedral flames in fuel-rich mixtures of higher hydrocarbons such as benzene, pentane and heptane burning in air. Later, Smith and Pickering (1929) conducted systematic experiments on PHF in rich propane/air and observed 3 to 7-sided polyhedrals and determined the characteristic cell size of the flames. Subsequently, Markstein (1964) performed comprehensive studies on the stability and structure of cellular and polyhedral flames. Also, the concentrations of some of the stable species in the trough and crest zones of

PHF have been measured (Jost, et al., 1958; Markstein, 1958). More recently, the influence of the burner-rim aerodynamics on PHF of butane/air on Bunsen burner was studied (Sohrab and Law, 1985) where some preliminary data on the angular velocity of rotating PHF was also presented.

Manton, et al. (1952) attributed the occurrence of cellular structures to the preferential diffusion of heat versus the deficient reactant. Thus, for Le (based on the diffusion coefficient of the deficient component) less than unity, the flame-front corrugations would grow because of the favorable stratification of the combustible mixture (Lewis and von Elbe, 1967).

The theoretical investigations of cellular flames were initiated by the introduction of the diffusional-thermal stability model (Barenblatt, et al., 1963; Sivashinsky, 1976) and have shown general qualitative agreement with the experimental observations (Markstein, 1964). Recently, more comprehensive models which include the influences of both hydrodynamic as well as thermo-diffusive effects have been reported (Clavin and Williams, 1982; Matalon and Matkowsky, 1982). The linear stability of non-adiabatic flames (Joulin and Clavin, 1979; Sohrab and Chao, 1984) and flames with two-reactant chemistry model (Joulin and Mitani, 1982) have also been analyzed.

Although most of the observations of cellular flames thus far do agree with the general hypothesis of the preferential-diffusion mechanism, there remain a few discrepancies which warrant further considerations. First, cellular structures were observed in rich methane/air flames (Botha and Spalding, 1959) which is not in accordance with the preferential-diffusion axioms. On the other hand, it was reported elsewhere (Behrens, 1953) that no polyhedral flames could be obtained in methane/air mixtures. Also, cellular structures have been observed in diffusion flames (Garside and Jackson, 1953) which do not possess any propagation velocity and as such do not fall into the

framework of the model developed for premixed systems. Finally, the physical extent and magnitude of the observed phenomena appear to be too large to be accounted on the basis of the small deviation of Le from unity.

In view of the above consideration, the role of chemical-kinetic effects through the active radical species in the formation, amplification and sustenance of flame-front corrugations was recently studied by Bidinger and Sohrab (1986). The results of this study showed that radical species, such as atomic hydrogen, indeed play some role in the thermo-diffusive flame instabilities. Therefore, it appears that a complete description of the flame-front stability may require the inclusion of chemical effects in addition to the hydrodynamic, thermal and diffusional effects. The present investigation is an extension of the previous study (Bidinger and Sohrab, 1986) and aims to further explore the chemical-kinetic and thermo-diffusive nature of cellular flame structures. Such effects are explored by examination of temperature in the trough/crest zones when either chemical inhibitor CF_3Br or nitrogen are gradually added to PHF of rich butane/air Bunsen flames. Also, the rotation speed and the periodic temperature fluctuations of rotating PHF are examined. Finally, for different flow rates of the combustible mixture through the burner, the flame temperature corresponding to the onset of cell formation are determined.

EXPERIMENTAL PROCEDURES

The PHF of rich butane-air mixtures are stabilized on the Bunsen burner shown in Fig. 1. The burner is a brass tube with 1.27 and 0.96 cm outside and inside diameters and is 1 m long such that fully-developed parabolic velocity profiles occur at the burner exit plane. An outer concentric tube with 3.5 cm

inside diameter is provided for the control of velocity/composition of the surrounding atmosphere. Four equally-spaced layers of small mesh-screens are placed within the annular region between the concentric tubes to obtain uniform velocity profile, as shown in Fig. 2a. The fuel, oxygen, nitrogen and CF_3Br are separately metered and may be introduced in the inner or outer tubes. The gases are thoroughly mixed in a mixing chamber before introduction into the burner tube. Precise adjustment of the fuel and CF_3Br flow rates are mandatory, because small changes in concentration of these species can alter the PHF substantially (Bidinger and Sohrab, 1986). Soap-bubble meters are therefore used to accurately measure the flow rates of the butane, CF_3Br and N_2 .

A stationary 6-sided PHF is chosen as a standard reference flame for the subsequent comparisons. For the reference flame, the fuel concentration ϕ (by volume) is 4.8 and the mean velocity at the burner exit plane V is 72.65 cm/s. The light-blue flame with a closed tip has the height of about 13 mm, and the dark-zone between the burner rim and the flame base is 0.3 mm. In order to prevent the flame rotation about the axis of symmetry, during the temperature measurements, a special stabilizer ring shown in Fig. 2b was designed. The stabilizer ring is mounted at the top, around the outer burner tube such that it can be rotated about the burner axis. Six platinum wires, 0.05 mm diameter, are circumferentially positioned such that they are 60 degrees apart and extend radially inward. The wires terminate 0.5 mm away from the inner-surface of the burner tube, close to the crest zones of the reference PHF. Rotation of the stabilizer ring results in rigid-body rotation of the entire PHF. It is established that the stabilizer ring has no visible effects on the reference PHF. This ring helps to prevent the unwanted rotation of the flames during the temperature measurements on stationary

PHF. A direct photograph of the standard PHF on the burner with stabilizer ring is shown in Fig. 3.

Temperature measurements are made by using a silica-coated, Pt-Pt-10% Rh thermocouple with 0.05 mm wire diameter, which can be traversed in both radial and axial directions. The response time of the thermocouple junction is estimated to be about 2 ms. Because of the local perturbations induced by the intrusion of the thermocouple, the precise positioning of the junction is very difficult. For example, if the junction is positioned too far upstream of the flame sheet the flame sheet may corrugate and anchor at the junction. However, since the luminous flame sheet is clearly identifiable, the approximate positioning of the junction in the vicinity of the reaction zone can be achieved. It is found necessary to employ two judgemental criteria for the positioning of the thermocouple junction.

The following criteria are used for the positioning of the thermocouple junction in the trough and crest zones of stationary PHF. The PHF is anchored on the burner and held stationary by the stabilizer ring. The ring is then rotated and the flame is positioned such that the center of trough zone radially points toward the thermocouple junction. The junction is then radially moved inward in such a way that the junction just touches the downstream edge of the luminous zone of the flame sheet. The criteria for positioning of the junction in the crest is different. Here, the junction is positioned at the outer edge of the dark crest cone and is symmetrically located between two adjacent cells. The adjustment of the position has to be done as precisely as possible, because the smallest deviations may cause rather large temperature variations. Falsification of the measurements can occur by attachment of the flame sheets of the adjacent cells to the junction located in the middle.

The procedure described above was developed such that good repeatability of the measurements could be achieved. The temperatures of the trough, T_c , and crest (ridge), T_r , zones are then measured with the junction located 5 mm above the burner rim. Variations of T_c and T_r are determined as the volumetric concentrations of the inhibitor, α_{CF_3Br} and nitrogen, α_{N_2} , are gradually increased in the reference PHF until complete disappearance of the cellular structure.

For conducting temperature measurements in rotating PHF, the thermocouple, an amplifier, and an oscilloscope are arranged according to the schematic drawing shown in Fig. 4. The stabilizer ring is removed for tests on rotating PHF. Tests on rotating PHF, consider butane concentration of 4.95 in air at velocity $V = 72.65$ cm/s suggested by the earlier observations (Sohrab and Law, 1985). The introduction of nitrogen into the outer jacket tube removes the surrounding diffusion-flame mantle and results into rapid rotation of the PHF. The thermocouple junction is located at a constant axial position 6 mm above the burner rim. If the junction is too close to the burner rim it will prevent the rotation of the PHF. Temperature of the upstream and downstream regions of the rotating flame are then measured by varying the radial position of the junction from 2.4 to 4.4 mm relative to the axis of symmetry.

In order to detect the number of cells of the rapidly rotating polyhedrals, two thermocouples are employed and connected in series, as shown in Fig. 5. The variation of the phase angles between the two thermocouples is then determined from the output signal when one junction is fixed and the other, at a fixed radial and axial position, is circumferentially rotated. When the signal of both junctions are in phase, say both located at the crest or trough position, the angle between the junction will correspond to the cell

angle. The number of sides of the rotating PHF is then determined from the knowledge of the cell angles. For example, for a 6-sided stationary PHF, the cell angle will be 60 degrees.

STATIONARY POLYHEDRAL FLAMES

As the additives CF_3Br and N_2 are gradually introduced into the reference PHF, the cellular flame structure is found to diminish and eventually a conical-flame with smooth surface is achieved. The minimum values of $\Omega_{\text{CF}_3\text{Br}}$ and Ω_{N_2} corresponding to smooth flame situation are respectively 0.36 and 5% in close agreement with the previous observations (Bidingger and Sohrab, 1986). Also, as CF_3Br (N_2) is added, the flame height increases from 18 mm to 32 mm (30 mm) at the smooth flame condition. Direct photographs of the reference PHF before and after addition of 0.36% CF_3Br are shown in Fig. 6. It is noted that the difference between influences of CF_3Br and N_2 cannot be accounted for on the basis of thermal effects alone. For the typical temperature of 1670 K, the molar specific heats, \bar{c}_{p_i} , of CF_3Br and N_2 are respectively 25.17 and 8.43 cal/mole-K. When account is made of the respective mole fractions, x_i , of these additives (0.36 and 5%), the ratio between $x_i \bar{c}_{p_i}$ is about 0.27. Therefore, similar to the flame inhibition studies (Sohrab, 1981) it is concluded that CF_3Br effects occur through chemical-kinetic interference with the flame structure.

The variations of T_c and T_f as a function of $\Omega_{\text{CF}_3\text{Br}}$ and Ω_{N_2} are shown in Figs. 7 and 8. Examination of the data shows that both T_c and T_f decrease with Ω_{N_2} , while they first increase and then decrease with $\Omega_{\text{CF}_3\text{Br}}$. It is interesting that the critical value of $\Omega_{\text{CF}_3\text{Br}}$ associated with the maximum temperatures T_c and T_f in Fig. 7, about 0.1, closely agrees with the critical

inhibitor mole fraction corresponding to the maximum inhibition efficiency of CF_3Br determined earlier (Sohrab, 1981). In the previous study, inhibition of diffusion flames burning in the stagnation-point flow above liquid pool of heptane was investigated (Sohrab, 1981). It was found that the maximum oxygen mass-fraction Y_{O_2} at extinction occurs when the mole fraction of inhibitor in $\text{CF}_3\text{Br}-\text{O}_2-\text{N}_2$ mixture is $x = 0.1$ as shown in Fig. 9. Therefore, the data in Figs. 7 further confirms that the inhibition efficiency of CF_3Br is related to the temperature-sensitivities of the kinetics of inhibition as was discussed previously (Sohrab, 1981). The comparisons of the data in Figs. 7 and 8 also show that temperatures T_c and T_f are higher in the flames inhibited by CF_3Br which is a manifestation of the chemical rather than thermal influence of this additive as compared to nitrogen.

In a series of tests, the temperature of the flames corresponding to the onset of cellular structure, T_0 , is determined at different gas velocities V . Here, onset of cellular instability is defined as the first appearance of a dark region over a narrow vertical strip on the smooth conical flames. Starting with smooth rich flames, Ω_f is steadily reduced until the first appearance of the dark zone at which point the temperature of the luminous zone of the flame is measured. The data, presented in Table 1, show that T_0 is nearly constant, $\pm 10^\circ\text{C}$, for various velocities V . Because of the uncertainties in the judgement concerning the initial appearance of instability, the data are qualitative in nature. However, the results appear to support the fact that chemical-kinetic mechanisms may be effective in sustenance or amplifications of the flame-front perturbations. Such behavior is somewhat similar to the well known constancy of the flame temperatures, about 1120°C , at the lean flammability limits of lower hydrocarbons, such as methane, propane and butane. This latter phenomenon suggests the possible

role of chemical-kinetic mechanisms in the description of the lean flammability limits of the lighter hydrocarbons. Such chemical-kinetic effects are further discussed in the following section.

PHENOMENOLOGICAL ARGUMENTS

The importance of molecular hydrogen in the formation of cellular flames was emphasized in the early reports by Behrens (1953) and Garside and Jackson (1953). It was found that addition of small quantities of hydrogen will enhance the tendency for PHF formation in propane-air flames (Garside and Jackson, 1953). In particular, no PHF could be obtained in methane-air mixtures unless some hydrogen was also added (Behrens, 1953). Certain phenomenological arguments were presented by Behrens (1953) in support of his experimental observations. It was also noted that the chemical-kinetics of methane combustion differs from that of the higher hydrocarbons in that CH_3 radical instead of the atomic-hydrogen plays an important role in methane combustion. In this pioneering work (Behrens, 1953) the author concluded that the molecular hydrogen, and the resulting atomic-hydrogens as reaction intermediaries, play a key role in the formation of cellular flames.

In the present study, the significant role of atomic-hydrogen is further isolated through the introduction of the chemical-inhibitor CF_3Br . On the basis of the earlier (Bidinger and Sohrab, 1986) and present observations, it may be concluded that chemical-kinetics effects have an appreciable influence on cellular flames. In particular, complete destruction of cellular flame structure is achieved through chemical interaction of CF_3Br with the reaction zone of the unstable flame. Therefore, the results of the present study are better understood when viewed within the framework of the kinetics of

inhibition by halogenated compounds reviewed previously (Sohrab, 1981). Here, in the same spirit as that considered by Behrens (1953), two phenomenological arguments will be presented which may in part describe how chemical-kinetic mechanisms can influence the flame-front stability. The arguments are based on the kinetics of branched-chain reactions which are relevant to hydrocarbon combustion (Lewis and von Elbe, 1967).

The central role of atomic hydrogen in the combustion of hydrocarbons was reviewed previously (Sohrab, 1981). It is known that within a thin radical-production zone, which is embedded in the relatively wider reaction zone, the following important reactions occur:



The rate of reactions (2) and (3) are orders of magnitude higher than that of reaction (1). Hence, the important chain-branching reaction (1) with activation energy of 17 kcal/mole is rate controlling.

The inhibitor CF_3Br is expected to first decompose according to the reaction (Sohrab, 1981),



The subsequent role of CF_3 is not significant and cyclic removal of atomic hydrogen by HBr is expected to occur through the regenerative reaction cycles (Sohrab, 1981).



and



Thus, the overall effect of the inhibitor is replacement of active H atoms by

less reactive bromine atoms, thereby reducing the overall reaction rate.

Since atomic hydrogen generation is controlled by the reaction (1) which has a large activation energy, the local peaks in temperature, say in the trough zones of PHF, are expected to result in H-atom concentration peaks. Also, high H concentration will enhance the consumption of O_2 by the reactions (1)-(3). This will result in larger concentration gradients of O_2 which will in turn enhance the diffusion of O_2 towards the trough zone. Thus, stratification of the mixture could be augmented through such chemical-kinetic mechanisms. As a result, the temperature perturbations which are originated by preferential-diffusion are amplified thereby increasing the propensity for cell formation.

We note that because of the nature of branched-chain reactions, only small deviation of Le from unity are needed in order to produce the original temperature corrugations whose subsequent amplification leads to large observable corrugations of the front. Also, in accordance with the observations, the amplification of corrugations is expected to be reduced in presence of CF_3Br , since the inhibitor removes the atomic-hydrogen radicals. A schematic drawing of the expected fluctuations of T , H , O_2 and fuel F , for a 6-sided PHF is shown in Fig. 10. Such fluctuations of O_2 and F are in qualitative agreement with the observations of Jost, et al. (1953). Also, the variation of T is in accordance with the observations made herein as well as the theoretical predictions (Sivashinsky, 1976). The schematic concentration profiles in Fig. 10 are also supported by the previous observations of soot formation in the crest zones of certain PHF (Smith and Pickering, 1929). In the crests, CO and O_2 concentrations are larger (Jost, et al., 1953) while H , and therefore OH , concentrations as well as the temperature are lower as compared with the troughs. Therefore, formation of soot in the crests is

anticipated on the basis of high concentration of CO, possible catalytic effects of O_2 (Lin and Sohrab, 1986) as well as the well known role of OH in the combustion of soot precursors.

The second phenomenological argument concerning the role of chemical-kinetics in flame instability is based on the concept of the critical cross-over temperature (Sohrab, 1981). Because of their different activation energies, the rates of bimolecular and termolecular reactions may cross each other when plotted as functions of $1/T$. The cross-over point between the rate of an important biomolecular reaction, such as reaction (1), and an important termolecular reaction, such as reaction



can be defined as the critical cross-over temperature T_c as shown in Fig. 11. When temperature perturbations about T_c occur, for $T > T_c$ and $T < T_c$ the reaction rate is expected to respectively accelerate or decelerate. This will result in corrugation of the flame front as shown in Fig. 11. Again, because of the nature of branched-chain reactions, only small perturbations about T_c are necessary to produce substantial change in the reaction rate leading to formation of cellular structure. The small temperature fluctuations about T_c could be initiated by the preferential-diffusion mechanism. Such a phenomenological description is supported by the constancy of temperature T_0 corresponding to the onset of cell formation mentioned in the previous section.

ROTATING POLYHEDRAL FLAMES

In this section, the periodic variation of the temperature field in the vicinity of rapidly rotating PHF is discussed. The fuel concentration of the

reference PHF is now changed to $\Omega_T = 4.95$, with $V = 72.67$ cm/s and the stabilizer ring is removed. The resulting stationary 6-sided PHF will start a rapid counter-clockwise rotation when small flow, 72 cm³/s, of nitrogen is introduced in the outer annular tube as discussed before. A direct photograph of the rotating PHF is shown in Fig. 12. The luminous zone of the rapidly rotating PHF is fuzzy and thicker while the flame height is smaller compared to the stationary PHF. Also, the rotation of PHF is found to predominantly occur in the counter-clockwise direction in agreement with the previous observations (Sohrab and Law, 1985).

The number of sides and the rotation speed of the PHF are measured using the two-thermocouple connections, Fig. 5, discussed earlier. It is found that in-phase signal of the two thermocouples are obtained when the second junction is located at 90° , 180° and 270° angles relative to the first junction. Therefore, the original stationary 6-sided PHF has changed to a 4-sided structure after rotation is induced by nitrogen flow in the outer annulus. This result is in agreement with the previous observation of rapidly rotating PHF using high speed cinematography (Sohrab and Law, 1985). Also, from the period of temperature fluctuations, 32 ms, the rotation speed, $\omega = 7.8$ rotations per second (rps), is calculated in qualitative agreement with the previous observation (Sohrab and Law, 1985).

The circumferential temperature fluctuations at different radial positions are obtained from the tracing of the direct photographs of the oscilloscope screen and are shown in Fig. 13a-i. The variations of periodic temperature profiles at different radial positions are qualitatively understood on the basis of the residence time of the thermocouple junction in the downstream (hot) or upstream (cold) sides of the rotating PHF. In general, the trough zones are circumferentially wider than the crest zones, as

reflected by the longer time intervals of high versus low temperatures in Fig. 13. Also, the magnitude of the temperature fluctuations are a function of the relative instantaneous position of the junction with respect to the corrugated flame-front. We note that the temperature gradients downstream of the flame are much smaller than those in the upstream region, as is to be expected. The results in Fig. 13 also show that temperature fluctuations occur about a mean temperature plateau of approximately 1408 °C. Hence, rotation of different cells of the PHF occur in preheated gas. It is known that the rotation of the flame, reaction zone, is not accompanied with any appreciable circumferential rotation of the combustible gas (Smith and Pickering, 1929; Sohrab and Law, 1985).

Rotating PHF was also examined in oxygen-enriched air. For the fuel and oxygen concentrations of $\Omega_F = 7.76$ and $\Omega_O = 26$, a stationary 8-sided PHF is obtained with well defined cells and a stream of soot is observed to emanate from the flame tip. However, this flame was found to be only marginally stable, and under small laboratory fluctuations, it could spontaneously start a rapid counter-clockwise rotation. We note that such rapidly rotating PHF in butane/air mixtures could only occur in the presence of nitrogen flow in the outer annulus (Sohrab and Law, 1985). Therefore, the present observation shows that rapidly rotating flames may occur in oxygen-rich air in absence of inert surrounding atmosphere. Here, the period of temperature fluctuation is 20 ms, and the PHF is found to be 4-sided, resulting in $\omega = 12.5$ rps. According to some preliminary observations, the rotation speed of the flame was found to increase with Ω_O .

CONCLUDING REMARKS

Through comparisons of the minimum mole fractions of the additives CF_3Br and N_2 required for destruction of cellular structure of butane/air PNF, the significance of chemical versus thermal effects in the formation/amplification of cellular flame structures was investigated. The small changes in the mean specific heats and velocities induced by the additives, on the other hand, revealed that the observed cell destruction does not appear to have thermal or hydrodynamic origins. It was therefore concluded that the influence of CF_3Br primarily occurs through chemical-kinetic modification of the structure of PNF. It is emphasized that the kinetic mechanisms discussed herein are complementary to the well-known thermo-diffusive, $\text{Le} \neq 1$, mechanisms of cell formation. Indeed, the observations are consistent with both mechanisms working in conjunction with each other.

Since pyrolysis of fuel molecules occurs prior to their consumption in the reaction zone, more than one Lewis number, $\text{Le}_i = \alpha/D_i$, each corresponding to the diffusion coefficient D_i of specie i , could effect the flame front. Here, α refers to the thermal diffusivity of the mixture. Therefore, in general, thermo-diffusive description of flame-front instability could be based on the deviation of Le of reaction intermediaries, such as radical species, from unity. In fact, recent theoretical study of Peláez and Liñán (1985) has shown that thermo-diffusive stability of flames are influenced by the Lewis number of intermediate species. Such effects are particularly relevant to atomic hydrogen because of its high mobility. However, the role of chemistry is separate and fundamentally different from that of the transport, $\text{Le} \neq 1$, effects. The former may manifest itself through augmentation of preferential-diffusion effects by chemical-kinetic mechanisms

as discussed earlier.

Intrusive temperature measurements in rotating PHF proved to be difficult. However, the technique of employing two thermocouple junctions connected in series facilitated the determination of the number of cells as well as the rotation speed of PHF. So far, the reason for predominant rotation of PHF in counter-clockwise direction remains a mystery. The preliminary tests on the influence of applied magnetic field on rotating PHF showed no observable effects. Thus, influences associated with the asymmetry in the Earth's magnetic field were ruled out. Exploration of the possible effects of coriolis acceleration on this interesting phenomena through experiments on rotating PHF performed in the Southern hemisphere, may prove useful.

ACKNOWLEDGEMENT

This research has been sponsored by Air Force Astronautics Laboratory under Contract No. F04611-87-K-0067.

REFERENCES

1. Barenblatt, G. I., Zeldovich, Y. B. and Istratov, A. G. (1962). On Diffusional Thermal Instability of Laminar Flames, Prikl. Mekh. Tekh. Fiz. 2, 21.
2. Behrens, H. (1953). Flame instabilities and combustion mechanism, Fourth Symposium (International) on Combustion, Williams and Wilkins, Baltimore, MD., p. 535.
3. Bidingler, D. F. and Sohrab, S. H. (1986). Chemical kinetic mechanisms as amplifiers of diffusional-thermal instabilities, Central States Section, The Combustion Institute, May 5-6, Cleveland, OH.
4. Bocha, J. P. and Spalding, D. B. (1954). The laminar flame speed of propane/air mixtures with heat extraction from the flame, Proc. Royal Soc. A225, 71-96.
5. Clavin, P. and Williams, F. A. (1982). Effects of molecular diffusion and of thermal expansion on the structure and dynamics of premixed flames in turbulent flows of large scale and low intensity, J. Fluid Mech. 116, 251.
6. Garside, J. E. and Jackson, B. (1953). The formations and some properties of polyhedral burner flames, Fourth Symposium (International) on Combustion, Williams and Wilkins, Baltimore, MD., p. 545.
7. Jost, W., Krug, J. and Sieg, L. (1953). Observations on disturbed flames, Fourth Symposium (International) on Combustion, Williams and Wilkins, Baltimore, p. 535.
8. Joulin, G. and Clavin, P. (1979). Linear stability analysis of nonadiabatic flames: a thermal-diffusional model, Combust. Flame 35, 139.
9. Joulin, G. and Mitani, T. (1981). Linear stability analysis of two-reactant flames, Combust. Flame 40, 235.
10. Lewis, B., and Von Elbe, G. (1967). Combustion, Flames and Explosions of Gases, Academic Press, New York.
11. Lin, T. H. and Sohrab, S. H. (1986). Influence of vorticity on counterflow diffusion flames, Combust. Sci. Tech. 12, 75.
12. Manton, J., von Elbe, G. and Lewis, B. (1952). Nonisotropic propagation of combustion waves in explosive gas mixtures and the development of cellular flames, J. Chem. Phys. 20, 153.
13. Markstein, G. H. (1964). Nonsteady Flame Propagation, Pergamon Press.
14. Markstein, G. H. (1958). Composition traverses in curved laminar flame fronts, Seventh Symposium (International) on Combustion, The Combustion Institute, p. 289.

15. Matalon, M. and Matkowsky, B. J. (1982). Flames as Gasdynamic discontinuities, J. Fluid Mech. 124, 239.
16. Peláez, J. and Liñan, A. (1985). Structure and stability of flames with two sequential reactions, SIAM J. Appl. Math. 45, 303.
17. Sivashinsky, G. I. (1977). Diffusional-thermal theory of cellular flames, Combustion Science and Technology 15, 137-165.
18. Smith, F. A. and Pickering, S. F. (1929). Bunsen flames of unusual structure, Bureau of Standards Journal of Research, 3, 65.
19. Smithells, A. and Ingle, H. (1892). The structure and chemistry of flames, J. Chem. Soc. 61, 204.
20. Sohrab, S. H. (1981). Diffusion Flame Extinction, Ph.D. Thesis, University of California, San Diego.
21. Sohrab, S. H. and Chao, B. H. (1984). Influences of upstream versus downstream heat loss/gain on stability of premixed flames, Combust. Sci. Tech. 38, 245.
22. Sohrab, S. H. and Law, C. K. (1985). Influence of burner rim aerodynamics on polyhedral flames and flame stabilization, Combust. Flame 62, 243.
23. Williams, F. A. (1985). Combustion Theory, 2nd Ed., Benjamin/Cummings Publishing Co., Menlo Park, CA.

LIST OF FIGURES

- Figure 1. Schematic of Bunsen burner apparatus.
- Figure 2. Details of (a) burner tubes, (b) stabilizer ring.
- Figure 3. Direct photograph of the reference PHF.
- Figure 4. Thermocouple-amplifier-oscilloscope assembly.
- Figure 5. Series-connection of two thermocouple junctions used for measurements in rotating PHF.
- Figure 6. Butane PHF (a) reference flame, (b) after addition of 0.36% (by volume) of CF_3Br .
- Figure 7. Variations of T_c and T_f with $\dot{Q}_{\text{CF}_3\text{Br}}$.
- Figure 8. Variations of T_c and T_f with \dot{Q}_{N_2} .
- Figure 9. Oxygen mass fraction in air at extinction Y_{O_2} versus $\dot{Q}_{\text{CF}_3\text{Br}}$ stagnation flow diffusion flames above heptane, $V = 50$ cm/s. Area under the curve corresponds to the extinction condition.
- Figure 10. Schematic profiles of H, O_2 , F (fuel) and T in 6-sided stationary PHF.
- Figure 11. Critical cross-over temperature, T_c .
- Figure 12. Direct photograph of rapidly rotating PHF. $\dot{Q}_{\text{N}_2} = 4.95$, $V = 72.67$, outer N_2 flow = $72 \text{ cm}^3/\text{s}$, $\omega = 7.8$ rps.
- Figure 13. Circumferential temperature fluctuations in rotating PHF at 2 mm radial intervals from $R = 2.4$ to 4.0 mm. $\dot{Q}_{\text{N}_2} = 4.95$, $V = 72.67$ cm/s, $\omega = 7.8$ rps. Outer N_2 flow = $72 \text{ cm}^3/\text{s}$.

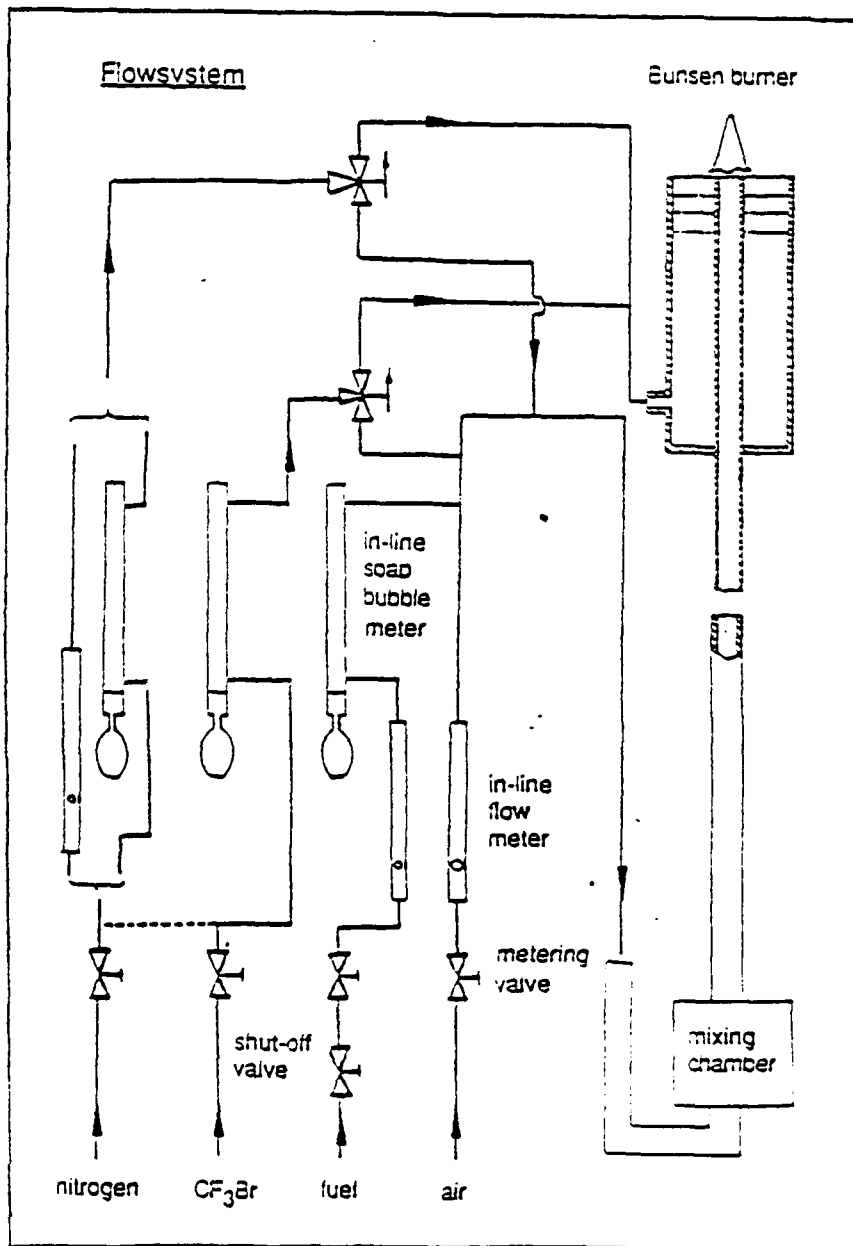
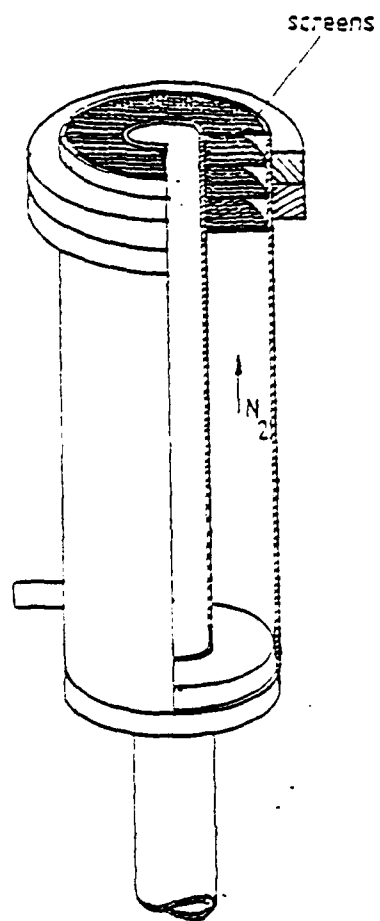
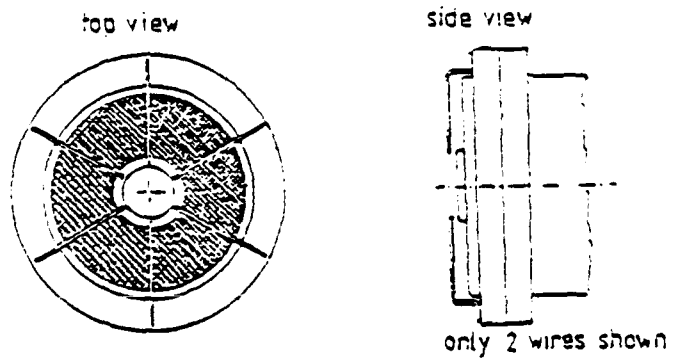


Figure 1

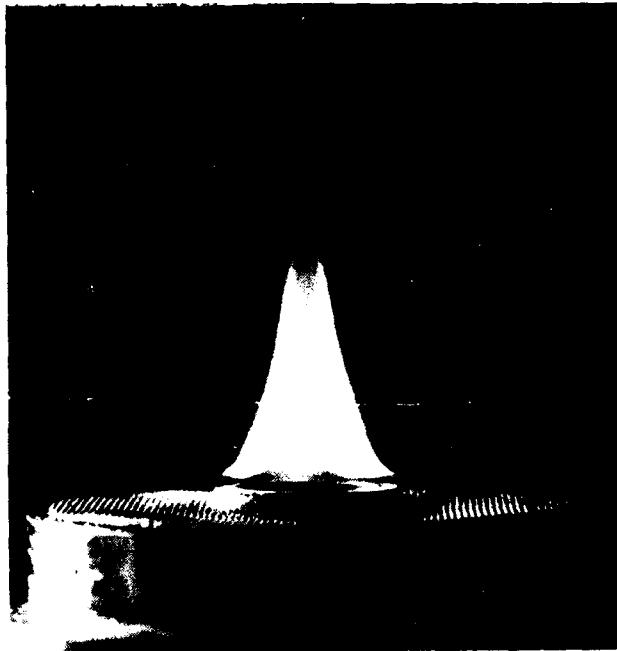


(a)



(b)

Figure 2



Measurement of Temperature Fluctuations in Rotating Polyhedral Flames

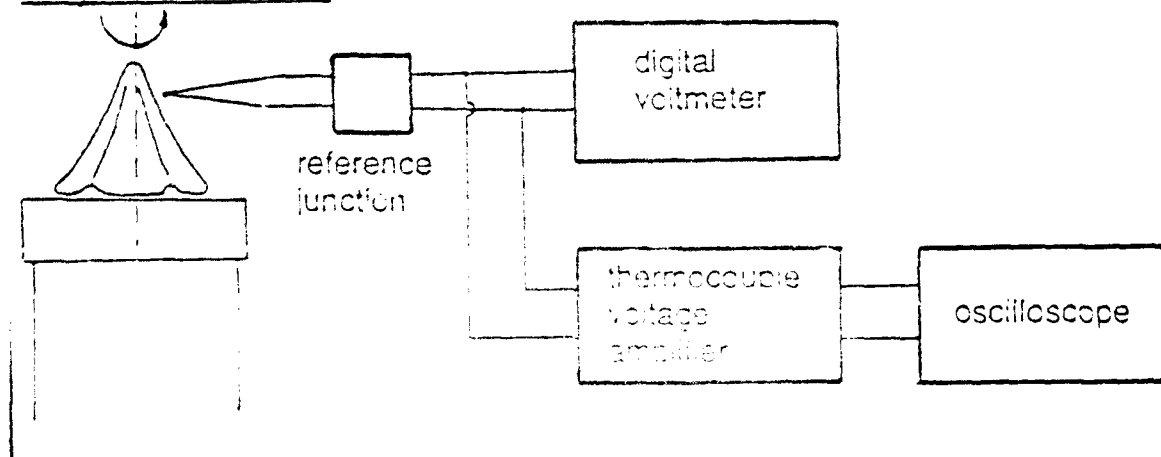
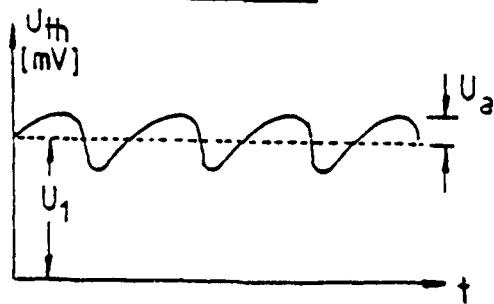
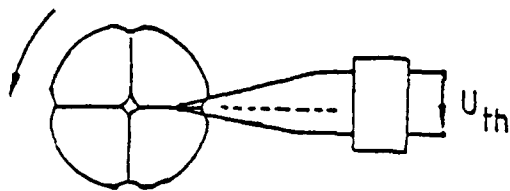


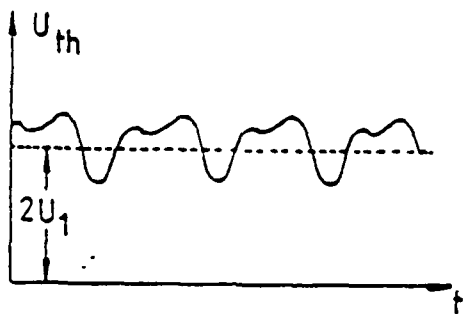
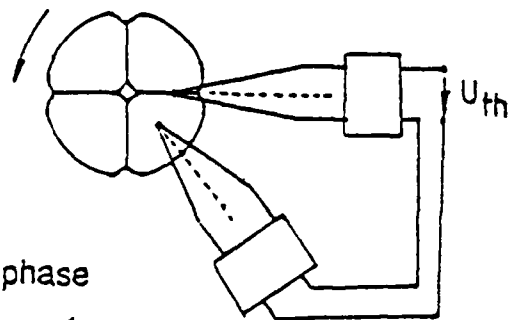
Figure 1

Cell Number Detection in Rotating Polyhedral Flames

single thermocouple



series of 2 thermocouples:
out of phase



in phase

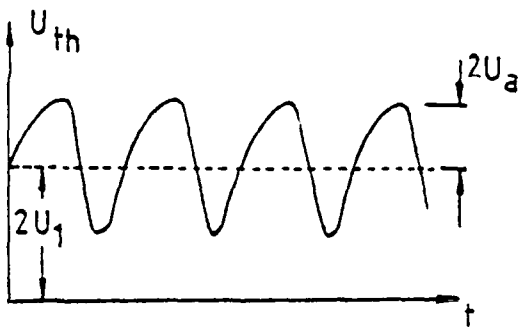
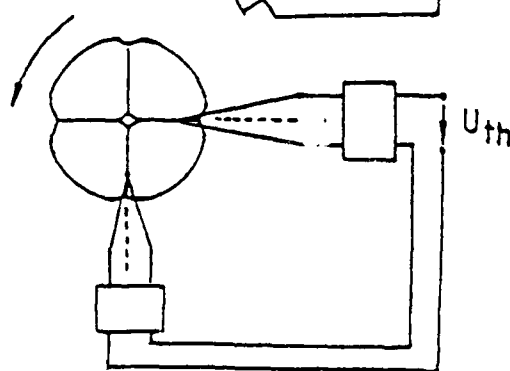
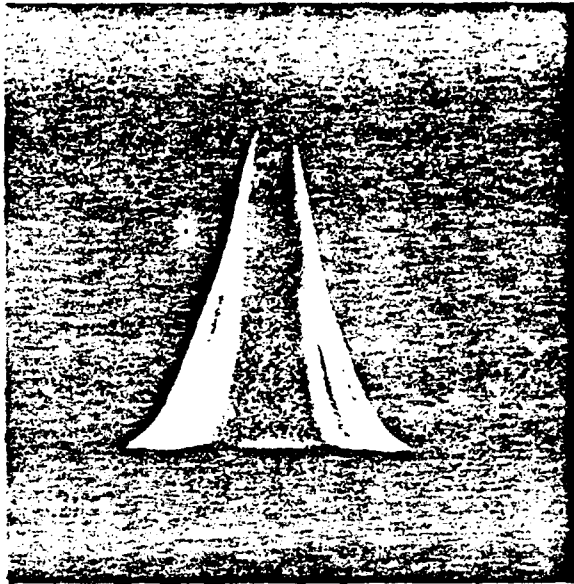
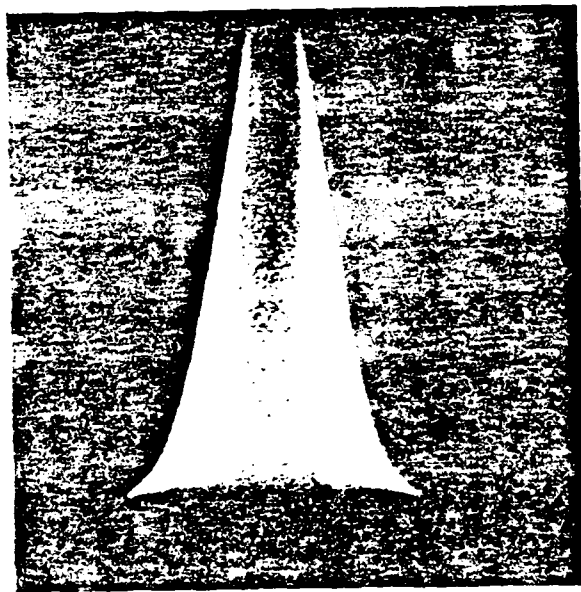


Figure 5



(a)



(b)

Figure 6

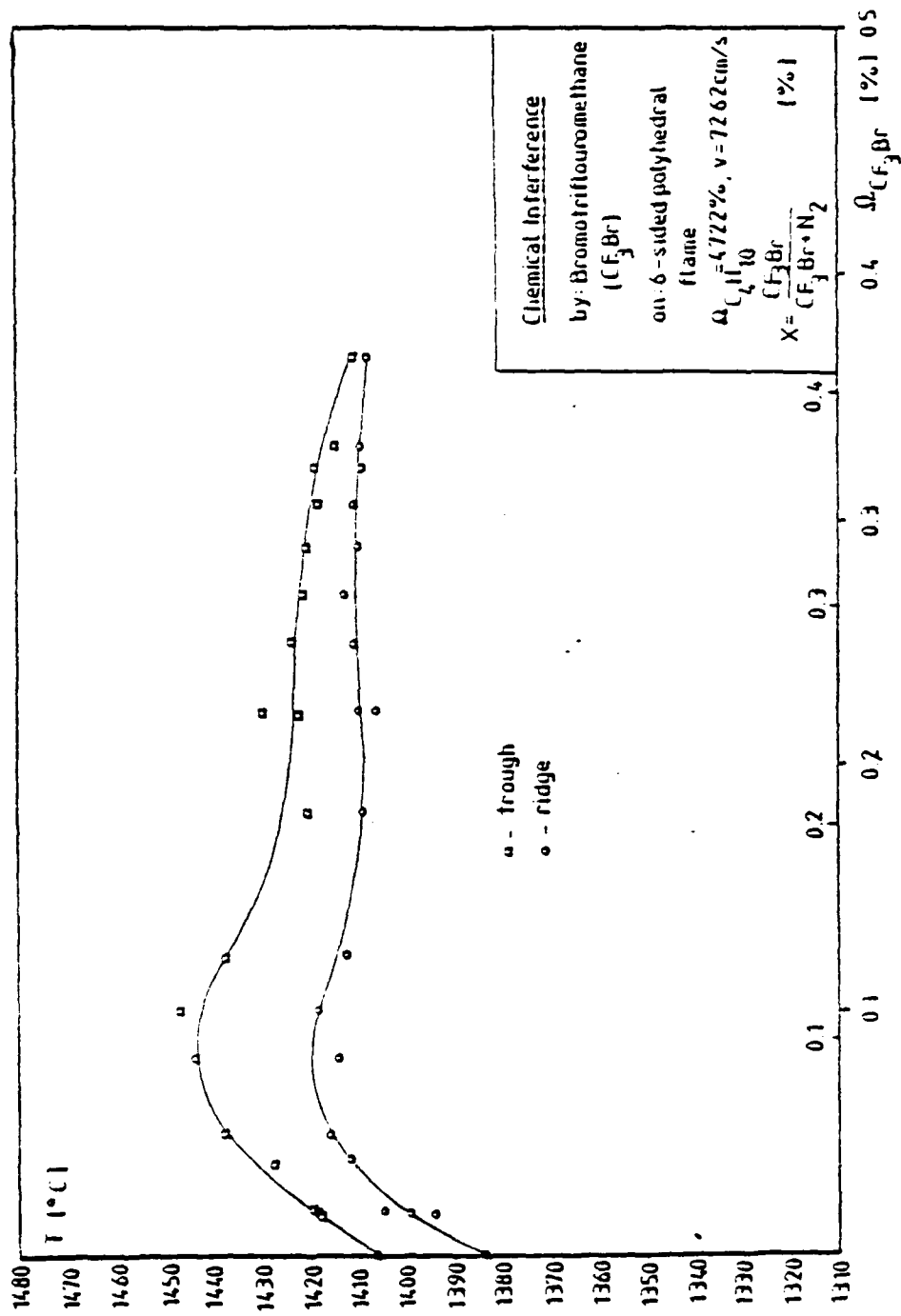


Figure 7

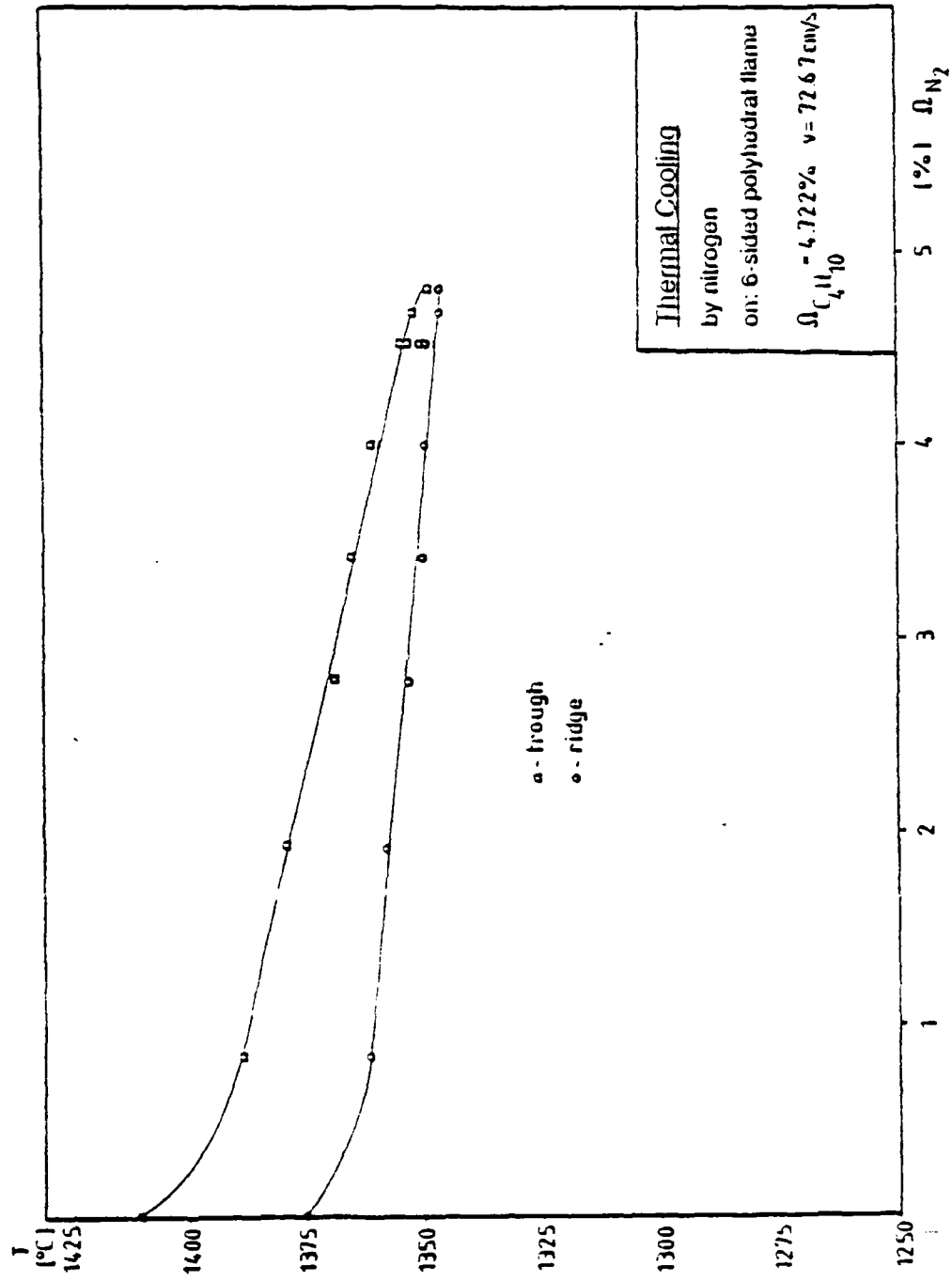


Figure 8

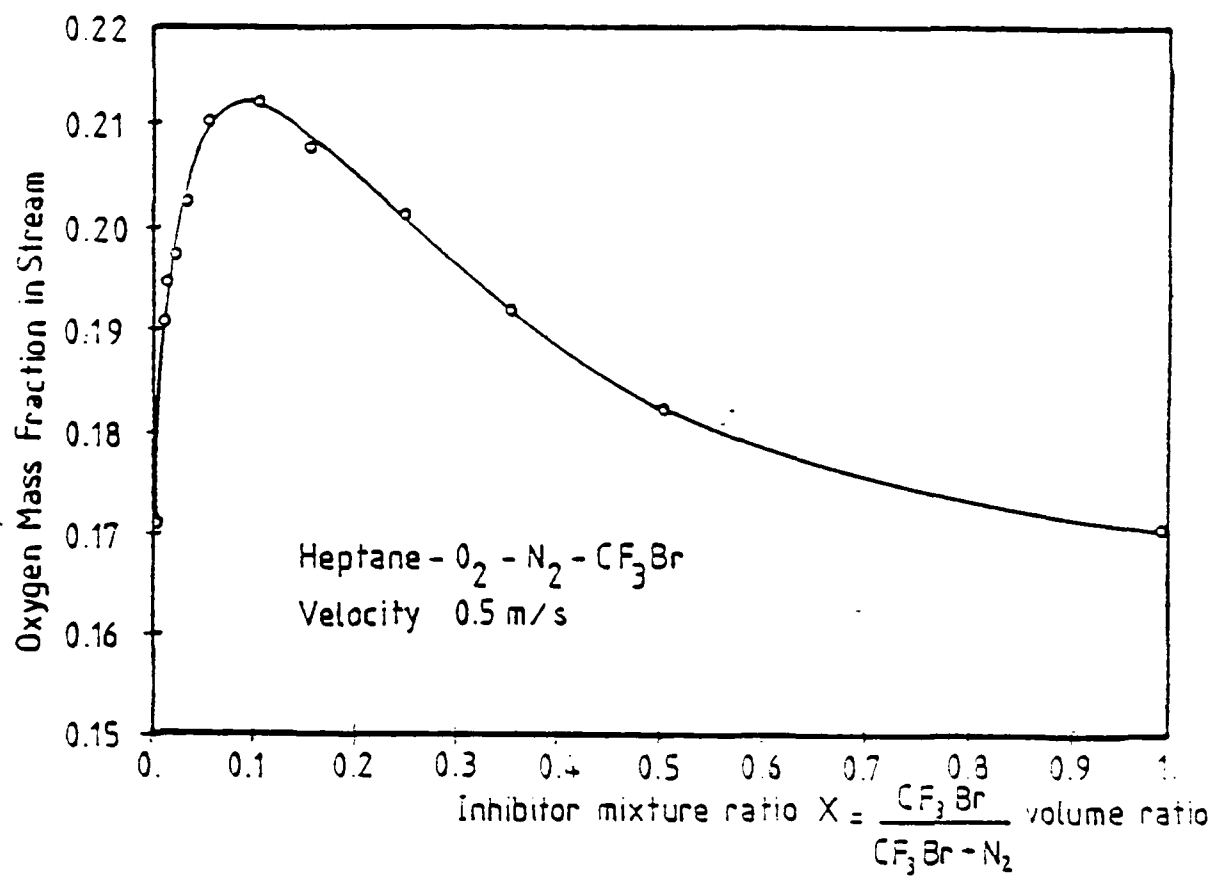


Figure 9

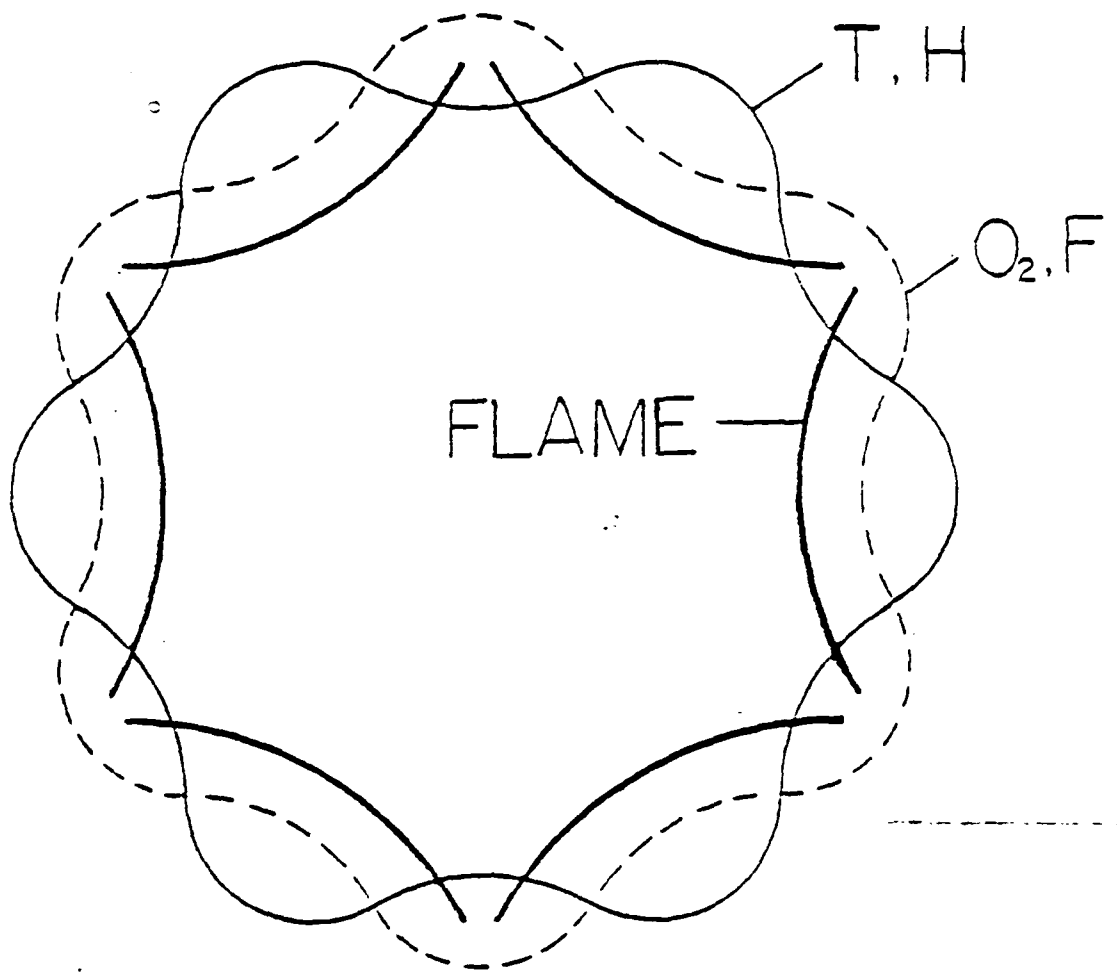


Figure 10

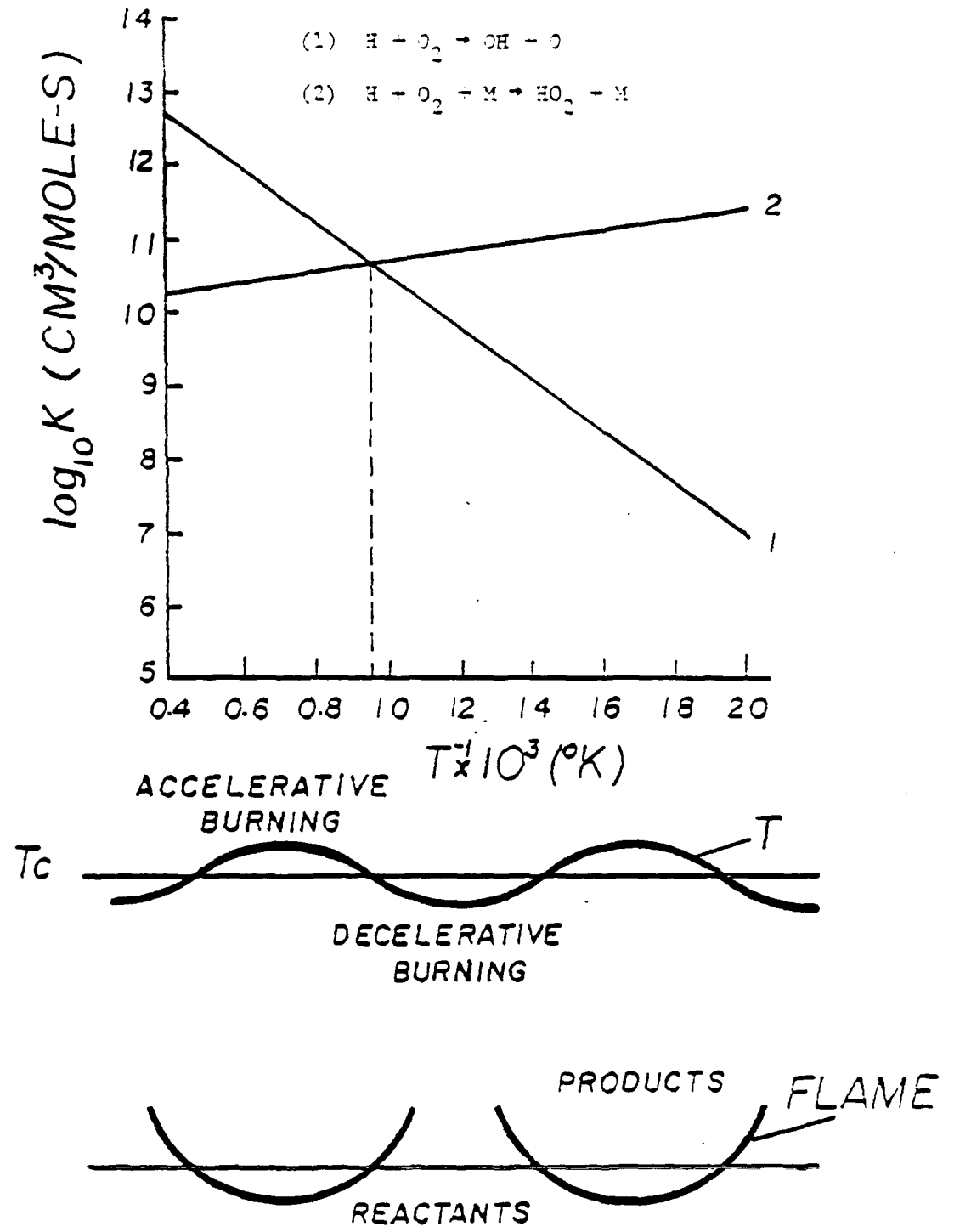
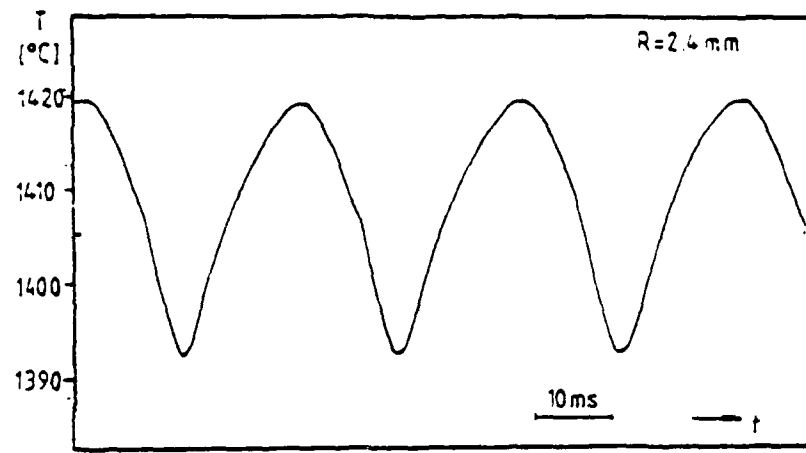


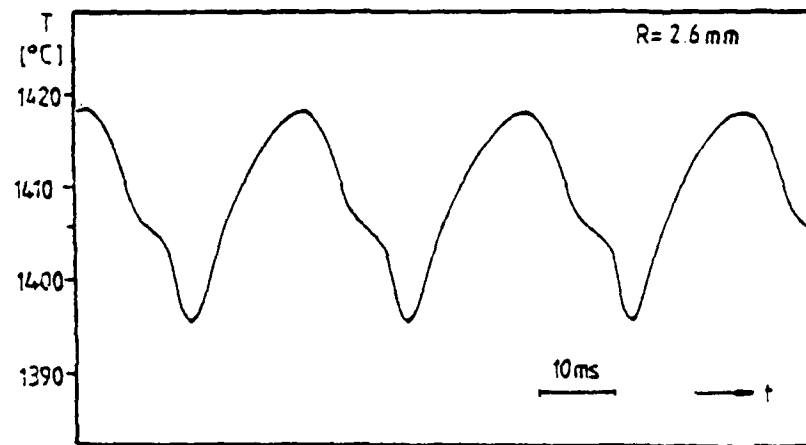
Figure 11



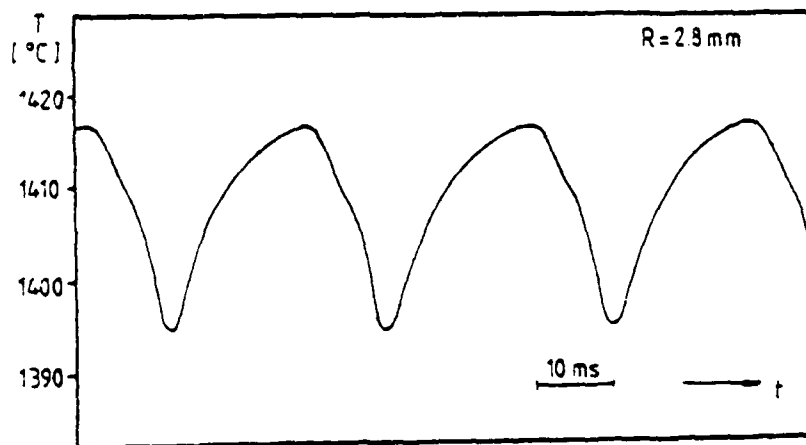
Figure 12



(a)

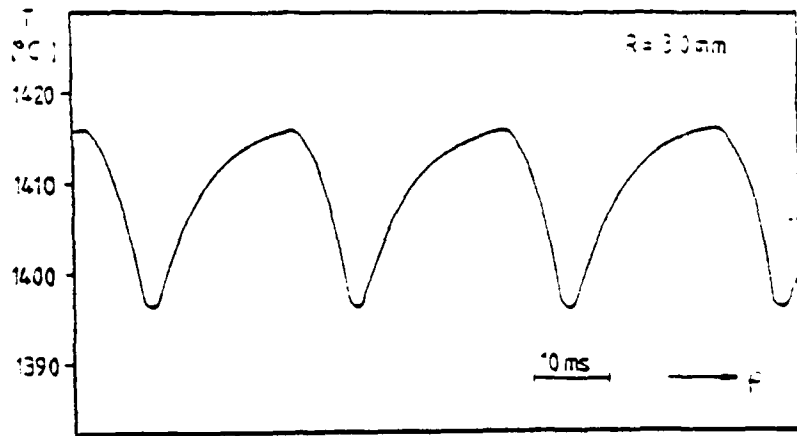


(b)

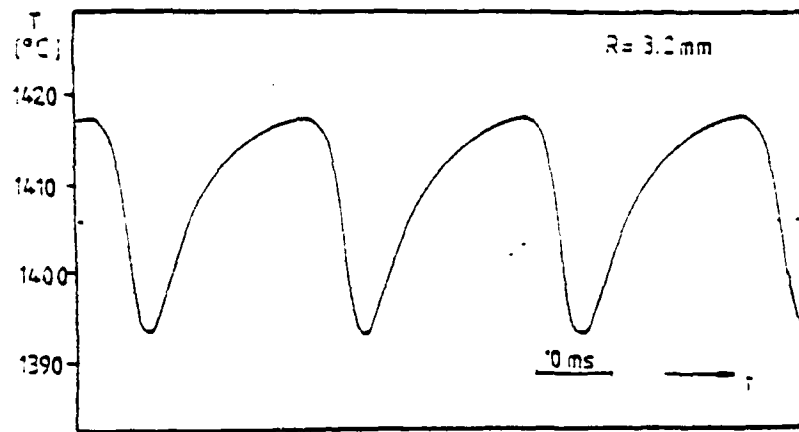


(c)

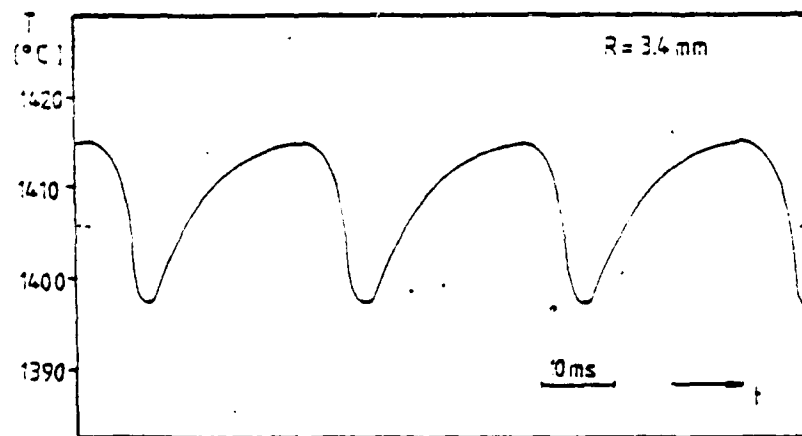
Figure 13



(d)

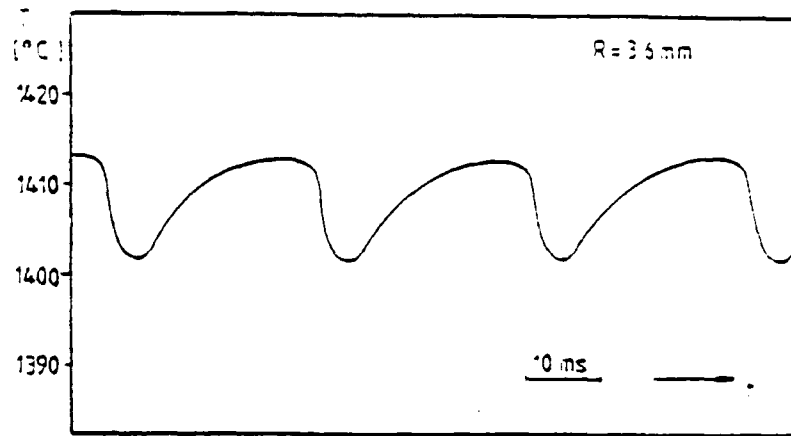


(e)

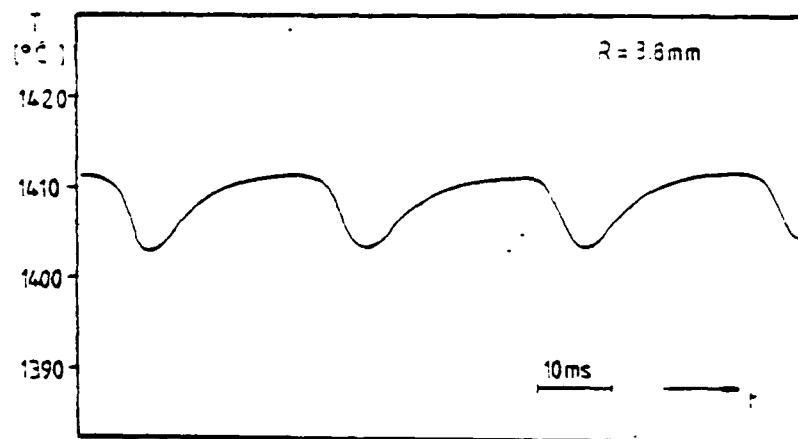


(f)

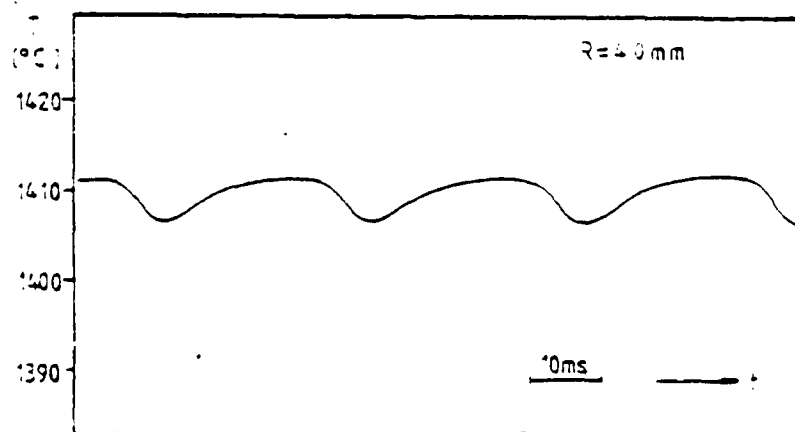
Figure 10



(g)



(h)



(i)

Figure 13

Table 1

TEST #	$\Omega_{C_4H_{10}}$	V [cm/s]	T_j [°C]
1	5.2	46.16	1381
2	5.36	50.249	1378
3	5.43	52.05	1384
4	4.6	70.1	1387
5	4.6	80.27	1385
6	4.68	91.01	1388
7	4.22	105.38	1383

APPENDIX IV

Flame Propagation in a Rotating Gas

G. I. SIVASHINSKY and Z. RAKIB *Department of Mathematical Sciences, Tel-Aviv University, Ramat-Aviv, Tel-Aviv, 69978, Israel*

M. MATALON and S. H. SOHRAB *The Technological Institute, Northwestern University, Evanston, Illinois 60201, U.S.A.*

(Received August 15, 1986; in final form August 17, 1987)

Abstract—In this paper we consider the influence of centrifugal and Coriolis accelerations on the form and stability of a flame propagating in a rotating tube. We detect a discrete sequence of angular velocities, near which the flame propagation velocity undergoes an unlimited amplification. We show that sufficiently rapid rotation may suppress cellular instability of the flame front. We construct a self-similar solution that describes a flame propagating in a rotating gas in free space. Our predictions of the flame shape and of the suppression of cellular instability in the presence of rotation have been verified in a simple experiment we have performed.

INTRODUCTION

It is well known that variations in the density of a burning gas make the latter sensitive to external acceleration (see, e.g., Rakib and Sivashinsky, 1987). In the present paper we shall investigate the influence of centrifugal and Coriolis accelerations on the form and stability of a premixed flame propagating in a rotating cylindrical tube.

In order to capture the nature of the rotation-induced effects, we begin with the simplest hydrodynamic model, considering the flame to be a geometric surface moving at constant velocity U_b relative to the burnt gas. Transport and chemical effects are ignored, but the change in gas density across the flame front is taken into consideration (Landau, 1944).

In a coordinate frame rotating together with the tube about the z -axis, at angular velocity ω , the Euler equations are:

$$\frac{\partial v_r}{\partial t} + v_r \frac{\partial v_r}{\partial r} + \frac{v_\varphi}{r} \frac{\partial v_r}{\partial \varphi} + v_z \frac{\partial v_r}{\partial z} - \frac{v_\varphi^2}{r} = -\frac{1}{\rho} \frac{\partial p}{\partial r} - \omega^2 r + 2\omega v_\varphi, \quad (1.1)$$

$$\frac{\partial v_\varphi}{\partial t} + v_r \frac{\partial v_\varphi}{\partial r} + \frac{v_\varphi}{r} \frac{\partial v_\varphi}{\partial \varphi} + v_z \frac{\partial v_\varphi}{\partial z} + \frac{v_r v_\varphi}{r} = -\frac{1}{\rho r} \frac{\partial p}{\partial \varphi} - 2\omega v_r, \quad (1.2)$$

$$\frac{\partial v_z}{\partial t} + v_r \frac{\partial v_z}{\partial r} + \frac{v_\varphi}{r} \frac{\partial v_z}{\partial \varphi} + v_z \frac{\partial v_z}{\partial z} = -\frac{1}{\rho} \frac{\partial p}{\partial z}, \quad (1.3)$$

$$\frac{\partial v_r}{\partial r} + \frac{1}{r} \frac{\partial v_\varphi}{\partial \varphi} + \frac{\partial v_z}{\partial z} + \frac{v_r}{r} = 0. \quad (1.4)$$

Here (r, φ, z) are nondimensional cylindrical coordinates, with r, z measured in units of the radius R of the tube (see Figure 1); t is the nondimensional time, measured in units of R/U_b ; ω is the nondimensional angular velocity, measured in

units of $U_b R$; ρ is the nondimensional density measured in units of the density ρ_b of the combustion products; p is the nondimensional pressure, measured in units of $\rho_b U_b^2$ and $(v_r, v_\varphi, v_z) = \mathbf{v}$ is the nondimensional velocity of the gas, measured in units of U_b .

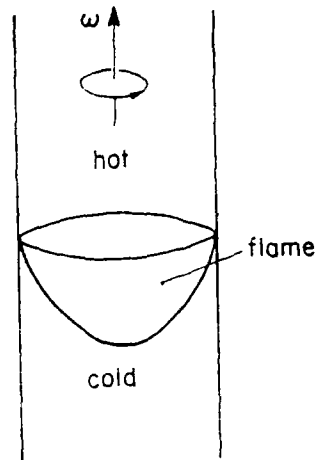


FIGURE 1 Schematic representation of a flame propagating in a rotating channel.

The following conditions must hold at the flame front [$z = \Phi(r, \varphi, t)$]:

- i) Continuity of mass flow

$$[\rho(\mathbf{v} \cdot \mathbf{n} - D)] = 0, \quad (1.5)$$

- ii) Continuity of momentum flow

$$[\rho \mathbf{v}(\mathbf{v} \cdot \mathbf{n} - D) + p \mathbf{n}] = 0, \quad (1.6)$$

- iii) Constant velocity of the flame front relative to the gas

$$\rho(\mathbf{v} \cdot \mathbf{n} - D) = 1, \quad (1.7)$$

where

$$\mathbf{n} = \frac{\left(-\Phi_r, -\frac{1}{r} \Phi_\varphi, 1 \right)}{\sqrt{1 + (\nabla \Phi)^2}}, \quad D = \frac{\Phi_t}{\sqrt{1 + (\nabla \Phi)^2}}. \quad (1.8)$$

Hydrodynamic quantities corresponding to the burnt gas region [$z \geq \Phi(r, \varphi, t)$] will be assigned the index (+); those corresponding to the fresh gas region [$z \leq \Phi(r, \varphi, t)$] the index (-). With this convention,

$$\rho_+ = 1, \quad \rho_- = (1 - \gamma)^{-1}, \quad (1.9)$$

FLAME PROPAGATION IN ROTATING GAS

where

$$\gamma = \frac{\rho_- - \rho_+}{\rho_-} \quad (1.10)$$

is the thermal expansion coefficient of the gas.

Using (1.7), (1.9), we can transform conditions (1.5) and (1.6) to the following form, which will facilitate further treatment:

$$[\mathbf{v} \cdot \mathbf{n}] = \gamma, \quad (1.11)$$

$$[\mathbf{v} \times \mathbf{n}] = 0, \quad (1.12)$$

$$[p] = -\gamma. \quad (1.13)$$

For the sequel, it will also be convenient to introduce the reduced pressure

$$q = p - \frac{1}{2} \rho r^2 \omega^2 \quad (1.14)$$

by eliminating the centrifugal acceleration from Eqs. (1.1)-(1.3). In terms of the reduced pressure, condition (1.13) becomes

$$[q] = -\frac{1}{2} \omega^2 [\rho] r^2 - \gamma = \frac{\gamma \omega^2}{2(1-\gamma)} r^2 - \gamma. \quad (1.15)$$

SELECTION OF SCALINGS

In the absence of rotation ($\omega = 0$), one of the possible states of the system is a plane (p) flame:

$$\Phi'' = 0, \quad v_1'' = (0, 0, 1), \quad v_2'' = (0, 0, 1 - \gamma), \quad p_1'' = q_1'' = 1, \quad p_2'' = q_2'' = 1 - \gamma. \quad (2.1)$$

If the flame is propagating in a rotating tube, the plane flame can no longer be an equilibrium state of the system. Rotation-induced acceleration produces a radial flow which curves the flame front. However, if the thermal expansion of the gas is weak ($\gamma \ll 1$) the curving will be slight. Thus, one expects the equation for the flame front dynamics to be weakly nonlinear. The structure of this equation is largely determined by condition (1.7), which assumes a simpler form when $\gamma \ll 1$:

$$\Phi' + \frac{1}{2} (\nabla \Phi)^2 = v_1'' - 1. \quad (2.2)$$

Condition (1.15) suggests that when $\omega = O(1)$ the perturbation of the reduced pressure q due to rotation is of the order of magnitude of γ . It is natural to assume

that the perturbation of the velocity v due to rotation will be of the same order of magnitude. According to this estimate and (2.1), we introduce scaled quantities V_r^\pm , V_φ^\pm , V_z^\pm , Q^\pm :

$$\begin{aligned} v_r^\pm &= \gamma V_r^\pm, & v_\varphi^\pm &= \gamma V_\varphi^\pm, \\ v_z^\pm &= 1 + \gamma V_z^\pm, & v_z^- &= 1 - \gamma + \gamma V_z^-, \\ q^+ &= 1 + Q^+, & q^- &= 1 + \gamma + \gamma Q^-. \end{aligned} \quad (2.3)$$

Since $r \sim 1$ in terms of the selected nondimensional units, the relationships (2.2) and (2.3) suggest the following scalings for the time t and the front amplitude Φ :

$$\Phi = \sqrt{\gamma} F, \quad t = \tau / \sqrt{\gamma}. \quad (2.4)$$

In terms of the scaled variables (2.3), (2.4), we obtain from (1.1)–(1.4) the following equations for the principal term of the asymptotic expansion ($\gamma \ll 1$):

$$\frac{\partial V_r^\pm}{\partial z} + \frac{\partial Q^\pm}{\partial r} = 2\omega V_r^\pm, \quad (2.5)$$

$$\frac{\partial V_\varphi^\pm}{\partial z} + \frac{1}{r} \frac{\partial Q^\pm}{\partial \varphi} = -2\omega V_r^\pm, \quad (2.6)$$

$$\frac{\partial V_z^\pm}{\partial z} + \frac{\partial Q^\pm}{\partial z} = 0, \quad (2.7)$$

$$\frac{\partial V_r^\pm}{\partial r} + \frac{1}{r} \frac{\partial V_\varphi^\pm}{\partial \varphi} + \frac{\partial V_z^\pm}{\partial z} + \frac{V_r^\pm}{r} = 0. \quad (2.8)$$

Substituting $z = \Phi = \sqrt{\gamma} F$ in condition (1.11)–(1.13) and (1.7) and taking the zeroth approximation with respect to γ , we obtain the following conditions at $z = 0$:

$$V_r^+ = V_r^-, \quad V_r^+ = V_r^-, \quad V_z^+ = V_z^- \quad (2.9)$$

$$Q^+ - Q^- = G(r) = \frac{1}{2} \omega^2 r^2, \quad (2.10)$$

$$F_r + \frac{1}{2} (\nabla F)^2 = V_z^+, \quad (2.11)$$

Impermeability conditions are imposed at the tube walls ($r = 1$):

$$V_r^+ = V_r^- = 0 \quad \text{at} \quad r = 1. \quad (2.12)$$

We shall also assume that, far ahead of the flame front, the gas rotates as a rigid body. Thus, in a rotating coordinate system, we have the following conditions as $z \rightarrow -\infty$:

$$V_r^\pm \rightarrow 0, \quad V_\varphi^\pm \rightarrow 0, \quad V_z^\pm \rightarrow 0 \quad \text{as} \quad z \rightarrow -\infty. \quad (2.13)$$

DERIVATION OF THE FLAME-FRONT EQUATION

In the limit considered above, the flame front configuration $[z = F(r, \phi, \tau)]$ appears only in condition (2.11). Hence the gas flow is completely determined by Eqs. (2.5)–(2.8) and conditions (2.9), (2.10), (2.12) and (2.13)[†]. Since the problem possesses circular symmetry, the flow is independent of the angular coordinate ϕ .

Hence, we seek a solution of the linear system (2.5)–(2.8) in the form

$$\begin{aligned} V_z &= \sum_{n=1}^{\infty} \tilde{V}_z(z, k_n) J_0(k_n r), \\ V_r &= \sum_{n=1}^{\infty} k_n \tilde{V}_r(z, k_n) J_0'(k_n r), \\ V_\phi &= \sum_{n=1}^{\infty} k_n \tilde{V}_\phi(z, k_n) J_0'(k_n r), \\ Q &= \sum_{n=1}^{\infty} \tilde{Q}(z, k_n) J_0(k_n r), \end{aligned} \tag{3.1}$$

where, by condition (2.12),

$$J_0'(k_n) = 0. \tag{3.2}$$

We also express the right-hand side of (2.10) as a Fourier-Bessel expansion:

$$G(r) = \sum_{n=1}^{\infty} \tilde{G}(k_n) J_0(k_n r), \tag{3.3}$$

where

$$\tilde{G}(k_n) = \frac{2}{J_0^2(k_n)} \int_0^1 r G(r) J_0(k_n r) dr = \frac{2\omega^2}{J_0(k_n) k_n^2}. \tag{3.4}$$

Inserting (3.1) into the system (2.5)–(2.8) and the conditions (2.9), (2.10), we obtain:

$$\frac{d\tilde{V}_z^z}{dz} + \tilde{Q}^z = 2\omega \tilde{V}_\phi^z, \tag{3.5a}$$

$$\frac{d\tilde{V}_\phi^z}{dz} = -2\omega \tilde{V}_r^z, \tag{3.5b}$$

[†]The independence of the hydrodynamic field on the flame front configuration completely excludes the effect of spontaneous flame instability due to thermal expansion (Landau, 1944), which turns out here to be negligibly small compared with the effects of rotation.

$$\frac{d\tilde{V}_z^{\pm}}{dz} + \frac{d\tilde{Q}^{\pm}}{dz} = 0, \quad (3.5c)$$

$$\frac{d\tilde{V}_z^{\pm}}{dz} - k_n^2 \tilde{V}_r^{\pm} = 0. \quad (3.5d)$$

$$[\tilde{V}_z] = 0, \quad [\tilde{V}_r] = 0, \quad [\tilde{V}_\varphi] = 0, \quad [\tilde{Q}] = \tilde{G}, \quad (3.6)$$

$$\tilde{V}_r^- \rightarrow 0, \quad \tilde{V}_\varphi^- \rightarrow 0, \quad \tilde{V}_z^- \rightarrow 0, \quad \text{as } z \rightarrow -\infty. \quad (3.7)$$

The characteristic equation corresponding to the exponential solutions [$\sim \exp(pz)$] of the system (3.5) is

$$p^2(p^2 + 4\omega^2 - k_n^2) = 0. \quad (3.8)$$

Hence

$$p = 0 \quad \text{or} \quad p = \pm \sqrt{k_n^2 - 4\omega^2}. \quad (3.9)$$

Thus, one has two essentially different cases:

$$\text{i) } k_n^2 > 4\omega^2$$

and

$$\text{ii) } k_n^2 \leq 4\omega^2.$$

In case (i), taking condition (3.7) into account, we obtain from (3.5)–(3.6):

$$\begin{aligned} \tilde{V}_z^- &= \frac{\tilde{G}k_n^2}{2(k_n^2 - 4\omega^2)} \exp(\sqrt{k_n^2 - 4\omega^2} z), \\ \tilde{V}_z^+ &= -\frac{\tilde{G}k_n^2}{2(k_n^2 - 4\omega^2)} \exp(-\sqrt{k_n^2 - 4\omega^2} z) + \frac{\tilde{G}k_n^2}{(k_n^2 - 4\omega^2)}. \end{aligned} \quad (3.10)$$

In case (ii), Eqs. (3.5)–(3.7) give:

$$\begin{aligned} \tilde{V}_z^- &= 0, \\ \tilde{V}_z^+ &= -\frac{\tilde{G}k_n^2}{(k_n^2 - 4\omega^2)} \cos\sqrt{4\omega^2 - k_n^2} z + \frac{\tilde{G}k_n^2}{(k_n^2 - 4\omega^2)}. \end{aligned} \quad (3.11)$$

Thus,

$$\tilde{V}_z^+(0) = \begin{cases} \frac{\tilde{G}k_n^2}{2(k_n^2 - 4\omega^2)}, & k_n^2 > 4\omega^2 \\ 0, & k_n^2 \leq 4\omega^2. \end{cases} \quad (3.12)$$

Hence

$$V_r^2(r, 0) = \frac{1}{2} \sum_{k_n^2 > 4\omega^2} \frac{G(k_n)k_n^2}{(k_n^2 - 4\omega^2)} J_0^2(k_n r). \quad (3.13)$$

From (2.11) and (3.13) we obtain a single equation for the flame front dynamics

$$F_r + \frac{1}{2} (\nabla F)^2 = W(r), \quad (3.14)$$

where

$$W(r) = \sum_{4\omega^2 < k_n^2} \frac{\omega^2 J_0^2(k_n r)}{J_0(k_n) (k_n^2 - 4\omega^2)}, \quad (3.15)$$

and use have been made of (3.4) and (3.13).

Knowing $W(r)$, we look for solutions in a form of a progressive wave

$$F^{(0)} = -Vr + \psi(r) \quad (3.16)$$

where V and ψ are the equilibrium velocity and shape of the flame front, respectively. Substituting into (3.14) one obtains

$$\frac{1}{2} \psi_r^2 = W(r) + V. \quad (3.17)$$

In order for the solution $\psi(r)$ to exist over the entire tube cross-section $(0 < r < 1)$, the velocity V must satisfy the inequality

$$V \geq -W(r). \quad (3.18)$$

We assume that the actually realized situation corresponds to minimum flame propagation velocity, *i.e.*,

$$V = -\min W(r), \quad (0 < r < 1).$$

The need for this selection principle arises here because of the lack of natural boundary condition for the first order differential equation (3.14). This difficulty is easily eliminated if one introduces dissipative effects (diffusion and heat conduction) with the appropriate boundary conditions. Figures 2 and 3 exhibit the velocity V and the shape ψ of the flame front as functions of the parameter $4\omega^2$.

We note that V does not vary monotonically with increasing ω . As $4\omega^2$ approaches k_n^2 , the flame velocity undergoes an unlimited amplification. Near these resonance points the asymptotic approach proposed above is clearly not applicable. Description of the flame in the vicinity of these points requires special consideration. However, the non-monotonic behavior of the flame with increasing angular velocity is apparently captured correctly by our analysis. It would be interesting to conduct a systematic laboratory investigation of this phenomenon. As yet, to the best of our knowledge, the only experimental study in this area is the recent work of Chen, Liu and Sorhab (1987), devoted to the influence of rotation on counterflow premixed flames.

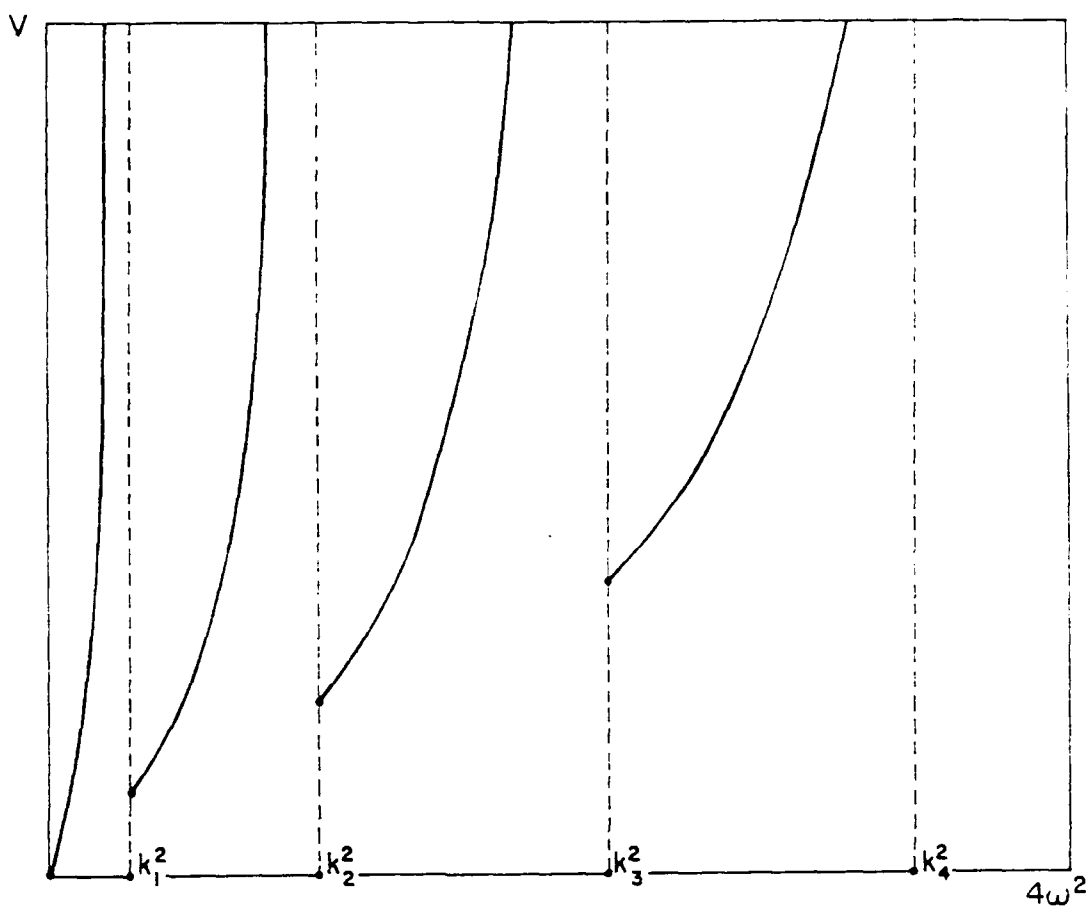


FIGURE 2 Flame velocity V as a function of the parameter $4\omega^2$.

THE CASE OF SLOW ROTATION

If $4\omega^2 < k_1^2$, it may be shown from (3.15) that $W(r)$ is a solution of the equation

$$\frac{d^2 W}{dr^2} + \frac{1}{r} \frac{dW}{dr} = \omega^2, \quad (4.1)$$

satisfying the additional conditions

$$\frac{dW(0)}{dr} = 0, \quad \int_0^1 rW(r)dr = 0. \quad (4.2)$$

Hence

$$W(r) = \frac{1}{4} + \frac{\omega J_0(2\omega r)}{4J_0'(2\omega)}. \quad (4.3)$$

FLAME PROPAGATION IN ROTATING GAS

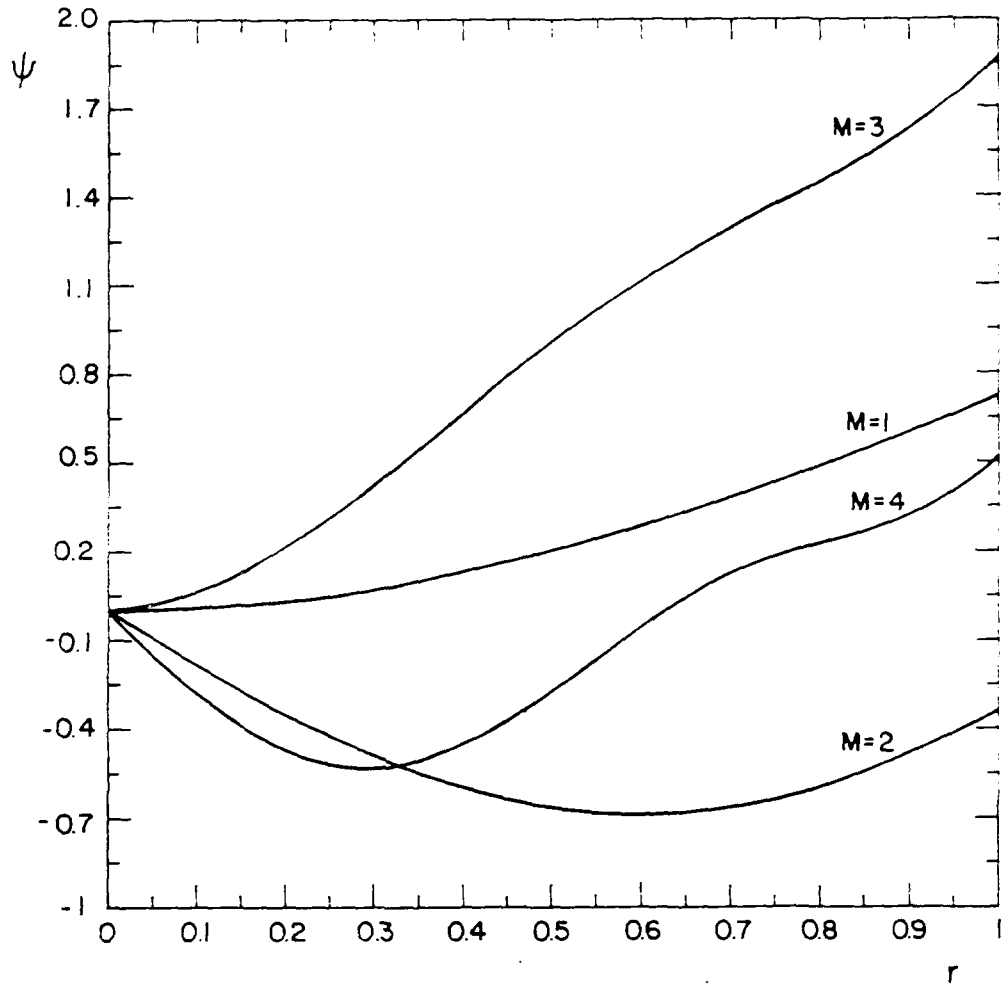


FIGURE 3. Flame front configuration for various values of the parameter $4\omega^2 = 3k_0^2 + k_1^2$ ($M=1, 2, 3, 4$).

If $\omega^2 \ll k_1^2$, this relationship simplifies to

$$W(r) = \frac{1}{4} \omega^2 \left(r^2 - \frac{1}{2} \right) \quad (4.4)$$

We then deduce from (3.14), (3.17) and (3.18) that

$$F^0 = -V\tau + \sqrt{V}r^2 \quad (4.5)$$

where $V = \omega^2/8$.

The stability of this solution will now be examined.

For a small perturbation $f = F - F^0$, Eq. (3.14) yields a linear equation

$$f_\tau + 2\sqrt{V}rf_r = 0, \quad f(r, 0) = f_0(r). \quad (4.6)$$

Here $f_0(r)$ is the initial perturbation. It follows from (4.6) that

$$f(r, \tau) = f_0(r) e^{-\lambda \tau}. \quad (4.7)$$

Thus, small perturbations are stretched and the flame front becomes smooth: the situation being similar to the one found in stagnation-point flow flames (Sivashinsky *et al.*, 1982), freely expanding flames (Sivashinsky, 1983) and upward propagating flames (Rakib and Sivashinsky, 1987).

It should be noted that when $4\omega^2 \ll k_1^2$ the effect of Coriolis acceleration turns out to be small compared with the effects of centrifugal acceleration, and the corresponding terms in Eqs. (1.1), (1.2) may be dropped.

THE EFFECT OF ROTATION ON CELLULAR INSTABILITY

Centrifugal acceleration creates a gradient of the tangential velocity which tends to smooth out any possible perturbations of the flame front. Thus, one may expect rotation to suppress diffusional-thermal (cellular) flame instability, frequently observed when the deficient reactant is of high mobility. We shall demonstrate this for the simple case of slow rotation considered in the previous section. As a first step, let us write the equation of the flame front (3.14), (4.4), in terms of dimensional variables denoted by (*):

$$\frac{\partial \Phi^*}{\partial t^*} + \frac{1}{2} U_b (\nabla \Phi^*)^2 = \frac{1}{4} \gamma \Omega^2 R^2 U_b^{-1} \left[\left(\frac{r^*}{R} \right)^2 - \frac{1}{2} \right], \quad (5.1)$$

where $\Omega = U_b \omega R$ is the dimensional angular velocity as noted earlier. Allowing for diffusional-thermal effects implies that these equations must be modified as follows (see Sivashinsky, 1983):

$$\frac{\partial \Phi^*}{\partial t^*} + \frac{1}{2} U_b (\nabla \Phi^*)^2 + \varepsilon D_{th} \nabla^2 \Phi^* + 4 D_{th} l_{th}^2 \nabla^4 \Phi^* = \frac{1}{4} \gamma \Omega^2 R^2 U_b^{-1} \left[\left(\frac{r^*}{R} \right)^2 - \frac{1}{2} \right], \quad (5.2)$$

where D_{th} is the thermal diffusivity of the gaseous mixture, l_{th} is the thermal thickness of the flame ($D_{th} = U_b l_{th}$) and $\varepsilon = (E/2R^0 T_b)(1 - Le)^{-1}$, with E the activation energy, R^0 the universal gas constant, T_b the adiabatic temperature of the combustion products, $Le = D_{tr}/D_{mol}$ the Lewis number and D_{mol} the molecular diffusivity of the deficient reactant.

Transforming to scaled nondimensional variables \tilde{F} , \tilde{r} , \tilde{t}

$$\Phi^* = \varepsilon l_{th} \tilde{F}, \quad r^* = 2l_{th} \tilde{r} / \sqrt{\varepsilon}, \quad t^* = 4l_{th} \tilde{t} / \varepsilon^2 U_b, \quad (5.3)$$

we bring Eq. (5.2) to the following form:

$$\tilde{F}_t + \frac{1}{2} \nabla \tilde{F}^2 + \nabla^2 \tilde{F} + \nabla^4 \tilde{F} = \lambda (\tilde{r}^2 - \frac{1}{2}) \quad (5.4)$$

where $\langle \cdot \rangle$ denotes the spatial average over the cross-section and

$$\lambda = 4\gamma \varepsilon^{-1} \Omega^2 l_{th}^2 U_b^2 \quad (5.5)$$

is the centrifugal acceleration parameter.

FLAME PROPAGATION IN ROTATING GAS

Figure 4(a, b, c) exhibits the results of a numerical solution of the axially-symmetric version of Eq. (5.4) in a tube $0 < \tilde{r} < 50$, with boundary conditions

$$\tilde{F}_r = 0, \quad (\nabla^2 \tilde{F})_r = 0, \quad \text{at } \tilde{r} = 50, \quad (5.6)$$

corresponding to the thermally insulated tube walls (Margolis and Sivashinsky, 1984). At $\lambda = 0$, *i.e.*, a freely propagating flame in a nonrotating channel, since $\varepsilon > 0$ the flame exhibits thermo-diffusive instability which manifest itself in the form of a wavy (cellular) surface (Figure 4a). At $\lambda = 0.001$, cellular structure is superimposed on the paraboloid profile induced by rotation (Figure 4b). Finally, when $\lambda = 0.005$, centrifugal acceleration totally suppresses the cellular structure (Figure 4c). The flame exhibits a smooth, paraboloid profile, as in the absence of diffusional-thermal instability, *i.e.*, when $\varepsilon < 0$.

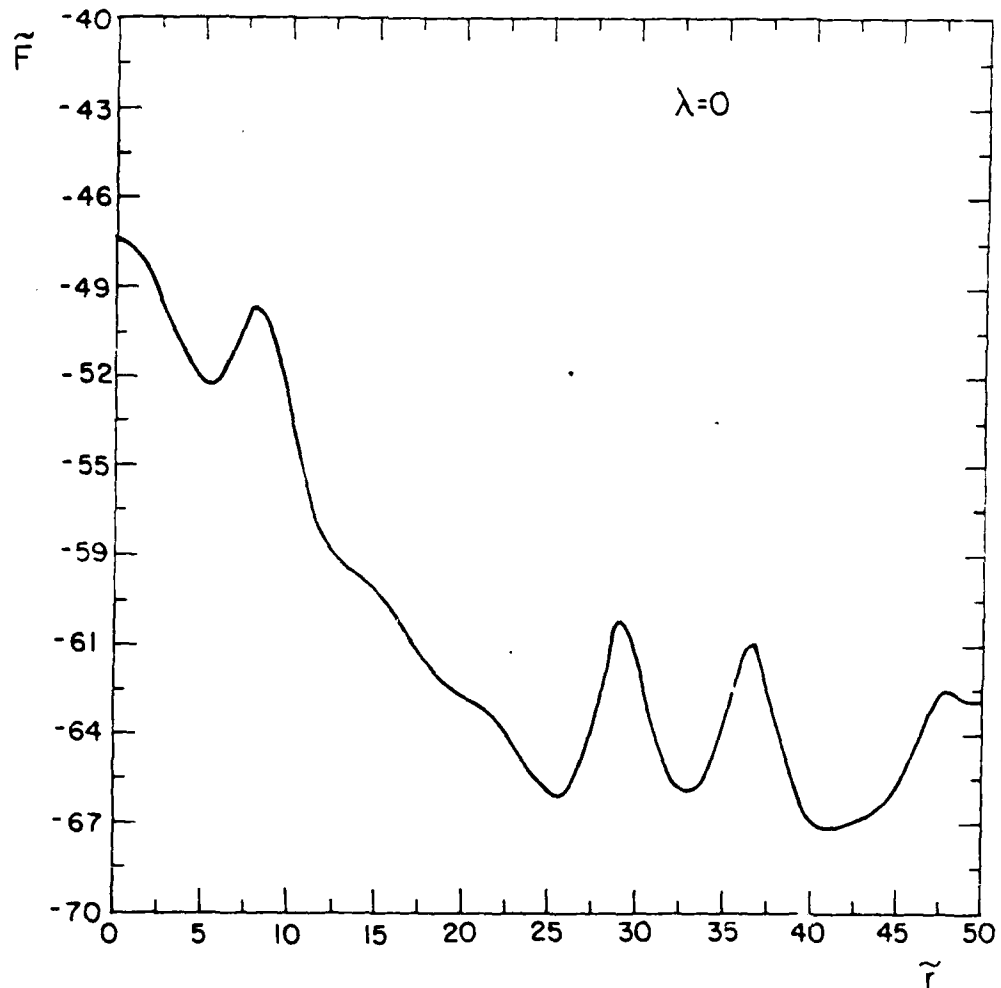


Fig. 4 (a)

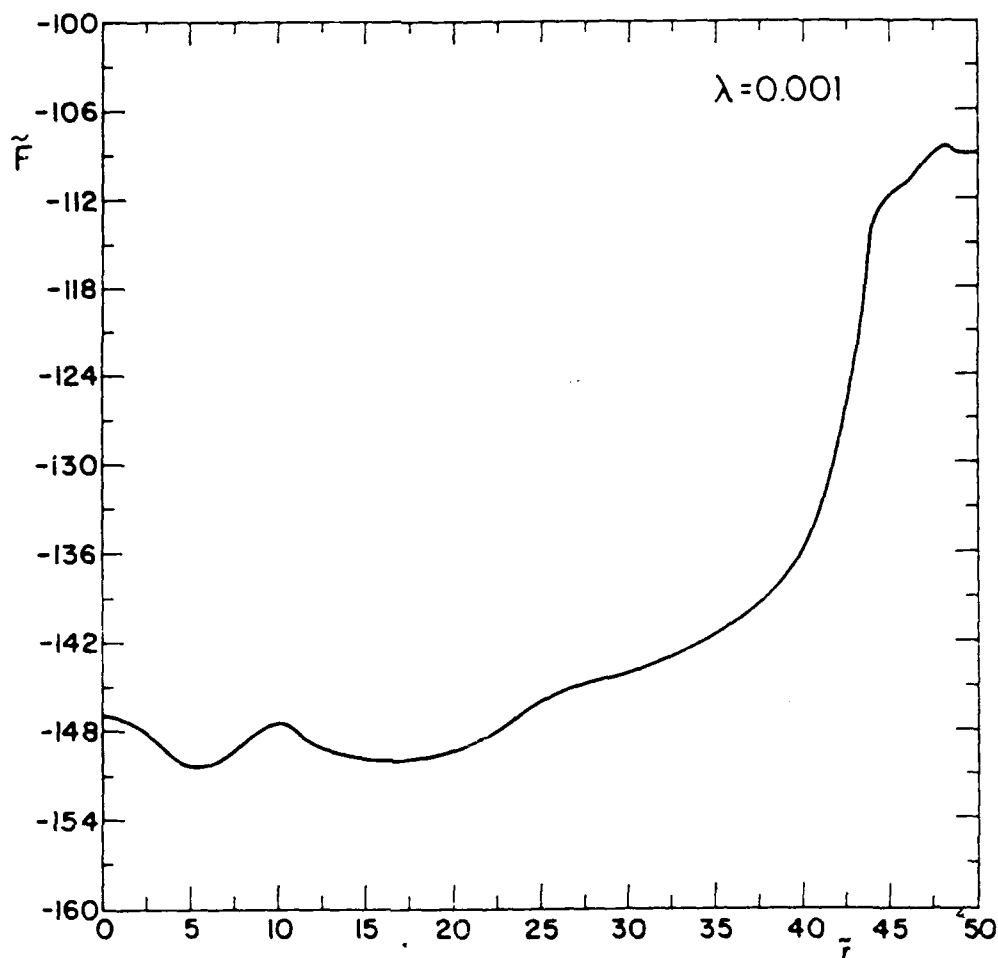


Fig. 4 (b)

EXPERIMENTAL OBSERVATIONS

The evolution of the flame front shown in Figure 4 is substantiated by our preliminary experiments performed on a rotating Bunsen burner. In the experiment, a cellularly unstable, polyhedral flame in rich butane/air mixture with volumetric fuel concentration of 6.6 percent is stabilized at the exit plane of the burner. The burner tube is made of pyrex and is 15 cm long with inside diameter of 2.0 cm, and the mean axial velocity of the gas over the cross-section is 44 cm/s. The tube is co-axially attached to a cylindrical burner which contains layers of small mesh screens and honeycombs and can be rotated by a DC-motor as described previously (Chen *et al.*, 1987). As the angular velocity Ω is increased, the cellular structure of the flame is observed to gradually diminish. At larger Ω , $\Omega \approx 9$ rps, the central position of the flame cone is flattened until it eventually becomes convex towards the unburnt gas. At still larger Ω , $\Omega = 12$ rps, the flame moves into the rotating tube and remains almost stationary near the middle, about 8 cm below the rim, and appears as an inverted smooth paraboloid. A direct

FLAME PROPAGATION IN ROTATING GAS

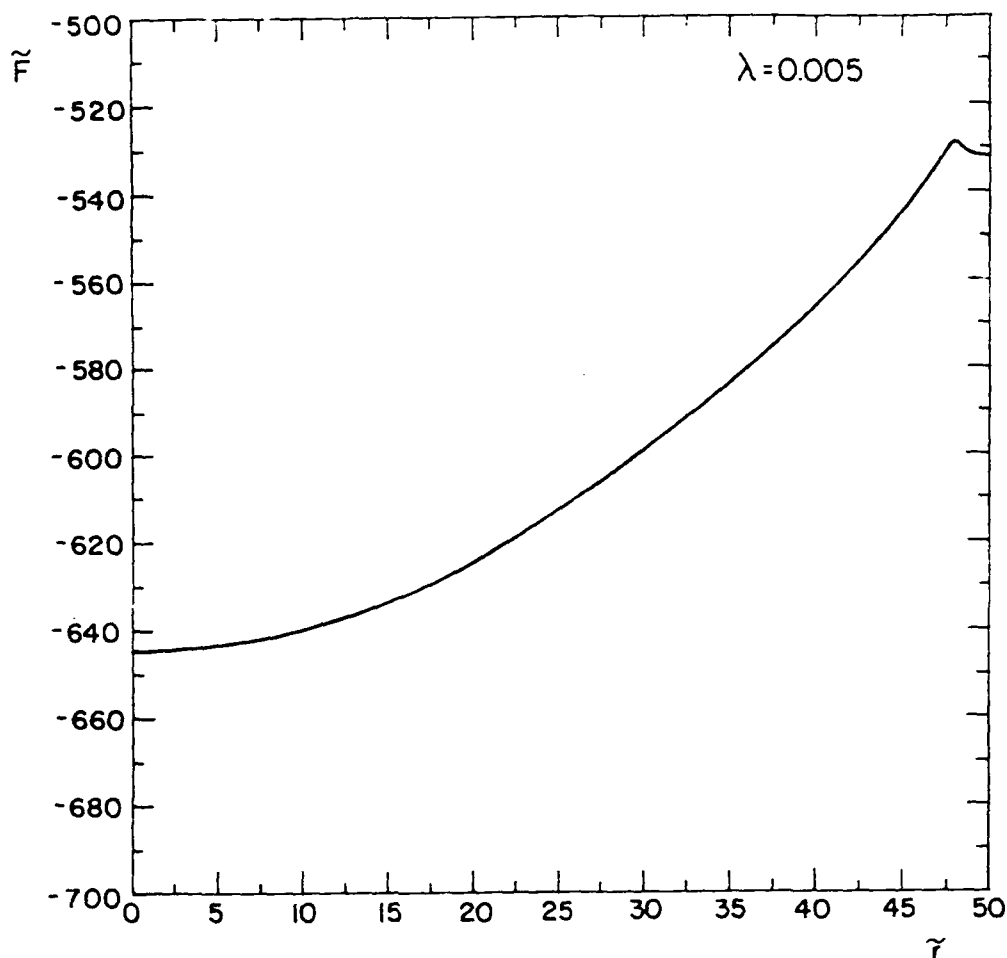


Fig. 4 (c)

FIGURE 4 Flame front configuration for various values of the parameter λ .

photograph of this flame is shown in Figure 5. Qualitatively similar observations were made for lean butane/air mixtures with the exception that the initial cellular structure was absent. The more complex peculiarities predicted for still larger values of Ω are as yet not observed because of limitation of the maximum angular velocity, $\Omega_{\max} = 29$ rps, of the DC-motor. Further studies of this interesting phenomena and experiments at larger Ω will be considered in the future.

FLAME PROPAGATION IN FREE SPACE

Hitherto we have been considering a flame propagating in a rotating tube. Under these conditions, the flame front is curved. It turns out that, if the walls are removed, a flame propagating in a rotating gas may remain planar. Moreover, the corresponding gas flow is described by a self-similar solution of the Euler equations, which can be constructed with no restrictions imposed on the parameter γ .

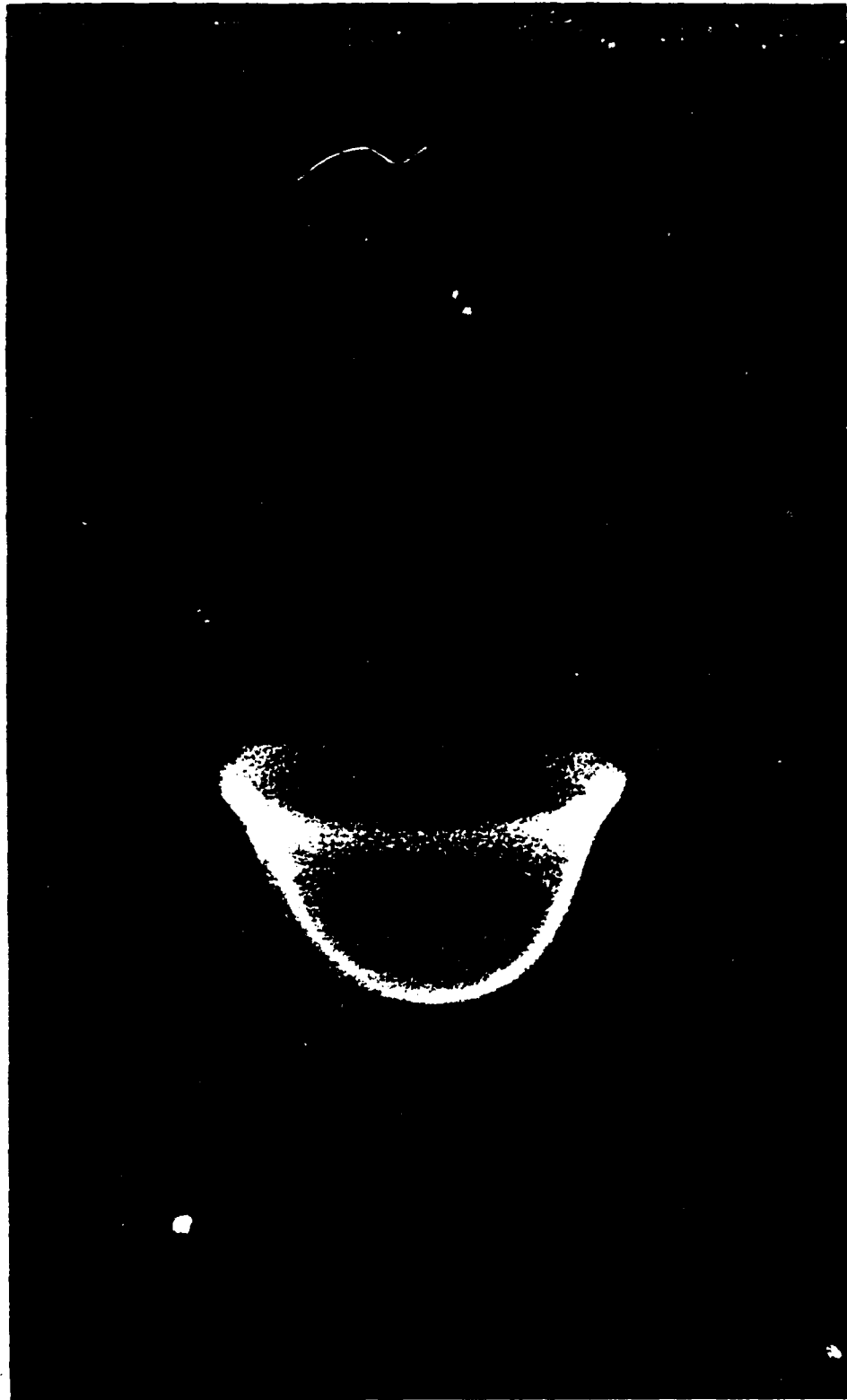


FIGURE 5 Rich butane/air flame in a rotating tube.

FLAME PROPAGATION IN ROTATING GAS

Let us assume that the flow in the region of the fresh mixture (in a rotating coordinate frame) is unidirectional:

$$\begin{aligned} \bar{v}_z^- &= 1 - \gamma, \quad \bar{v}_r^- = 0, \quad \bar{v}_\phi^- = 0, \\ \bar{q}^- &= \bar{p}^- - \frac{\omega^2 r^2}{2(1 - \gamma)} = \gamma. \end{aligned} \quad (6.1)$$

In the burnt-gas region, we seek a solution of the following form:

$$\begin{aligned} v_z^+ &= 2a(z), \quad v_r^+ = -a'(z)r, \quad v_\phi^+ = b(z)r, \\ q^+ &= p^+ - \frac{1}{2} \omega^2 r^2 = \frac{\gamma \omega^2}{2(1 - \gamma)} r^2 + c(z). \end{aligned} \quad (6.2)$$

At the flame front, which is assumed to be plane ($z = \Phi = 0$), we have the following conditions, derived from (1.5), (1.11), (1.12) and (1.15):

$$a(0) = 1/2, \quad a'(0) = 0, \quad b(0) = 0, \quad c(0) = 0. \quad (6.3)$$

Inserting (6.2) into the Euler equations (1.1)–(1.4), (1.14), we obtain

$$ab' - a'b = \omega a', \quad (6.4)$$

$$2aa'' - (a')^2 + b^2 + 2\omega b = \frac{\gamma \omega^2}{1 - \gamma}, \quad (6.5)$$

$$4aa' + c' = 0. \quad (6.6)$$

Note that here the continuity equation is automatically satisfied.
From (6.4), (6.6) and conditions (6.3), we obtain

$$b(z) = 2\omega a(z) - \omega. \quad (6.7)$$

$$c(z) = \frac{1}{2} - 2a^2(z). \quad (6.8)$$

Equations (6.7) and (6.5) yield a closed equation for $a(z)$:

$$2aa'' - (a')^2 + 4\omega^2 a^2 = \frac{\omega^2}{1 - \gamma}. \quad (6.9)$$

Hence the solution satisfying conditions (6.3) is

$$a(z) = \frac{1}{4(1 - \gamma)} (2 - \gamma - \gamma \cos 2\omega z). \quad (6.10)$$

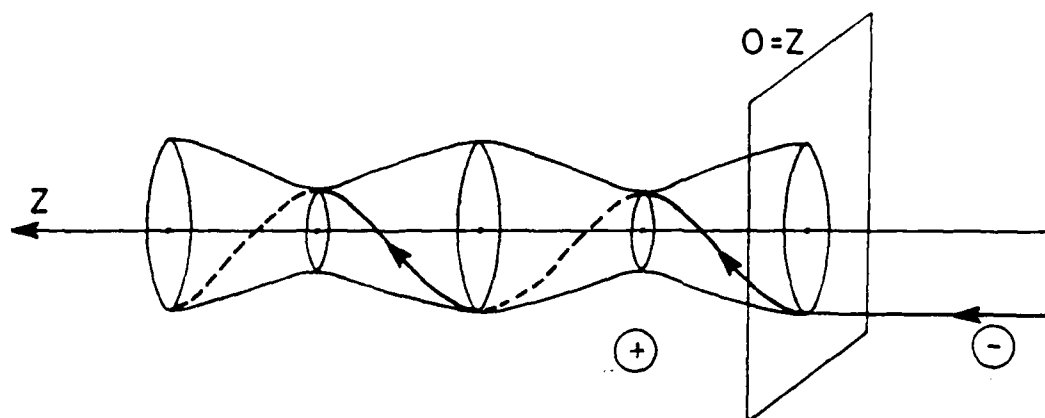


FIGURE 6 Streamline (represented by the solid line) in propagation of a plane flame in a rotating gas. The profile of the surface of revolution (6.11) is represented by a thin line.

The streamlines corresponding to the flow (6.2) are spirals winding around the surface of rotation [see Eq. (1.4)].

$$r = \frac{\text{const}}{\sqrt{a(z)}} \quad (6.11)$$

One of these streamlines and the corresponding surface (6.11) are illustrated in Figure 6.

CONCLUDING REMARKS

Using the weak thermal expansion approximation we derived an equation describing the dynamics of a flame propagating in a rotating tube. The velocity and shape of the equilibrium flame front were calculated. A discrete sequence of angular velocities are predicted near which the flame propagation velocity undergoes a considerable amplification. When the angular velocity of rotation is sufficiently high, we predict that cellular structure due to thermo-diffusive flame instability may be suppressed. The variation of the flame shape and the suppression of instabilities as a result of the rotation, were experimentally substantiated. We finally remark that, although the analysis assumes weak thermal expansion and in real flames density variations are quite appreciable, this limit may give a qualitatively correct description of some features of real flames.

ACKNOWLEDGEMENT

G. I. S. was supported in part by DOE grants DE-AC02-80ER-10559 and DE-FJ02-88ER13822 while visiting the Institute of Applied Chemical Physics (CCNY). M. M. was supported in part by NSF grants CBT-8521352 and DMS-8601903 and by DOE grant DE-FG02-87ER-25027. S. H. S. was supported by the Air Force Astronautics Laboratory, contract No. F04611-87-K-0067.

FLAME PROPAGATION IN ROTATING GAS

REFERENCES

- Chen Z. H., Liu G. E., and Sohrab S. H. (1987). Premixed flames in counterflow jets under rigid-body rotation. *Combust. Sci. and Tech.* **51**, 39.
- Landau, L. D. (1944). On the theory of slow combustion. *Acta Physicochim. URSS.* **19**, 77.
- Margolis, S. B., and Sivashinsky, G. I. (1984). Flame propagation in vertical channels: bifurcation to bimodal cellular flames. *SIAM J. Appl. Math.* **44**, 349
- Rakib, Z., and Sivashinsky, G. I. (1987). Instabilities in upward propagating flames. *Combust. Sci and Tech.*, to appear.
- Sivashinsky, G. I., Law, C. K., and Joulin, G. (1982). On stability of premixed flames in stagnation-point flow. *Combust. Sci. and Tech.* **28**, 155.
- Sivashinsky, G. I. (1983). Instabilities, pattern formation, and turbulence in flames. *Ann. Rev. Fluid. Mech.* **15**, 79.

APPENDIX V

Effect of Rotation on Bunsen Flame

W. J. SHEU, S. H. SOHRAB and G. I. SIVASHINSKY*

Department of Mechanical Engineering
Northwestern University
Evanston, Illinois 60208

Abstract

The influence of centrifugal accelerations on the form and stability of the Bunsen burner stabilized flame is studied. It is shown that as the angular velocity of rotation increases, the classical Bunsen cone first slightly buckles at the tip. Buckling then becomes more prominent and eventually the flame enters the burner. At sufficiently rapid rotation flame stabilization by the burner rim becomes impossible and the flame flashes back. The theoretical findings are in favorable agreement with the experimental observations made on a rotating Bunsen burner.

*Department of Applied Mathematics, Tel-Aviv University, Ramat Aviv, Israel.

I. INTRODUCTION

Flame propagation in situations of practical interest occurs as a rule, in turbulent flow fields and involves complex flame-flow interactions. One of the basic interactions of this type is that which is imposed by rotation of the gas flow crossing the flame front.

Recently, studying the influence of centrifugal and Coriolis accelerations on the shape, stability and extinction limits of premixed flames [1] (cf. also [2-5]), a number of new observations were made on a rotating Bunsen burner. Among other observations, it was found that flame stabilization by the burner rim is possible only at sufficiently low angular velocities. Under rapid rotation, the flame flashes back inside the burner tube.

As we show in this paper, the main features of the phenomena are describable within the framework of a simple mathematical model recently proposed in the study of premixed flames freely propagating in rotating tubes [5].

II. EXPERIMENTAL OBSERVATIONS

Premixed flames are stabilized at the rim of a 50 cm long pyrex tube with 11 (13) mm inner (outer) diameter. The tube is vertically supported at 20 and 30 cm from the rim and at the bottom by bearings and connected through a pulley-belt system to a DC-motor. The variable speed motor is calibrated such that a desired constant angular velocity in either CW or CCW direction can be maintained. To insure rigid-body rotation of the gas within the tube, three cylindrical layers of honeycomb, each 1 cm thick with 2 mm hexagonal holes, are successively positioned within the tube near the middle. The honeycombs also help to prevent flame flash-back into the inlet supply chamber. Butane (commercial grade) and air are respectively metered by soap-bubble meter and rotameter and fully mixed prior to introduction into the burner.

For lean flames, which have closed tips (Fig. 1a) it is found that the rotation first results in the buckling of the central region of the flame cone as shown in Fig. 1b. This flame corresponds to the fuel concentration (percent by volume), the mean velocity over the tube cross section $\Omega_F = 2.69$ (percent by volume), the mean velocity over the tube cross section $V = 122$ cm/s, and the burner angular velocity $\omega = 51$ RPS (rotations per second). At larger ω , the flame cone begins to enter the tube (Fig. 1c) and eventually at $\omega = 69$ RPS the flame flashes back into the tube and assumes the inverted conical shape shown in Fig. 1d. The inverted flame cone is convex towards the fresh gas with peripheries bending towards the tube walls, such that the flame surface near the walls is almost concave towards the fresh gas. When similar experiments are performed with a larger diameter tube, 20 mm, the transition from buckled state (Fig. 1b) to flash-back (Fig. 1d) occurs very rapidly. In such cases, direct photography of the intermediate state such as shown in Fig. 1c will be quite difficult.

The tip of the initial rich butane/air flames $\Omega_F = 5.60$, $V = 129$ cm/s and $\omega = 0$, is open [6-8] (Fig. 2a). As ω is increased to 44 RPS, the height of the original flame cone is reduced and a new inverted conical flame surface, convex towards the fresh gas, appears in the middle of the outer curtain-flame (Fig. 2b). The inner conical flame is separated from the outer flame by a dark ring of extinction region. As ω is further increased, the inner conical flame begins to enter the tube (Fig. 1c). Eventually, at $\omega = 50$ RPS, the inner conical flame flashes back into the tube while the outer flame

cone vanishes (Fig. 2d). Now, as opposed to the lean flame (Fig. 1d), the peripheries of the conical flame are nearly parallel to the tube wall.

III. MATHEMATICAL MODEL

In a recent study of the effects of centrifugal and Coriolis acceleration on the form and stability of a premixed flame freely propagating in a rotating tube, the following evolution equation for the asymptotic flame-front has been derived [5],

$$\frac{\partial F}{\partial t} + \frac{1}{2} v_n \left(\frac{\partial F}{\partial r} \right)^2 = D_{th} \frac{1}{2} \frac{\partial}{\partial r} \left(r \frac{\partial F}{\partial r} \right) + \frac{1}{4} \gamma \omega^2 v_n^{-1} \left(r^2 - \frac{1}{2} R^2 \right) \quad (3.1)$$

where $-z = F(r,t)$ is the flame front surface; v_n is the normal velocity of flame propagation; D_{th} is the thermal diffusivity of the gas; ω is the angular velocity of rotation; R is the radius of the tube; γ is the thermal expansion coefficient ($\gamma = (\rho_u - \rho_b)/\rho_b$); ρ_u, ρ_b - densities of the unburned and burned gas.

If the tube is thermally insulated, Eq. (3.1) should be solved subject to the boundary condition

$$\frac{\partial F}{\partial r} (R,t) = 0 \quad (3.2)$$

Equation (3.1) corresponds to the limit of weak thermal expansion ($\gamma \ll 1$) and slow rotation ($\omega R/v_n \ll 1$). For simplicity, the Lewis number is taken to be unity, since the basic features of the flame response to rotation (buckling and flash-lock) do not seem to be very sensitive to the composition of the mixture (Figs. 1 and 2). Equation (3.1) is written in the frame of reference in which the velocity of the oncoming gas flow v_∞ is equal to the normal flame speed v_n , i.e., $v_\infty = v_n$. For the subsequent analysis it is convenient to consider the flame front dynamics in the frame of reference where $v_\infty \neq v_n$.

The corresponding evolution equation is obtained from Eq. (3.1) via simple transformation

$$F = \tilde{F} - (v_\infty - v_n)t \quad (3.3)$$

Hence, the modified evolution equation reads

$$\frac{\partial F}{\partial t} + \frac{1}{2} v_n \left(\frac{\partial F}{\partial r} \right)^2 = D_{th} \frac{1}{r} \frac{\partial}{\partial r} \left(r \frac{\partial F}{\partial r} \right) + \frac{1}{4} \gamma \omega^2 v_n^{-1} \left(r^2 - \frac{1}{2} R^2 \right) + v_\infty - v_n \quad (3.4)$$

Replacing the adiabatic boundary condition (3.2) by

$$\tilde{F}(R,t) = 0 \quad (3.5)$$

one obtains the system describing an axisymmetric flame held inside the rotating tube, when the axial velocity of the oncoming flow is v . (Fig. 3a). With all its dissimilarity to the Bunsen burner (Fig. 3b) this system proves capable of capturing the main ingredients of the phenomenon observed in rotating Bunsen flames. Introducing new nondimensional variables

$$\Phi = \frac{v_n}{D_{th}} \tilde{F}, \quad \rho = \frac{r}{R}, \quad \tau = \frac{D_{th} t}{R^2} \quad (3.6)$$

the problem (3.4), (3.5), may be written as

$$\frac{\partial \Phi}{\partial \tau} + \frac{1}{2} \left(\frac{\partial \Phi}{\partial \rho} \right)^2 = \frac{1}{\rho} \frac{\partial}{\partial \rho} \left(\rho \frac{\partial \Phi}{\partial \rho} \right) + \lambda \left(\rho^2 - \frac{1}{2} \right) + \mu \quad (3.7)$$

$$\Phi(1,\tau) = 0 \quad (3.8)$$

where

$$\lambda = \frac{\gamma \omega^2 R^4}{4 D_{th}^2}, \quad \mu = \frac{(v_\infty - v_n) v_n R^2}{D_{th}^2} \quad (3.9)$$

IV. TRANSFORMATION TO LINEAR PROBLEM

For the further analysis it is convenient to make the following transformation

$$\Phi = -2 \ln |u| \quad (4.1)$$

which converts the nonlinear problem (3.7), (3.8) to the linear one:

$$\frac{\partial u}{\partial \tau} = \frac{1}{\rho} \frac{\partial}{\partial \rho} \left(\rho \frac{\partial u}{\partial \rho} \right) - \frac{1}{2} \left[\mu + \lambda \left(\rho^2 - \frac{1}{2} \right) \right] u = 0 \quad (4.2)$$

$$u(1, \tau) = 1 \quad (4.3)$$

To exclude singular solutions one has to impose the additional condition:

$$\frac{\partial u}{\partial \rho} (0, \tau) = 0 \quad (4.4)$$

The time-independent solution $u^{(0)}(\rho)$ of the problem (4.2), (4.3), and (4.4) corresponds to a steady configuration of the Bunsen flame $\Phi^{(0)}(\rho)$. For the subsequent arguments it is convenient to convert the problem (4.2-3) as

$$\frac{\partial u}{\partial s} = \frac{1}{\xi} \frac{\partial}{\partial \xi} \left(\xi \frac{\partial u}{\partial \xi} \right) + (L - \xi^2) u \quad (4.5)$$

$$\frac{\partial u}{\partial \xi} (0, s) = 0, \quad u(\rho' \sqrt{\lambda/2}, s) = 1 \quad (4.6)$$

where

$$\xi = 4\sqrt{\lambda/2} \rho, \quad s = \sqrt{\lambda/2} \tau, \quad (0 < \xi < 4\sqrt{\lambda/2}) \quad (4.7)$$

and

$$L = \frac{1}{2} \sqrt{\lambda/2} - \frac{\mu}{2} \sqrt{2/\lambda} \quad (\text{Fig. 4})$$

Let us consider an auxiliary time-independent problem

$$\frac{1}{\xi} \frac{d}{d\xi} \left(\xi \frac{dv^{(0)}}{d\xi} \right) + (L - \xi^2) v^{(0)} = 0 \quad (4.8)$$

$$v^{(0)}(0) = 1, \quad \frac{dv^{(0)}}{d\xi}(0) = 0, \quad 0 < \xi < \infty$$

Thus,

$$v^{(0)}(\xi) = u^{(0)}(\xi)/u^{(0)}(0) \quad (4.9)$$

For sufficiently small L (e.g. $L < 0$) $v^{(0)}(\xi)$ does not have zeros at $\xi > 0$ [9]. The zeros appear only at sufficiently large values of L . The first zero $\xi_1(L)$ of $v^{(0)}(\xi)$ emerges from $+\infty$ at L exceeding some critical value L_1 and then monotonically decreases to zero as $L \rightarrow \infty$ (Fig. 5). The point $\xi = \xi_1$ corresponds to the singularity of the function

$$\Phi^{(0)} = -2 \ln|u^{(0)}|. \quad (4.10)$$

For sufficiently small L , the function $\Phi^{(0)}(\xi)$ has no singularities in the interval $0 < \xi < 4\sqrt{\lambda/2}$. Since $\partial L/\partial \lambda > 0$ (Fig. 4), the interval $(0, 4\sqrt{\lambda/2})$ expands as L increases. Therefore, when λ exceeds some critical value λ_1 the first zero (singularity) $\xi = \xi_1$ will enter the interval $(0, 4\sqrt{\lambda/2})$. With further increase of the parameter λ , the second singularity $\xi_2 > \xi_1$ will enter the interval $(0, 4\sqrt{\lambda/2})$, then the third $\xi_3 > \xi_2$, and so on.

V. BASIC PROPERTIES OF THE EQUILIBRIUM SOLUTION

When μ is of order of unity, the transition from one equilibrium configuration $\Phi^{(0)}$ to another occurs quite gradually. However, in typical laboratory situations μ is a rather large parameter. Indeed, let $v_n = 25$ cm/s, $v_\infty = 1.5 v_n$, $R = 1$ cm, $D_{th} = 0.25$ cm²/s. Then, according to (3.9) $\mu = 5 \times 10^3$. In this case the buckling (i.e. change of sign of $\Phi_{pp}^{(0)}$) occurs at $\lambda = 2\mu = 10^4$. In this domain of parameters, even very small variations of μ and λ causes a drastic change in the flame front shape. This phenomena may be easily explained. Since $d\xi_1/dL \rightarrow \infty$ as $L \rightarrow L_1$ (Fig. 5), large ξ_1 is very sensitive to small variations in L (i.e. λ and μ). On the other hand, the singular solution emerges at $\xi_1 = 4\sqrt{\lambda/2}$, which is a gradually increasing function of λ . As a result, transition from a slightly buckled flame configuration to a singular one at sufficiently large λ occurs in an almost jump like manner.

Such strong parameter dependence (stiffness) of the rotating flames makes numerical (and laboratory) study of the system a rather difficult task. Figures (6,7) show some samples of the numerical experiments which we have performed. Figure 6 corresponds to flame configurations at $\lambda = 32$ and different values of L (i.e. μ). The buckling occurs at $L = 0$ ($\mu = 16$), the first singularity at $L \approx 2.25$ ($\mu \approx -2$), i.e. when the flow in the burner is lower than v_n (3.9).

Figures 7(a,b,c) show flame shapes at $\lambda = 2 \times 10^4$. The buckling emerges at $L = 0$ ($\mu = 10^4$). Transitions from the buckled state to the singular one occurs in virtually a discontinuous fashion somewhere between $L = 3.4935286$ and $L = 3.4935287$ (Fig. 7b). Double precision Runge-Kutta method was used for the numerical calculations, providing up to 20 significant figures, with local error

of about 10^{-10} . The integration was initiated from $R = 1$ to avoid the singular behavior at the axis of symmetry. In Figure 7c ($L = 20$, $\mu = 6 \times 10^3$) flame front exhibits several singular points.

As L increase singularities shown in Figures 7(b,c) actually appear first at the wall. The configuration represented by the curve 7(b) corresponds to the situation in which the singularity is already shifted from the wall towards the axis of the tube.

VI. STABILITY

It is not difficult to show that nonsingular configurations ($\lambda < \lambda_1(\mu)$, Sec. IV) are stable and singular ones ($\lambda < \lambda_1$) are not stable. Indeed, let us put

$$u(\xi, s) = u^{(0)}(\xi) + w(\xi, s) \quad (6.1)$$

where disturbance $w(\xi, s)$ is a solution of the problem

$$\frac{\partial w}{\partial s} = \frac{1}{\xi} \frac{\partial}{\partial \xi} \left(\xi \frac{\partial w}{\partial \xi} \right) + (L - \xi^2)w = 0 \quad (6.2)$$

$$w_{\xi}(0, s) = 0 \quad , \quad w(4\sqrt{\lambda/2}, s) = 0$$

$w(\xi, s)$ may be sought in the form

$$w(\xi, s) = \sum_{n=1}^{\infty} w_n(\xi) e^{\sigma_n s} \quad (6.3)$$

One obtains the following eigenvalue problem for $w_n(\xi)$

$$\frac{1}{\xi} \frac{d}{d\xi} \left(\xi \frac{dw_n}{d\xi} \right) + (\Lambda_n - \xi^2)w_n = 0 \quad (6.4)$$

where $w_n'(0) = 0 \quad , \quad w_n(0) = 0$

$$\Lambda_n = L - \sigma_n \quad , \quad L = \frac{1}{2} \sqrt{\lambda/2} - \frac{\mu}{2} \sqrt{2/\lambda} \quad (6.5)$$

It is known from the general Sturm-Liouville Theory [9], $w_n(\xi)$ has $(n-1)$ zeros in the interval $(0, 4\sqrt{\lambda/2})$ and $\Lambda_{n+1} > \Lambda_n$ (or $\sigma_{n+1} < \sigma_n$). Hence, as follows from the results of Sec. IV,

$$\Lambda_1 = L - \sigma_1 > \lambda \text{ or } \sigma_1 < 0 \text{ for } \lambda < \lambda_1 \quad (6.6)$$

Thus, $\sigma_n < 0$ for any n , and therefore at $\lambda < \lambda_1$ the equilibrium solutions are stable. For the same reason at $\lambda > \lambda_1$

$$\Lambda_1 = L - \sigma_1 < L \text{ or } \sigma_1 > 0 \quad (6.7)$$

Therefore, at $\lambda > \lambda_1$ the equilibrium solution will be unstable at least to the disturbances corresponding to the first eigenfunction $w_1(\xi)$. In other words, all the equilibrium configurations involving singularities (Fig. 7c) are unstable.

Let us now look at the nonlinear evolution of the perturbed solution $\Phi^{(0)}(\xi)$ in the case of instability

$$\Phi(\xi, s) = -2\ln|u(\xi, s)| = -2\ln\left|u^{(0)}(\xi) + \sum_{n=1}^{\infty} w_n(\xi)e^{\sigma_n s}\right|. \quad (6.8)$$

Since $\sigma_n > \sigma_{n+1}$,

$$\Phi(\xi, s) \simeq -2\ln|u^{(0)}(\xi) + w_1(\xi)e^{\sigma_1 s}| \quad (6.9)$$

as $s \rightarrow \infty$. Hence, outside of the boundary layer (near $\xi = 4\sqrt{\lambda/2}$, (6.9) yields

$$\Phi(\xi, s) \simeq -2\sigma_1 s \quad \text{as } s \rightarrow \infty \quad (6.10)$$

Thus, at $\lambda > \lambda_1$ as a result of instability flame flashes back into the burner tube. Flame stabilization by the burner rim is possible only at sufficiently slow rotation.

VII. CONCLUDING REMARKS

The proposed mathematical model shows that the observed buckled flames (Figs. 1,2) emerge not as a result of an instability of the classical Bunsen cone, but as the only possible equilibrium configuration. The pertinent smooth solutions, however, exist only at sufficiently slow rotations. When the angular velocity ω exceeds a critical value ω_c smooth solutions are replaced by oscillating singular solutions (Fig. 7c). The singular solutions (unlike the smooth ones) are, however, unstable. Thus, at $\omega > \omega_c$ and fixed velocity of the oncoming flow (v_*), flame stabilization in a rotating tube becomes impossible and the flame flashes back.

The physical reason for the flashback is quite simple. If $\omega > \omega_c$ the rate of fuel supply (v_*) turns out to be insufficient to provide equilibrium flame configuration in the gas such that the flame breaks away towards the oncoming flow of the fresh mixture.

To verify this interpretation in a more formal way it is instructive to consider flame stabilization in a wide tube, where the dissipative effects (D_{th}) may be ignored. The corresponding mathematical problem is thus reduced to consideration of the first order differential equation

$$\frac{1}{2} v_n \left(\frac{d\tilde{F}}{dr} \right)^2 = \frac{1}{4} \gamma \omega^2 v_n^{-1} \left(r^2 - \frac{1}{2} R^2 \right) + v_\infty - v_n \quad (7.1)$$

Equation (7.1), as is readily seen, admits a real-valued solution (defined over the entire cross section of the tube, $0 < r < R$) only at

$$\omega < \omega_g = \frac{2}{R} \sqrt{2v_n \gamma^{-1} (v_\infty - v_n)} \quad (7.2)$$

It is interesting that at small nonzero D_{th} , the real-valued equilibrium solutions of Eq. (3.4) survive at $\omega > \omega_g$ due to the 'tunnel effect', i.e., emergence of high frequency singular solutions. These solutions are, however, dismissed via stability arguments (Sec. VI).

Acknowledgement

This research was supported by Air Force Astronautics Laboratory under Contract No. F04611-87-K0067 and DOE Grant DE-FG02-88ER13822.

REFERENCES

1. Bidinger, D. F. and Sohrab, S. H. (1985) unpublished.
2. Chen, Z. H., Liu, G. E., and Sohrab, S. H. (1987) Combust. Sci. and Tech. 51, 39-50.
3. Lin, T. H. and Sohrab, S. H. (1987) Combust. Sci. and Tech. 52, 73-79.
4. Sivashinsky, G. I. and Sohrab, S. H. (1987) Combust. Sci. and Tech. 53, 67-74.
5. Sivashinsky, G. I., Rakib, Z., Matalon, M., and Sohrab, S. H. (1987) Combust. Sci. and Tech., to appear.
6. Sivashinsky, G. I. (1975) J. Chem. Phy. 62(2), 638-643.
7. Buckmaster, J. D. (1979) Combust. Sci. and Tech. 20, 33.
8. Mizomoto, M., Asaka, Y., Ikai, S., and Law, C. K. (1984) 19th Symposium (Int.) on Combustion. The Combustion Institute, Pittsburgh, p. 1933.
9. Courant, R. and Hilbert, D. (1953) Methods of Mathematical Physics. John Wiley, New York, Vol. 1.

Figure Captions

- Figure 1. Direct photographs of lean butane/air Bunsen flames with $\Omega_F = 2.69$ and (a) $\omega = 0$. (b) $\omega = 51$ RPS (c) $\omega = 69$ RPS (d) $\omega = 69$ RPS.
- Figure 2. Direct photographs of rich butane/air Bunsen flames (a) $\Omega_F = 5.6$, $\omega = 0$ (b) $\Omega_F = 5.6$, $\omega = 44$ RPS (c) $\Omega_F = 5.6$, $\omega = 50$ RPS (d) $\Omega_F = 7.12$, $\omega = 67$ RPS.
- Figure 3. Diagram illustrating Bunsen flames stabilized inside the tube (a) and at the rim of the burner (b) under absence of rotation.
- Figure 4. The λ -dependence of the parameter L .
- Figure 5. The L -dependence of the first zero ξ_1 of the function $v^{(0)}(\xi)$.
- Figure 6. Flame configurations at $\lambda = 32$ and different values of the parameter L .
- Figure 7a. Stable flame configurations with $\lambda = 2 \times 10^4$ and $L < L_c = 3.49357287$.
- Figure 7b. Transition from (1) stable, $L = 3.49357286$ to (2) unstable, $L = 3.49357287$ flame configuration at $\lambda = 2 \times 10^4$.
- Figure 7c. Unstable flame with multiple singular points with $\lambda = 2 \times 10^4$, $L = 20$.

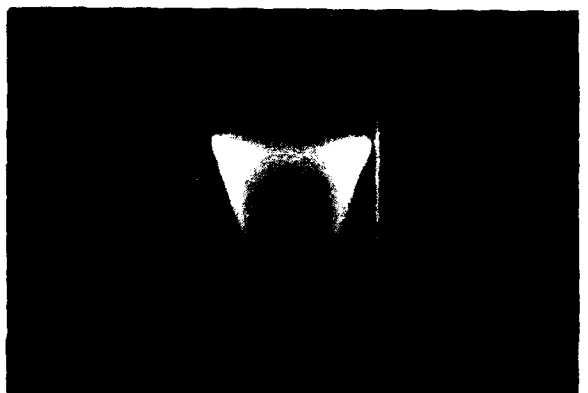
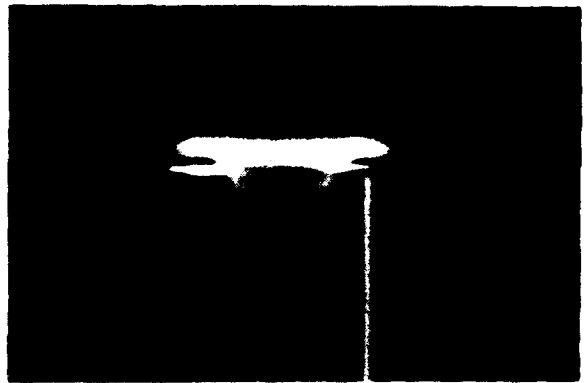


Figure 1.

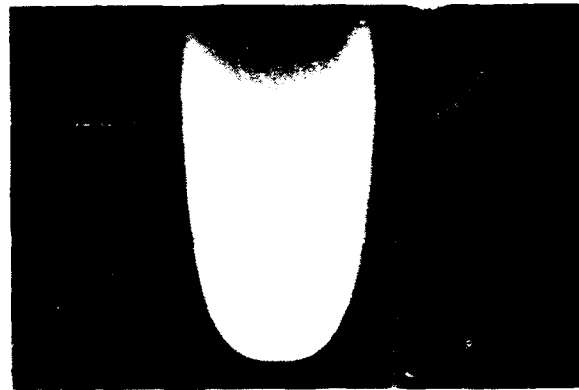
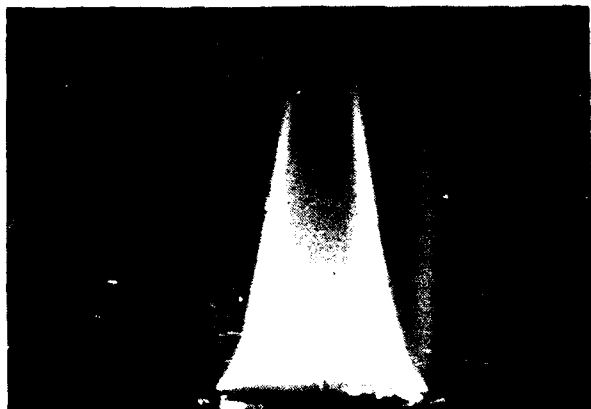
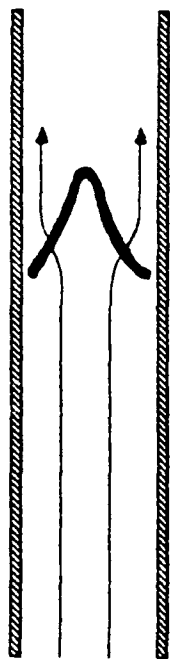
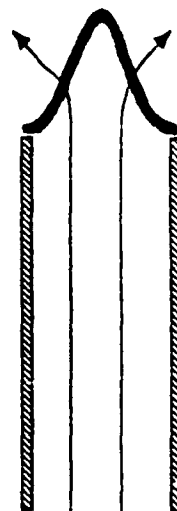


Figure 2.



(a)



(b)

Figure 3.

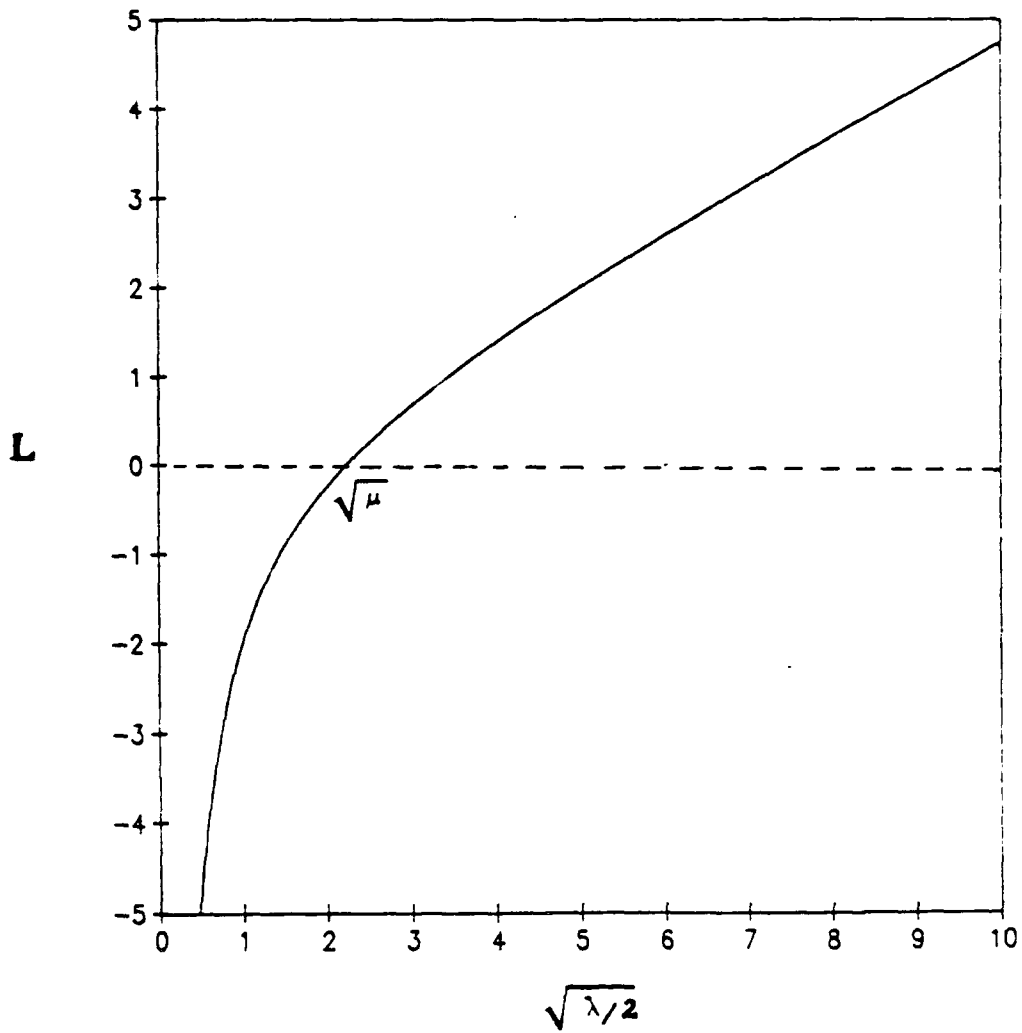


Figure 4.

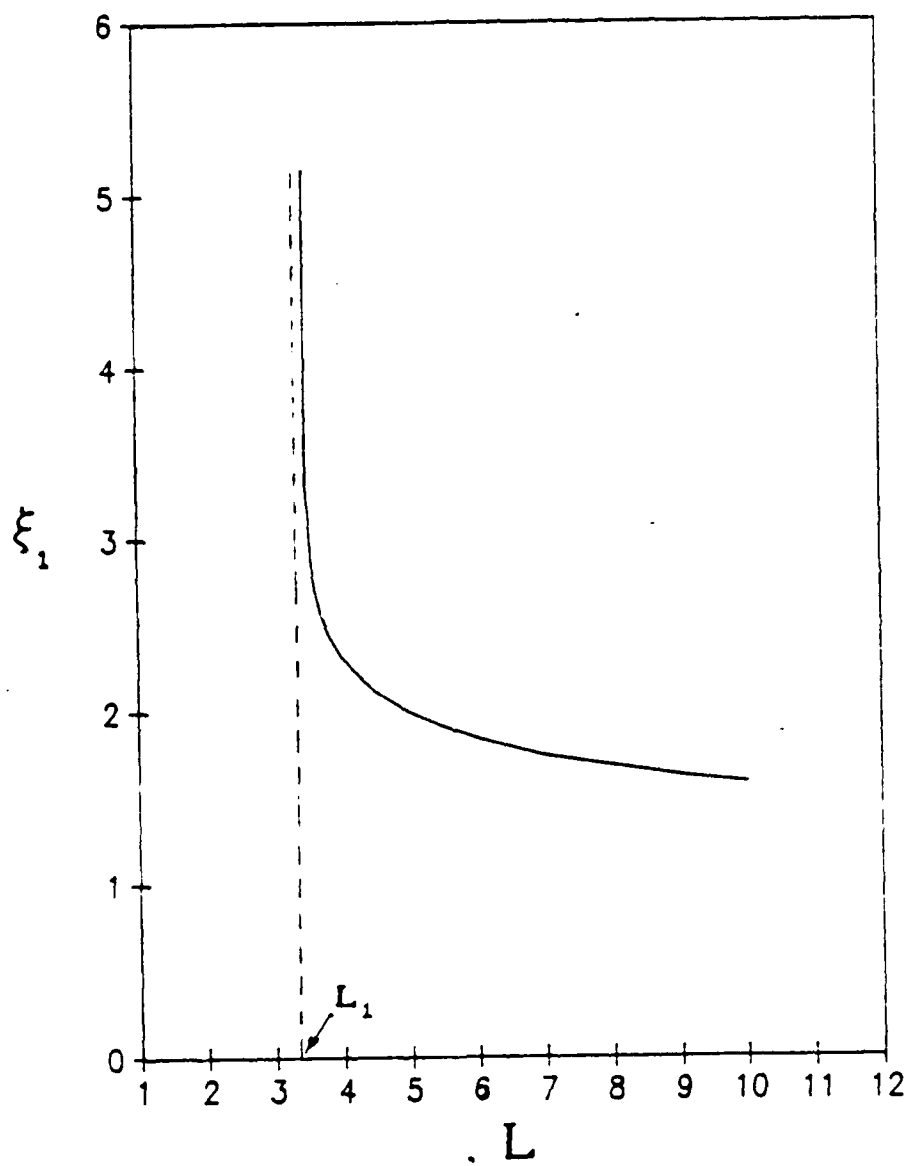


Figure 5.

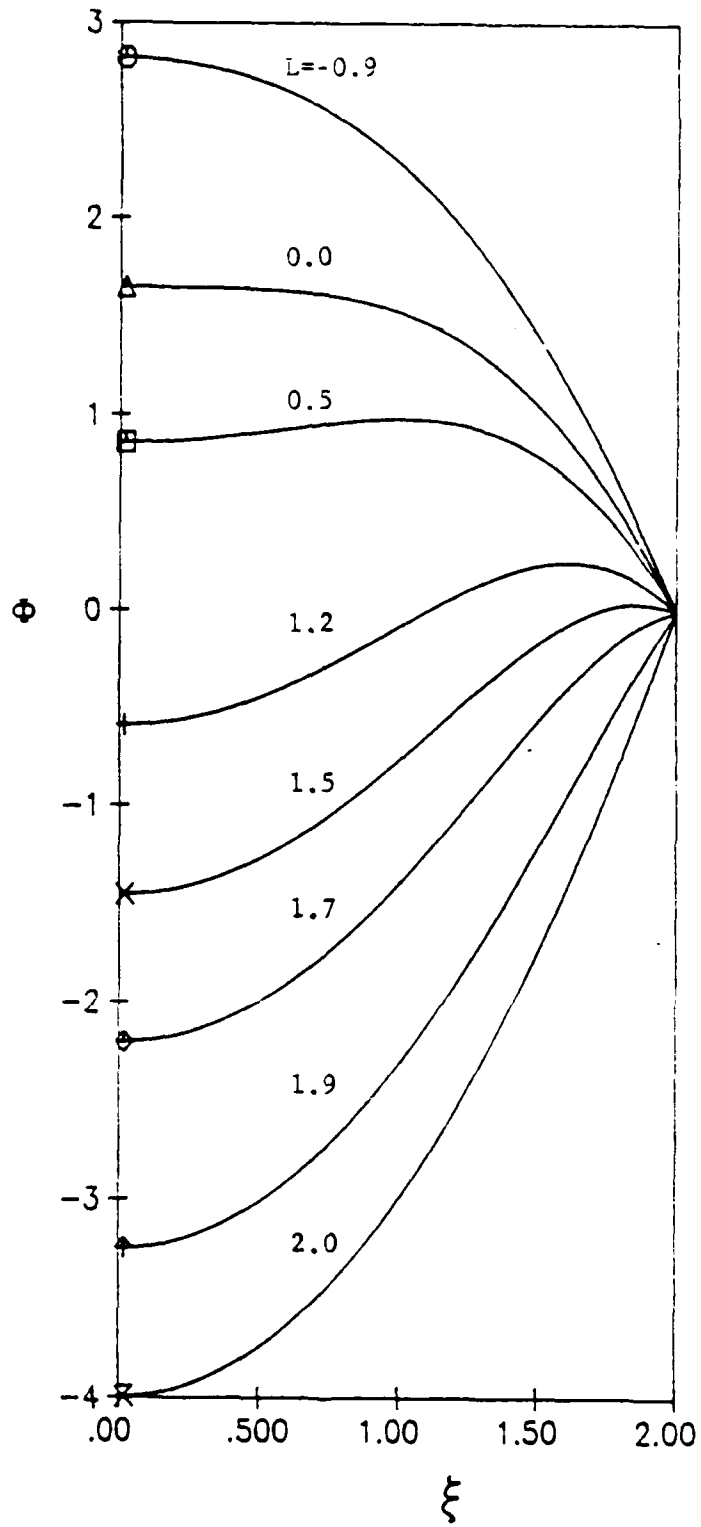


Figure 6.

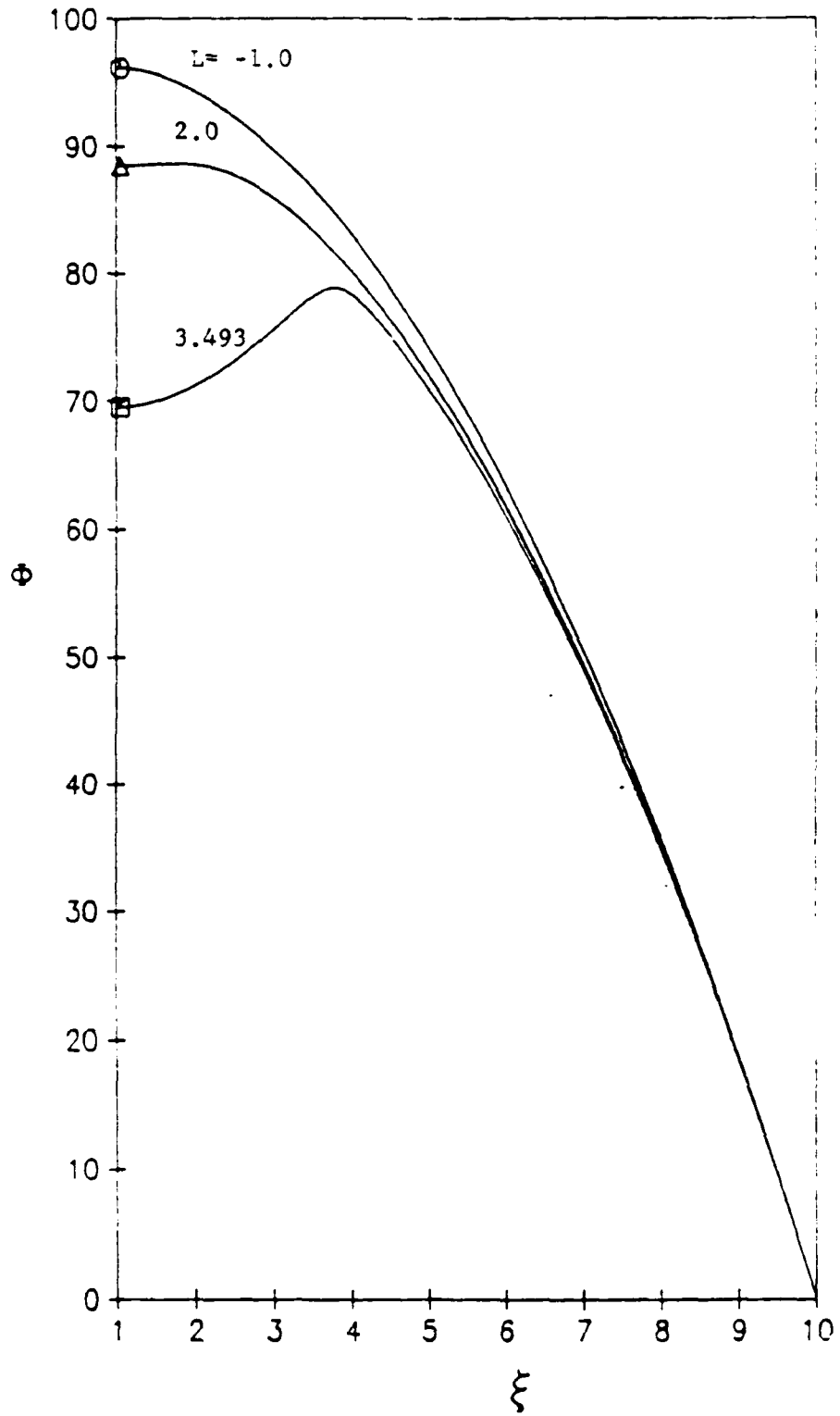


Figure 7a.

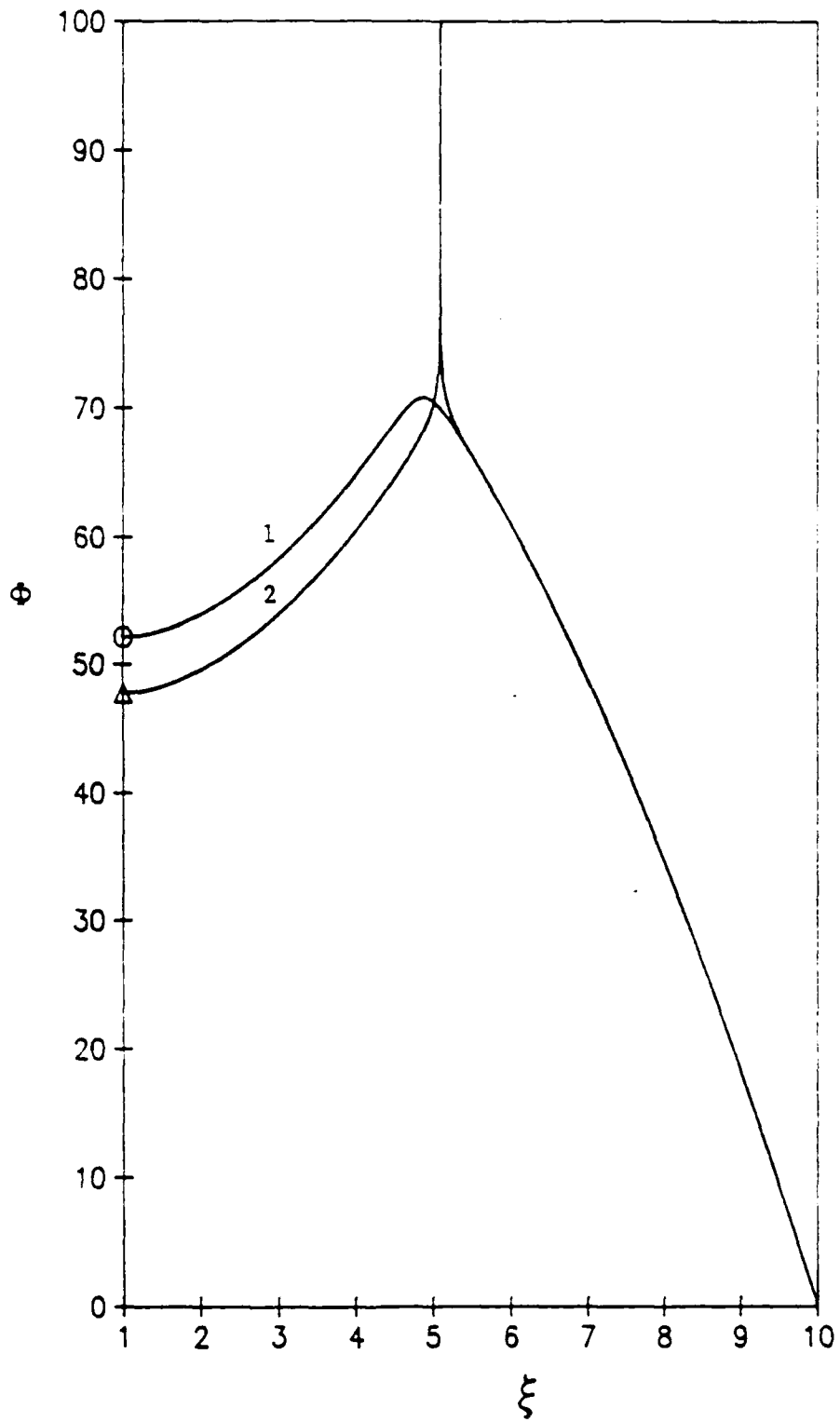


Figure 7b.

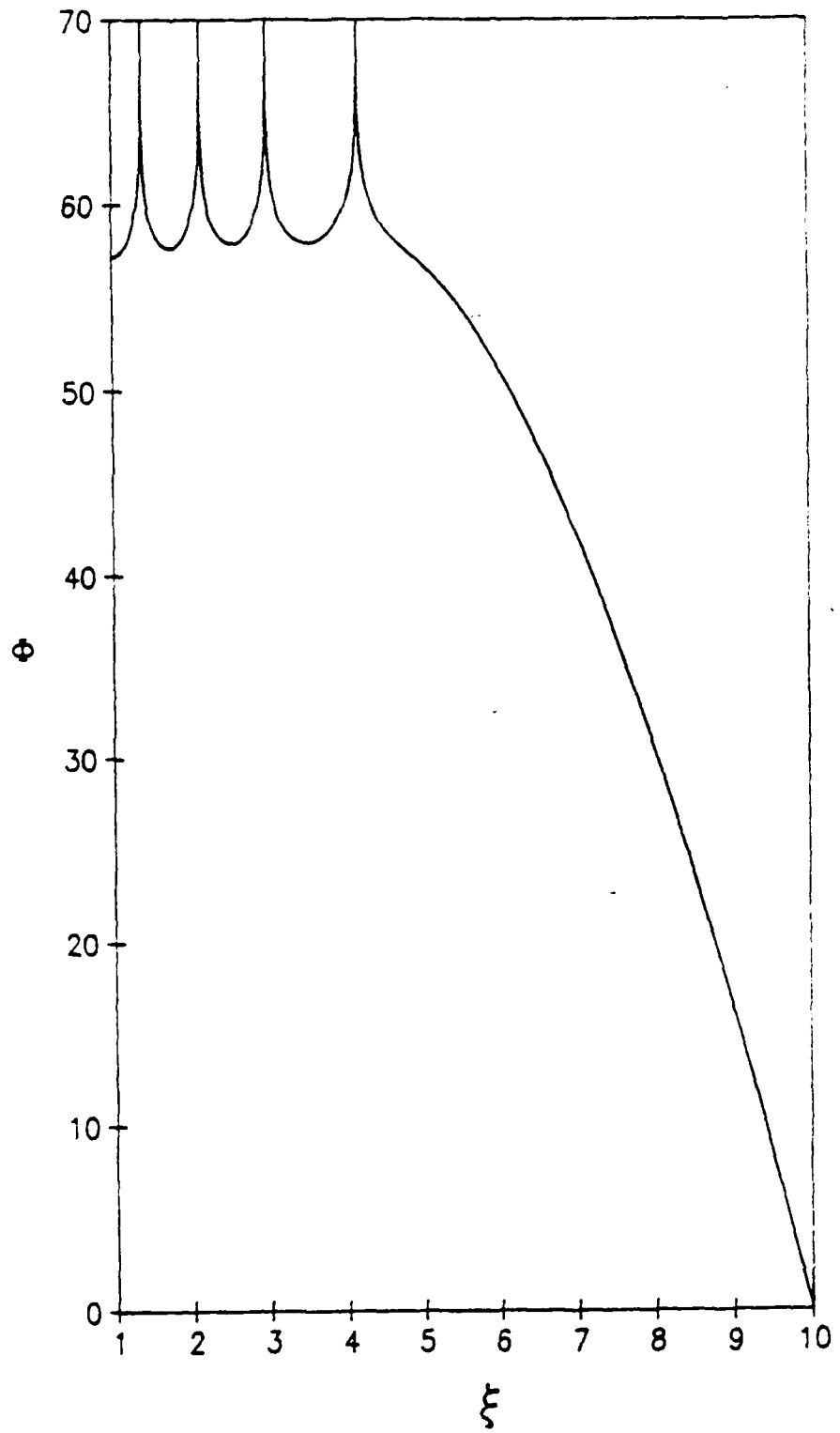


Figure 7c.

**NONPLANAR FLAME CONFIGURATIONS IN
STAGNATION POINT FLOW**

W. J. SHEU and G. I. SIVASHINSKY..

**Department of Mechanical Engineering
Northwestern University
Evanston, Illinois 60208 USA**

**School of Mathematical Sciences
Tel-Aviv University
Ramat-Aviv**

Tel-Aviv 69978, ISRAEL

ABSTRACT

Premixed flames stabilized in stagnation point flow are considered. It is shown that this classical flow field is capable of sustaining, apart from the known planar flames, also some nonplanar flame configurations similar to those recently observed in experiments.

1. INTRODUCTION

Stagnation point flow is one of the most convenient hydrodynamic systems for experimental and theoretical studies of premixed laminar flames. The remarkable feature of the stagnation point flow is that being essentially nonuniform it is capable of sustaining ideally planar flame fronts. However, recent experimental observations of Ishizuka, Miyasaka and Law (1982), Ishizuka and Law (1982) have shown that the stagnation point flow may stabilize also some nonplanar flame configurations. One of these new possibilities of the flame equilibrium is shown on Figure 1.

The present paper is aimed to show that the nonplanar equilibrium flame configurations are indeed admissible by the classical stagnation point flow field.

2. MATHEMATICAL MODEL

Consider the idealized scheme of Figure 2 in which the axisymmetric jet of the stagnation point flow field is assumed to be infinitely wide in diameter but of finite length (h). The coordinate frame is chosen in such a way that $z = 0$ corresponds to the stagnation plane. Assuming for simplicity the gas to be incompressible, the corresponding axisymmetric flow field $\vec{v} = (v_r, v_z)$ is given by

$$\begin{aligned}v_r &= V \left(\frac{r}{h} \right) \left[1 + \left(\frac{r}{h} \right) \right] \\v_z &= -V \left(\frac{z}{h} \right) \left[1 + \left(\frac{z}{h} \right) \right]\end{aligned}\tag{2.1}$$

where V is the velocity of the oncoming gas flow (at $z = -h$, Figure 2).

Define the flame as a geometrical surface, $F(r,z,t) = 0$, propagating relative to the gas flow with a prescribed speed V_0 .

The flame front evolution equation may then be written as

$$\vec{v} \cdot \vec{n} - D = -V_0\tag{2.2}$$

where

$$D = \frac{F_t}{|\nabla F|}\tag{2.3}$$

is the flame velocity relative to the fixed frame of coordinates (r,z) and

$$\vec{n} = -\frac{\nabla F}{|\nabla F|} \quad (2.4)$$

is the normal to the flame front.

To avoid dealing with implicit functions let us specify $F(r,z,t)$ in two different ways

$$F(r,z,t) = z - \phi(r,t) \quad (2.5)$$

and

$$F(r,z,t) = r - \psi(r,t) \quad (2.6)$$

In the first case

$$\vec{n} = \frac{(\phi_r, -1)}{\sqrt{1 + \phi_r^2}}, \quad D = -\frac{\phi_t}{\sqrt{1 + \phi_r^2}} \quad (2.7)$$

while in the second

$$\vec{n} = \frac{(-1, \psi_r)}{\sqrt{1 + \psi_r^2}}, \quad D = -\frac{\psi_t}{\sqrt{1 + \psi_r^2}} \quad (2.8)$$

Hence the evolution equation (2.2) may be written either as

$$\begin{aligned} v_r \phi_r - v_t + \dots &= -V_o \sqrt{1 + \phi_r^2} \\ (z = \phi(r,t)) \end{aligned} \quad (2.9)$$

or as

$$\begin{aligned} -v_r + v_z \psi_z + \psi_t &= -V_o \sqrt{1 + \psi_r^2} \\ (r = \psi(z,t)) \end{aligned} \quad (2.10)$$

Substituting (2.1), Eqs. (2.9) and (2.10) yield

$$V\left(\frac{r}{h}\right) \left[1 + \left(\frac{\phi}{h}\right)\right] \phi_r + V\left(\frac{\phi}{h}\right) \left[2 + \left(\frac{\phi}{h}\right)\right] + \phi_t = -V_o \sqrt{1 + \phi_r^2}, \quad (2.11)$$

$$-V\left(\frac{\psi}{h}\right) \left[1 + \left(\frac{z}{h}\right)\right] - V\left(\frac{z}{h}\right) \left[2 + \left(\frac{z}{h}\right)\right] \psi_z + \psi_t = -V_o \sqrt{1 + \psi_r^2} \quad (2.12)$$

Introduce the nondimensional quantities

$$\rho = z/h, \quad \xi = z/h, \quad \Phi = \phi/h, \quad \Psi = \psi/h, \quad (2.13)$$

$$\tau = V_0 t/h, \quad Q = VN_0 > 1$$

In terms of the new variables Eqs. (2.11) and (2.12) become

$$\Phi_\tau + \sqrt{1 + \Phi_\rho^2} + Q\rho(1 + \Phi)\Phi_\rho + Q\Phi(2 + \Phi) = 0 \quad (2.14)$$

$$\Psi_\tau + \sqrt{1 + \Psi_\xi^2} - Q\Psi(1 - \xi) - Q\xi(2 + \xi)\Psi_\xi = 0 \quad (2.15)$$

3. EQUILIBRIUM CONFIGURATIONS OF THE FLAME FRONT

From now on we confine ourselves to the study of the time-independent flame configurations only, i.e., we set $\Phi_\tau = \Psi_\tau = 0$. Equation (2.14) then yields

$$\Phi_\rho = \frac{Q^2\Phi^2(2 + \Phi)^2 - 1}{\sqrt{Q^2\Phi^2(2 + \Phi)^2 + Q^2\rho^2(1 + \Phi)^2 - 1} - Q^2\Phi(1 + \Phi)(2 + \Phi)\rho} \quad (3.1)$$

Here we have selected the branch for which Φ_ρ is negative at $\Phi = 0$.

Figure 3 shows the corresponding integral curves. Note that in the region marked by (#) (characterized by relatively low velocity of gas flow) flame stabilization is impossible. The flame configuration (Fig. 4b) corresponding to the solution (a) is of special interest since, despite its rather unusual appearance, it seems to be realizable experimentally in counterflow systems (Ishizuka and Law 1982). Similarly, the time-independent version of Eq. (2.5) yields

$$\Psi_\xi = \frac{Q^2(1 + \xi)^2\Psi^2 - 1}{\sqrt{Q^2(1 + \xi)^2 + Q^2\xi^2(2 + \xi)^2 - 1} - Q^2\xi(1 + \xi)(2 + \xi)\Psi} \quad (3.2)$$

This equation corresponds to the branch for which Ψ_ξ is positive at $\xi = 0$. The integral curves of Eq. (3.2) are shown on Fig. 5. In this case each flame front configuration seems to be experimentally feasible, provided the flame is held at the rim of the burner ($\xi = -1, \Psi = \Psi_0$). Curve (a) clearly corresponds to the Bunsen type flame, while (b) to the "grammophone" flame (Fig. 4d,c). Since Eqs. (3.1) and (3.2) are nothing but different branches of the same basic equation (2.2) their solutions may well coexist. In other words actual flame front shape may be composed from the elements generated by Eq. (3.1) as well as by Eq. (2.2).

Figure 4e shows one of such configurations, which clearly corresponds to the experimental situation shown on Fig. 1.

4. CONCLUDING REMARK

The simple geometrical model discussed above, shows that the classical stagnation point flow field apart from the known planar flame is indeed capable of sustaining other more complex flame configurations. In the present article we didn't discuss the question of dynamic stabilization, which due to apparent nonuniqueness of the possible equilibrium states may prove to be quite nontrivial.

ACKNOWLEDGMENTS

The authors wish to express their gratitude to Professor S. H. Sohrab for stimulating and helpful discussions.

This work was supported by the Air Force Astronautic Laboratory under Contract No. FO4611-87-KOO67 (W.J.S.) and by the U.S. Department of Energy under Grant DE-FG02-88ER13822 (G.I.S.).

REFERENCES

Ishizuka, S., Miyasaka, K., and Law, C. K. (1982) "Effects of heat loss, preferential diffusion, and flame stretch on flame-front instability and extinction of propane/air mixtures". Combustion and Flame, 45, 293-308.

Ishizuka, S., and Law, C. K. (1982) "An experimental study on extinction and stability of stretched premixed flames. Nineteenth Symposium (International) on Combustion. The Combustion Institute, 327-335.

LIST OF FIGURES

- Figure 1 Nozzle stabilized counter flow lean propane-air flame. (Courtesy of S. H. Sohrab, Northwestern University.)
- Figure 2 Diagram illustrating premixed flame moving in stagnation-point flow field. Shaded area represents the burnt gas region.
- Figure 3 Integral curves of Eq. (3.1) for $\phi = 2$. ($\alpha = 1/Q$, $\beta = -1 + \sqrt{1 - 1/Q}$)
- Figure 4. Integral curves of Eq. (3.2) for $\phi = 2$. ($\alpha = 1/Q$, $\beta = -1 + \sqrt{1 - 1/Q}$)
- Figure 5 Some of the possible equilibrium flame configurations in counter (stagnation point) flow fields.

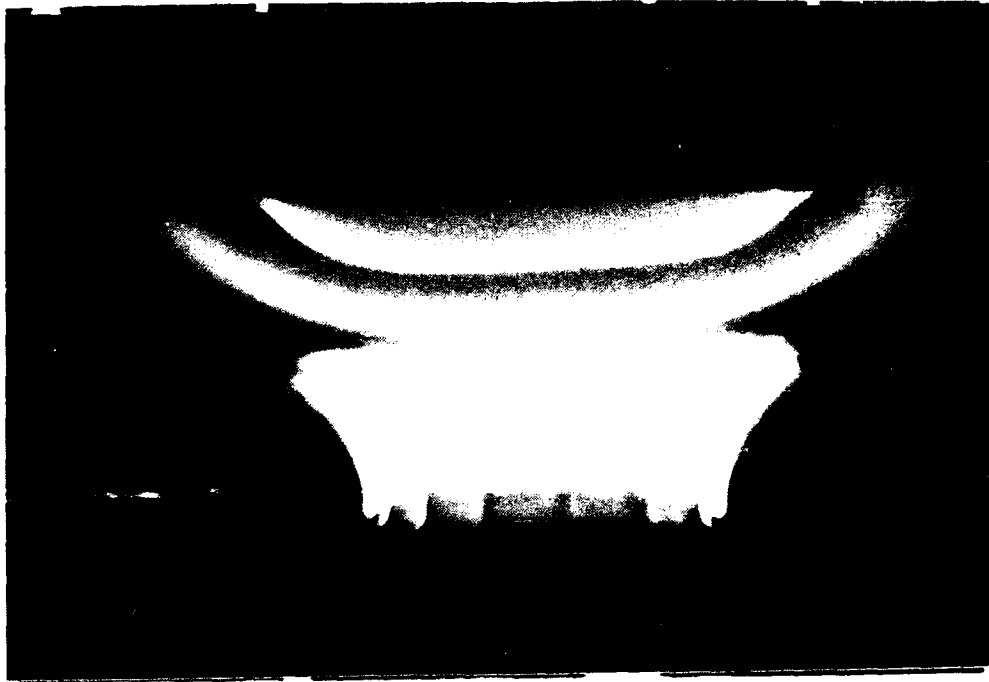


Figure 1

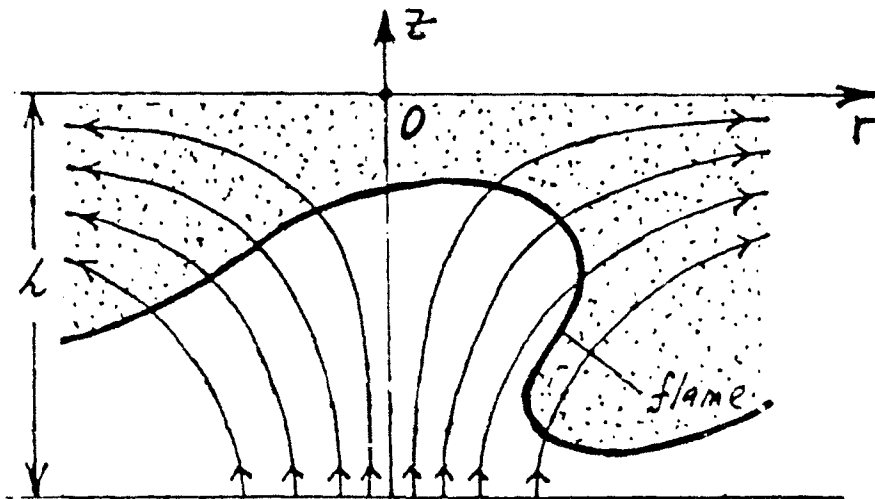


Figure 2

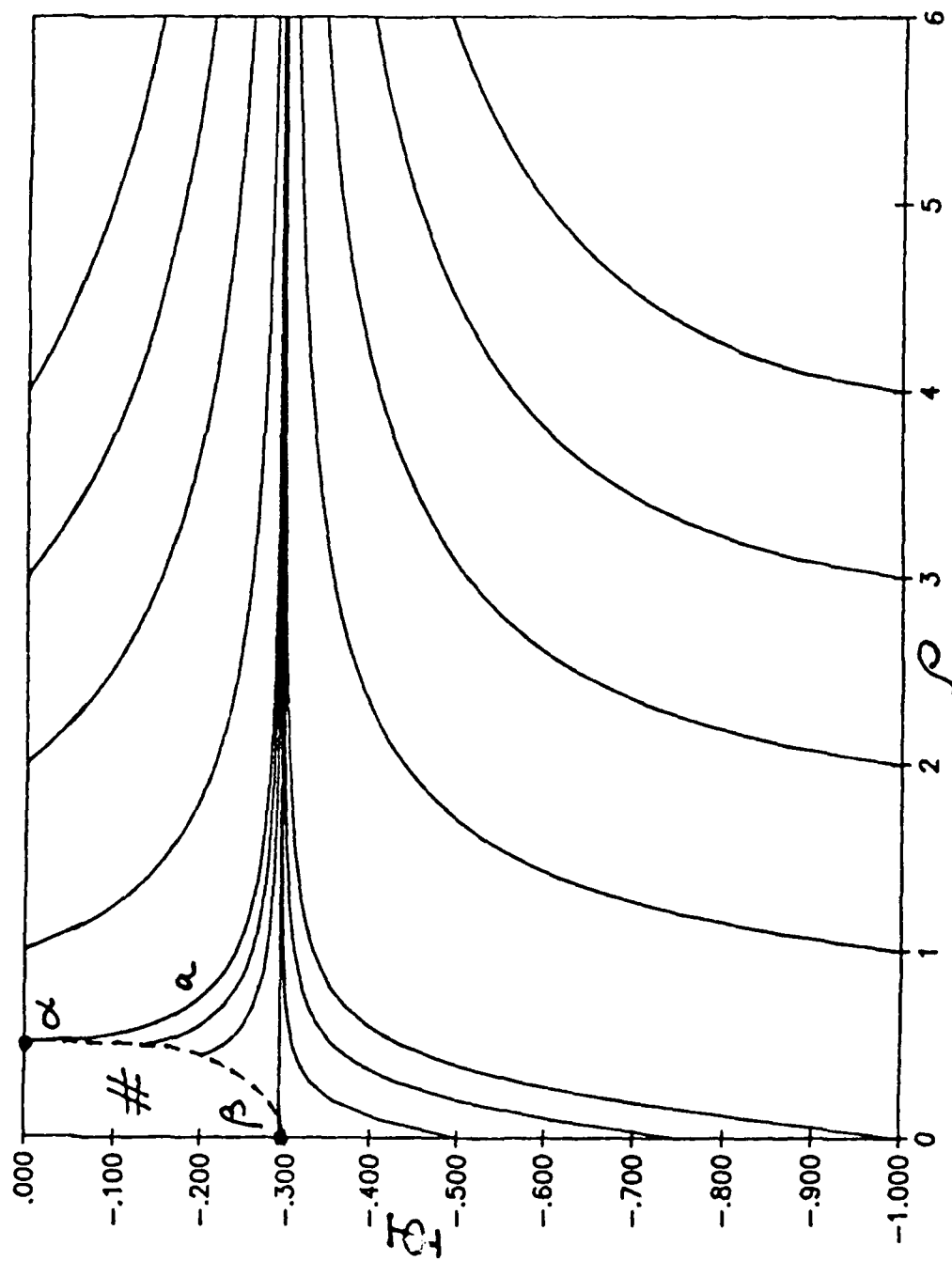


FIGURE 3

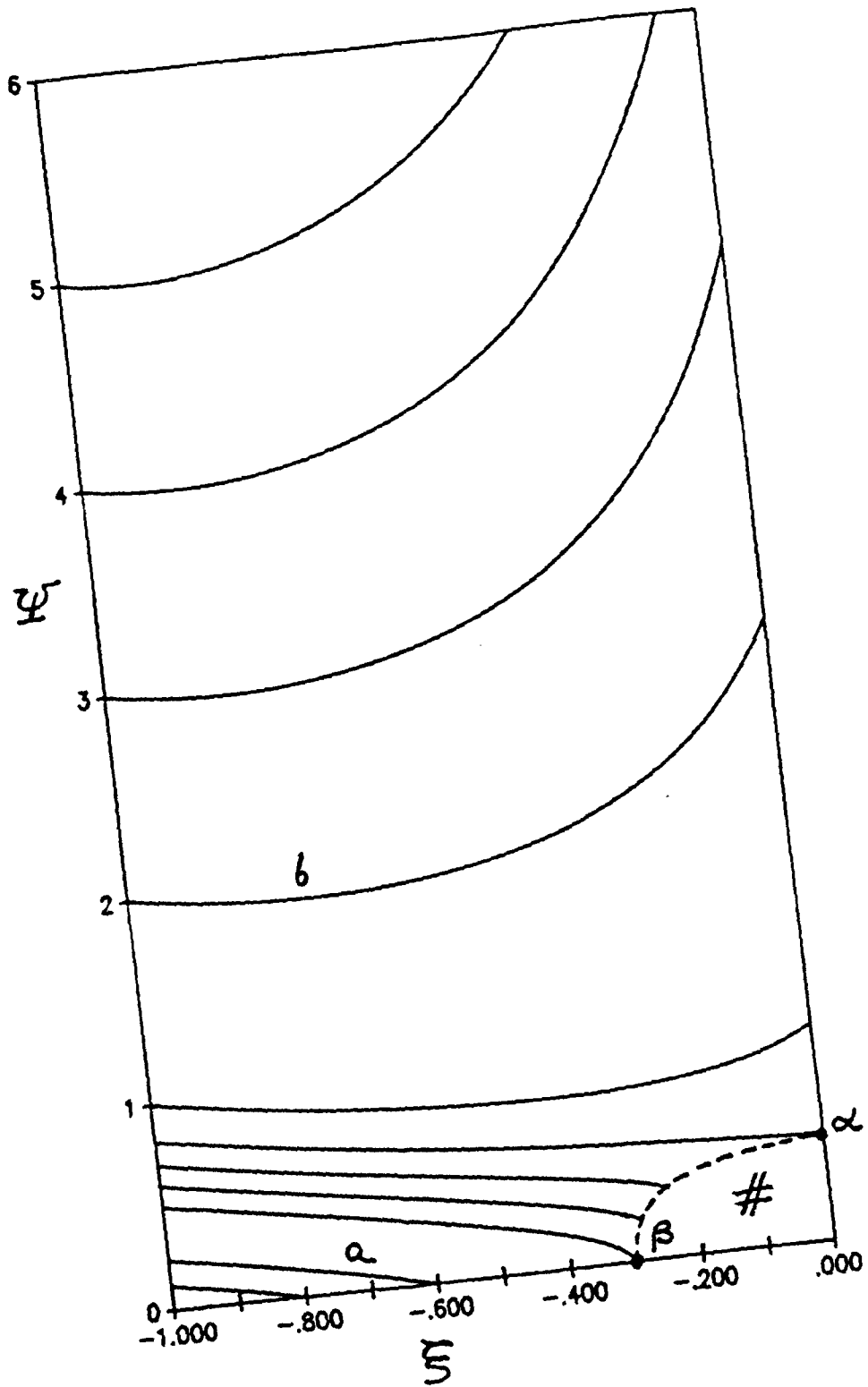
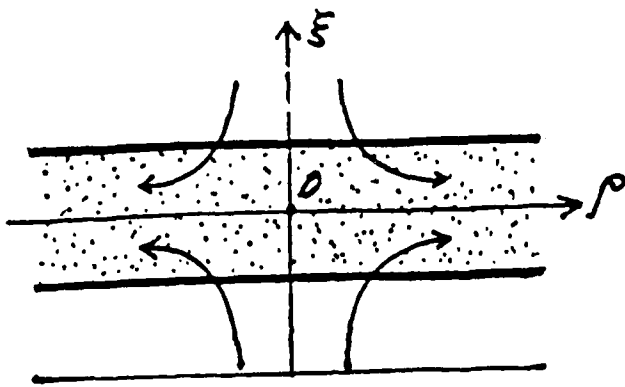
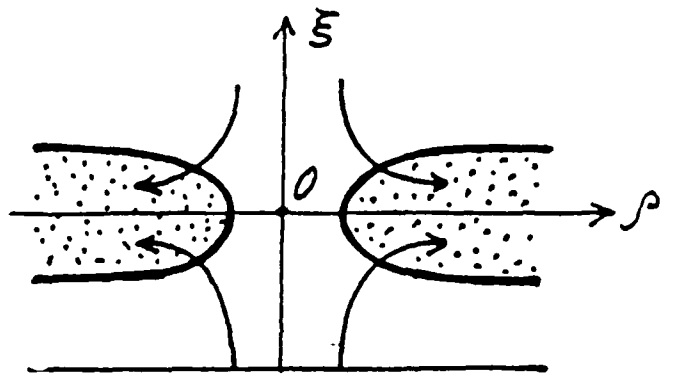


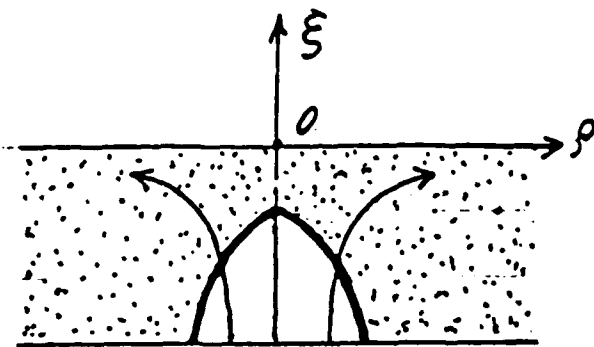
Figure 5



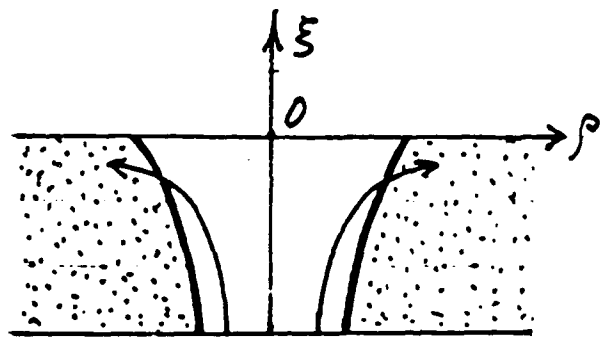
(a)



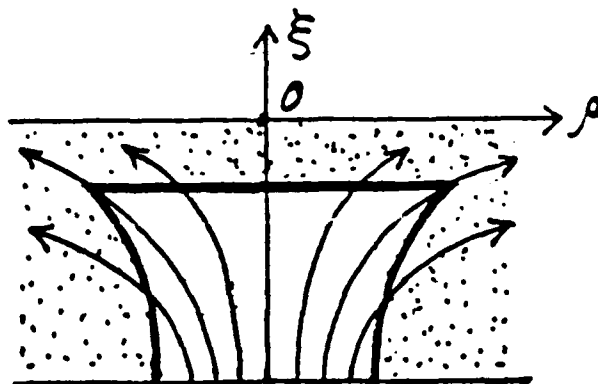
(b)



(c)



(d)



(e)